

**An Experimental Investigation into
Tool Wear in Micro-drilling of
Aluminium, Aluminium/Copper Metal
Alloys and Carbon Fibre Reinforced
Composites**

By

Ming-Yi Cheng

College of Engineering, Design and Physical Sciences

Brunel University London

April 2017

Abstract

Limitation of conventional machining equipment has become a growing concern over the past two decades due to the demands for greater machining accuracy in today's manufacturing. The development of micro-machining has therefore attracted significant attention; it signifies the advancement of national economy as well as the level of accuracy manufacturing industry could achieve.

While the connection between tool lifespan, cost of machining and throughput is well established, the factor of tool lifespan appears to have more significance since the miniaturization of tool could lead to further performance concerns such as its lack of strength and durability. On the other hand, raising feed rate and spindle rotation speed are the two common approaches for increasing manufacturing throughput. Such approaches tend to cause an increase in the thrust force subjecting the tool to greater stress, which is the main cause of tool wear and even tool failure.

Through literature review and preliminary experiments, it was found that spot-drill is often done prior to micro-drilling since it prepares a pre-drill countersunk hole that helps the alignment of tool for subsequent micro-drilling. Although such pre-drill step does improve the micro-drilling operation, the fundamental issue of tool diameter difference still remains. Often the tool used for pre-drill has a bigger diameter than the one for micro-drilling although a significant difference is always something to be avoided. This is because the difference has to be picked up by the tool used for micro-drilling and is directly linked to the wear caused by increased thrust force.

In this research the operation of micro-drilling is investigated via mathematical models. Such operation is further broken down into various steps and stages so more detailed description can be achieved. The findings are then further enhanced by simulation based on the 3D model of micro-drilling. Three materials were selected for this research: Al 6061T, Al/Cu metal alloy panel and Carbon fibre reinforced composites. Such a selection enables the study of individual characteristics of different materials and the variation in respective thrust forces.

Abstract

Finally, Conclusions present the summary of the main findings from micro-drilling process analysis based on research and investigation shown in earlier chapters. By combining actual measurements on micro-drilling and mathematic model this research hopefully would improve the understanding towards micro-drilling processes.

Acknowledgments

First and foremost I would like to take this opportunity to express my gratitude to my supervisor, Dr. Joe Au, for his enthusiastic science support, epitome of knowledge and patience throughout the course of this research.

I would like to thank Brunel University for their financial support which made this research possible. I would also like to express my thanks and gratitude to Prof. Kai Cheng and Dr. Atanas Ivanov for being helpful throughout the course

Special thanks to my friend Dr. Wang Chao, and Dr. Tommy Shyng for their invaluable support. Their friendship and encouragement have been a strong wind that helped lead this study safely to the harbour.

Finally, a big thanks to my family: my parents and brother, for their love and mental support, this research can be successful completion.

Table of contents

Abstract	I
Acknowledgments.....	III
Table of contents	IV
Nomenclature	VIII
List of figures	IX
List of tables	XV
Chapter 1: Introduction.....	1
1.1 Research background and motivation	1
1.2 Research aim and objectives.....	3
1.3 Organization of the thesis	4
Chapter 2: Literature review	6
2.1 Introduction	6
2.2 Theoretical analysis on the manufacturing machining	6
2.3 Theoretical analyses on the micro-drilling mechanics.....	9
2.4 Challenges with mechanical micro-drilling	13
2.4.1 Cutting force.....	13
2.4.2 Wandering motion	14
2.4.3 Tool breakage	15
2.4.4 Size effect of mechanical micro-drilling	16
2.5 Experimental measurements	17
2.5.1 Cutting parameters for micro-drilling	17
2.5.2 Rotation speed and feed rate.....	22
2.6 Surface quality in drilling composite.....	24
2.6.1 Mechanisms of composite delamination.....	24

Table of contents

2.6.2	Damage criteria on composite delamination.....	26
2.7	Modelling and simulation	27
2.7.1	Cero parametric 2.0.....	28
2.7.2	FEA simulation in ANSYS	29
2.7.3	LabVIEW 2014	29
2.7.4	MATLAB R2014a	30
2.8	Summary	31
Chapter 3:	Modelling and simulation of micro-drilling.....	32
3.1	Introduction.....	32
3.2	Geometry creation	33
3.2.1	Drill tool geometry	34
3.2.2	Geometry of the work-piece	37
3.3	Mesh generation	38
3.4	Boundary conditions	40
3.4.1	Engineering data	40
3.4.2	Fixed support.....	42
3.4.3	Displacement support	43
3.4.4	Velocity	44
3.4.5	End time	45
3.5	Results and discussion.....	46
3.6	Summary	50
Chapter 4:	Experimental methods	52
4.1	Introduction.....	52
4.2	Experimental set-up	52
4.2.1	KERN CNC milling machine tool	54
4.2.2	Force dynamometer	60

Table of contents

4.2.3	Aluminium work-piece fixture	62
4.2.4	Image acquisition	63
4.2.5	Drilling tools	65
4.2.6	Work-pieces.....	66
4.2.7	Ultrasonic cleaner	67
4.2.8	Mirror surface finishing process.....	68
4.3	Checking on the setting.....	69
4.3.1	Laser tool measuring system.....	70
4.3.2	Infrared touch probe system.....	71
4.3.3	Non-contact tachometer.....	72
4.3.4	Point angle and diameter of the drilling tool.....	73
4.4	Summary	74
Chapter 5:	Thrust force model for drilling	75
5.1	Introduction.....	75
5.2	Thrust force model.....	75
5.3	Stage 1: $x_0 < x_P \leq x_1$	78
5.4	Stage 2: $x_1 < x_P \leq x_2$	81
5.5	Stage 3: $x_2 < x_P \leq x_3$	83
5.6	Stage 4: $x_3 < x_P$	85
5.7	Summary	86
Chapter 6:	Experimental and theoretical results of micro-drilling manufacturing ..	87
6.1	Introduction.....	87
6.2	Force measurement	87
6.2.1	Aluminium 6061T work-piece	88
6.2.2	Al/Cu metal alloys	100
6.2.3	Carbon fibre reinforced composites	103

Table of contents

6.3	Hole quality and tool wear	105
6.4	Discussion between the numerical calculation with the drilling model and force gradient	110
6.5	Conclusion	112
Chapter 7:	Conclusions and recommendations for future work	113
7.1	Conclusions	113
7.2	Contribution to knowledge	114
7.3	Recommendations for future work.....	115
References.....		117
Appendix A: Engineering drawings for fixture design		131
Appendix B MATLAB programming for experimental data analysis		138

Nomenclature

A_d	Actual area of delamination damage
A_0	Area of the hole (mm ²)
D/D_{drill}	Drill diameter (mm)
D_{hole}	Diameter of the hole being enlarged
D_{max}	Maximum diameter of delamination damage
D_0	Diameter of the hole
F	Cutting force
F_{da}	New damage delamination evaluation index
f	Feed per revolution(in/rev)
f_m	Feed per minute
f_z	Feed per tooth
k'	Coefficient of the tip of the drill tool geometry
k_c	Specific cutting force
N	Rotational speed of the drill
T	Temperature of the work-piece material
T_m	Melting temperature
T_{room}	Room temperature
T_d	Drill tool temperature
V	Cutting velocity
w	Web thickness
δ	Helix angle
ϵ	Feed angle
θ	Clearance angle

List of figures

Figure 1-1: Micro manufacturing size/ precision domains	1
Figure 1-2: The industry applications of drilling.....	2
Figure 1-3: The chapter plan of thesis.....	5
Figure 2-1: Dimensional size for the micro-mechanical machining	7
Figure 2-2: Micro-drilling machine	10
Figure 2-3: Industrial precision machine with micro drilling capability: (a) Copyright KERN Microtechnik GmbH; (b) Makino Releases iQ300 Precision Micromachining Centre; (c) Haas Super Mini Mill Vertical Machining Centre; (d) Makino’s UPJ-2 Horizontal Wire EDM Machine; (e) 701S - 3-Axis Machining Centre with Parallekinematics; (f) F5 Vertical machining centre.....	13
Figure 2-4: Boundary conditions changes of micro-drilling process.....	15
Figure 2-5: Size effect the feed force	16
Figure 2-6: PCB Twist drill.....	17
Figure 2-7: Twist drill elements	18
Figure 2-8: The drilling speed used in different material.....	22
Figure 2-9: Feed rates used in drill diameter	23
Figure 2-10: Peel up at delamination entry point	25
Figure 2-11: Push out at delamination exit point	25
Figure 2-12: Examples of extreme delamination patterns when drilling FRP laminates (a) fine cracks and (b) uniform damage area	26
Figure 2-13: Simulation analysis process	28
Figure 2-14: Details of connection for transferring signal to user interface	30
Figure 3-1: ANSYS workbench explicit dynamics simulation	32
Figure 3-2: Process steps for FEA analysis on micro-drilling	33

List of figures

Figure 3-3: Drill diameter: 0.5mm.....	34
Figure 3-4: Body length: 10mm.....	34
Figure 3-5: Flute: Φ 0.25mm setting.....	35
Figure 3-6: Flute length: 7.5mm.....	35
Figure 3-7: Tool point angle drawing.....	36
Figure 3-8: Φ 0.5 mm tool solid	36
Figure 3-9: Geometry solid of work-piece	37
Figure 3-10: Assemble of geometry of tool and solid of work-piece.....	38
Figure 3-11: Mesh generation	39
Figure 3-12: Element size	39
Figure 3-13: Function of engineering Data	40
Figure 3-14: Fixed support	42
Figure 3-15: Displacement support.....	43
Figure 3-16: Tool rotational speed setting	44
Figure 3-17: Tool velocity setting	45
Figure 3-18: Action end time.....	46
Figure 3-19: Drilling action with time.....	47
Figure 3-20: The deformation of the Al work-piece during drilling process.....	47
Figure 3-21: The normal stress of the bottom surface of the Al work-piece during drilling process	48
Figure 3-22: Von-Mises stress of the work-piece during drilling process.....	49
Figure 3-23: Von-Mises stress change with time	49
Figure 3-24: Energy conservation in drilling simulation.....	50
Figure 4-1 Experimental process	53
Figure 4-2: KERN milling machine	54
Figure 4-3: Calibration of the aluminium fixture	55

List of figures

Figure 4-4: Set up the drilling parameter	55
Figure 4-5: The experiment test of micro-drilling	56
Figure 4-6: Drilling and monitor control	56
Figure 4-7: The Kistler dynamometer	60
Figure 4-8: The data collection and multichannel change amplifier	60
Figure 4-9: Force signal data collect.....	61
Figure 4-10: Smaller aluminium fixture	62
Figure 4-11: Bigger aluminium fixture	63
Figure 4-12: JCM-6000 Benchtop SEM.....	63
Figure 4-13: The operating of JCM-6000 Benchtop SEM	64
Figure 4-14: Specimen holder of JCM-6000 Benchtop SEM	64
Figure 4-15: PCB Tungsten carbide drill tool	65
Figure 4-16: Aluminium work-piece.....	66
Figure 4-17: Al/Cu metal matrix composite	67
Figure 4-18: Ultrasonic cleaner	68
Figure 4-19: Drill tool before clean and after.....	68
Figure 4-20: NANOTECH 250UPL Ultra-precision Lathe.....	69
Figure 4-21: The spindle of NANOTECH 250UPL Ultra-precision Lathe	69
Figure 4-22: To calibrate the Aluminium fixture remains parallel to the moving direction of the base plate	70
Figure 4-23: Laser tool position measuring system	71
Figure 4-24: Infrared probe 32.00-MINI.....	72
Figure 4-25: RS163-5348 Non-contact tachometer	72
Figure 4-26: Measured by the SEM photo	73
Figure 5-1: Twist drill tip moves into a work-piece	76
Figure 5-2: Cutting lip move with time	77

List of figures

Figure 5-3: Material removal during Stage 1: $x_0 < x_P \leq x_1$	78
Figure 5-4: Volume removal during Stage 1.....	80
Figure 5-5: Material removal during Stage 2: $x_1 < x_P \leq x_2$	81
Figure 5-6: Material removal during Stage 3: $x_2 < x_P \leq x_3$	83
Figure 5-7: Material removal during Stage 4: $x_3 < x_P$	85
Figure 6-1: Force signal of the 1st drilling process of Φ 0.2mm drilling tool and Al work-piece.....	88
Figure 6-2: Force signal of 1st pecking action of Φ 0.2mm drilling.....	89
Figure 6-3: Thrust forces of all 1st pecking with Φ 0.2mm tool on Al work-piece.....	89
Figure 6-4: Thrust force comparison over different feed rates of 1st pecking with Φ 0.2mm tool on Al work-piece.....	90
Figure 6-5: Force gradients of all 1st pecking with 0.2mm tool on Al work-piece.....	91
Figure 6-6: Force gradients comparison over different feed rates of 1st pecking with Φ 0.2mm tool on Al work-piece.....	92
Figure 6-7: Thrust Force of all 1st pecking with Φ 0.4mm tool on Al work-piece.....	92
Figure 6-8: Variation of maximum thrust force over 9 drilling processes on Al work-piece with drilling parameters: Φ 0.4mm drilling tool, 6000 rpm, 12mm/min feed rate.....	93
Figure 6-9: Variation of maximum force gradient over 9 drilling processes on Al work-piece with drilling parameters: Φ 0.4mm drilling tool, 6000 rpm, 12 mm/min feed rate.....	94
Figure 6-10: Variation of thrust force over 9 drilling processes on Al work-piece with drilling parameters: Φ 0.8mm drilling tool, 6000 rpm, 12 mm/min feed rate.....	94
Figure 6-11: Section between index time 0 and 100000, extracted from Figure 5.10	95
Figure 6-12: Variation of force gradient over 9 drilling processes on Al work-piece	

List of figures

with drilling parameters: Φ 0.8mm drilling tool, 6000 rpm, 12 mm/min feed rate	96
Figure 6-13: Influence of feed rates on thrust force over 9 drilling processes on Al work-piece with drilling parameters: Φ 0.4mm drilling tool, 6000 rpm.....	96
Figure 6-14: Influence of feed rates on thrust force over 9 drilling processes on Al work-piece with drilling parameters: 0.8mm drilling tool, 6000 rpm.....	97
Figure 6-15: Influence of feed rates on force gradient over 9 drilling processes on Al work-piece with drilling parameters: Φ 0.4mm drilling tool, 6000 rpm	97
Figure 6-16: Influence of feed rates on force gradient over 9 drilling processes on Al work-piece with drilling parameters: Φ 0.8mm drilling tool, 6000 rpm.....	98
Figure 6-17: Influence of drilling tool size on thrust force over 9 drilling processes on Al work-piece with drilling parameters: 6000 rpm, 12/min feed rate	99
Figure 6-18: Influence of drilling tool size on thrust force over 9 drilling processes on Al work-piece with drilling parameters: 6000 rpm, 24/min feed rate	99
Figure 6-19: Influence of drilling tool size on thrust force over 9 drilling processes on Al work-piece with drilling parameters: 6000 rpm, 36/min feed rate	100
Figure 6-20: Influence of rotation speed on thrust force on Al/Cu metal alloys work-piece with drilling parameters: Φ 0.5mm drilling tool, 24/min feed rate.....	101
Figure 6-21: Influence of feed rate on thrust force on Al/Cu metal alloys work-piece with drilling parameters: 0.5mm drilling tool, 9000 rpm	101
Figure 6-22: Influence of feed rate on gradient on Al/Cu metal matrix work-piece with drilling parameters: Φ 0.5mm drilling tool, 9,000 rpm.....	103
Figure 6-23: Comparison on the averaged thrust force with three levels of feed rate (0.4, 0.6 and 0.8 m/min) at a constant spindle speed of 20k rpm.....	104
Figure 6-24: Comparison on the averaged thrust force with three levels of spindle speed (20k, 40k and 60k rpm) at a constant feed rate of 0.8 m/min.	104
Figure 6-25: Countersink in Al work-piece	105

List of figures

Figure 6-26: Φ 0.2mm drilled in Al work-piece entry side.....	106
Figure 6-27: Φ 0.6mm drilled in Al work-piece entry and exit side.....	107
Figure 6-28: Φ 0.5mm drilled in Carbon fibre reinforced composite entry and exit side	107
Figure 6-29: Twist drill tip model moves into a work-piece.....	111
Figure 6-30: Drilling tool location after numerical calculation	112

List of tables

Table 2-1: Comparison between micro machining and typical ultra-precision machining.....	12
Table 3-1: Material property of aluminium 6061T for the work-piece.....	41
Table 3-2: Material property of structure steel for the drilling tool	41
Table 4-1: Drilling parameters for drilling aluminium 6061T	58
Table 4-2: Drilling parameter at aluminium/ copper metal alloy board	59
Table 4-3: Drilling parameter at carbon fibre reinforced plastics	59
Table 4-4: Drilling tool specification.....	65
Table 4-5: Spot drill tool specification.....	65
Table 4-6: The material element of aluminium 6061T.....	66
Table 4-7: The material element of Al/Cu metal matrix composite.....	67
Table 4-8: Each tool measured diameter and point angle	74
Table 6-1: SEM photo of Φ 0.2 and Φ 0.4mm new drilling tool and drilled 9 times after with 12, 24 and 36 mm/min feed rate in aluminium work-piece.....	108
Table 6-2: SEM photo of Φ 0.6, 0.8 and 1.0mm new drilling tool and drilled 9 times after with 12, 24 and 36 mm/min feed rate in aluminium work-piece	109

Chapter 1: Introduction

1.1 Research background and motivation

Micro-drilling has attracted growing attention over past two decades for its importance in advanced manufacturing process. In the United States, micro-drilling is also known as Micro-electromechanical Systems (MEMS), a technology extensively used for IC manufacturing, advanced electronics and precision machine components. In Europe the operation is called Micro-system Technology (MST) and typically used for precision manufacturing process that requires accuracy at millimetre and micrometre level. The operational range can be seen in Figure 1-1.

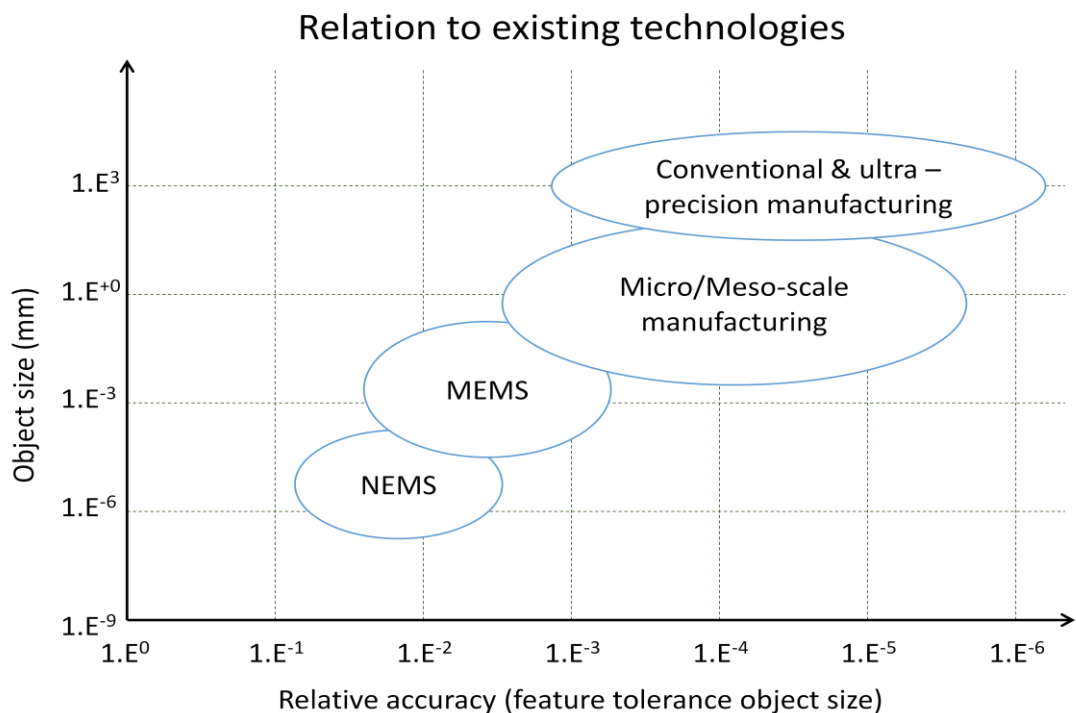


Figure 1-1: Micro manufacturing size/ precision domains (Kai, 2013)

Introduction

Although there is a clear separation between micrometre and nanometre level manufacturing, Nano Electric Mechanical System (NEMS), micrometre level accuracy is used in a much wider market and its application is also much more extensive.

Overall, there are three main metalworking techniques in the micro mechanical manufacturing: Micro turning, Micro drilling and Micro milling. Wherein, micro drilling has extensive industrial applications, such as in aircraft landing gear, oil field exploration, hydraulic cylinder inside bore, heat exchanger tube sheet, oil field downhole exploration, fuel injector bodies, and fluid assembly end.



Figure 1-2: The industry applications of drilling

For resolving the technical requirements of micro-drilling in the semiconductor industry, the ultra - precision manufacturing machine with a diameter below 1mm is in strong demand. Micro manufacturing normally refers to a process for making micro features no bigger than 1mm diameter on parts with an emphasis on the level of precision. The development of micro-machining continues to grow; it has been further used in small details such as 50 μ m (0.05mm) diameter holes. Micro-drilling involves not just small drill bits but also precision control over its cyclic rotation.

As the technology continued to develop, the scale of precision metal processing has reached a record high level at the end of 2001. Moreover, as a result of the Taiwanese Government's national support program for the semiconductor industry, there was an increasing number of titanium processing plants in 2002.

In order to compete with the developed countries, the first Taiwan Export Processing Zone (TEPZ) was established in 1966. As of the end of April 2015, the TEPZ has approved 621 manufacturers of the establishment and the total amount of

Introduction

investment has risen to over \$17,850 million dollars.

Owing to the features of micro-drilling that provides smooth clean walls, sharp, well defined edges and high volume production, high-tech industries today are heavily dependent on the technology. The advanced technology in micro-drilling does not only significantly improve the quality of the products and the processing performance but also avoid the possibility to exceed the allowable limit of the durability of the cutting tools. By doing so, the aim of extending the use of the cutting tools can be achieved, of which at the same time to reduce the cost of consumption, increase production as well as improve efficiency. Besides the size of the cutting tools, the processing of the cutting tools is also of vital importance for studying micro-drilling.

1.2 Research aim and objectives

It is well known that metal-machining tools, such as a drill bit, experiences significant stress during drilling because of effort required for metal removal and the friction at the tool/work-piece interface. It is therefore important to understand the drilling process and the factors that influence the machining mechanics. Moreover, by measuring and recording the force that the drill bit must endure, it would allow the process to be analysed via not only software simulation but also through real world experiment. The aim of this research is to offer a combined analysis and discussion of both aspects and provide applicable productions for the future developments in drill bit as well as references for other metal-machining tools.

The research objectives of this study are as follows:

- To identify the factors that influence the machining mechanics in micro-machining, such as part material, size of drill tool, operation parameters and the control over cooling.
- To evaluate tool wear on a drill using SEM and application software that offers precision measurements.
- To model by simulation the progression of thrust force during the drilling operation, followed by subsequent cross examination and comparison.

Introduction

- To model mathematically the metal removal rate of the drilling operation for the four stages of tool/work-piece engagement.
- To establish the relationship between metal removal rate and thrust force in drilling.
- To perform drilling tests on 3 types of work-piece materials, for drill diameters from 0.1mm to 1.0mm, and to capture the thrust force signal for tool wear monitoring analysis.

This research will follow the steps of model creation, Finite Element Analysis (FEA), experiment data collection and final analysis. It aims to improve scientific understanding in the development of micro-drilling process.

1.3 Organization of the thesis

This research consists of six chapters. Figure 1-3 is the schematic diagram of this thesis organization plan. Each step will be represented by one colour, and use arrows to represent the process of writing this thesis.

Chapter 1 starts with a general description on the significance of metal-machining industry and the importance of advanced tool applications. The background information leads to chapter 2 which gives detailed literature review as well as the theories, findings and discussions reported by other researchers.

As this research uses both experimental and simulation approaches, chapter 3 will focus on the design and excursion of software simulation whereas chapter 4 describes the setup and considerations for real world experiments. Chapter 5 provides further descriptions regarding the construction of mathematical model that is essential to the result interpretation. Systematic discussions on the data obtain through experimental measurements can be found in chapter 6 and chapter 7 presents an organised summary of the conclusion of this research.

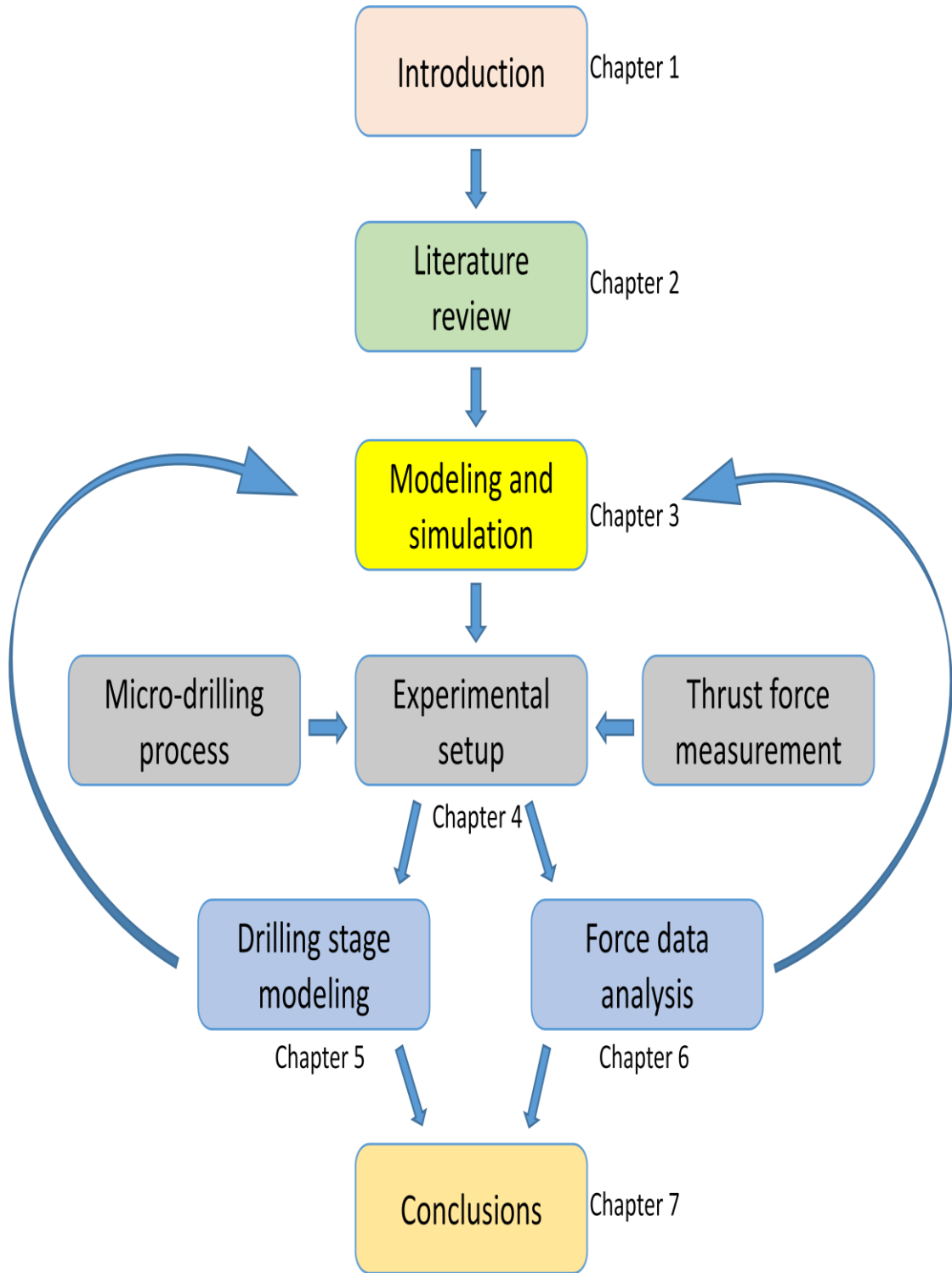


Figure 1-3: The chapter plan of thesis

Chapter 2:

Literature review

2.1 Introduction

In the last thirty years many papers on the basic mechanics of metal drilling have been written. Several models to describe the process have been developed. Analysis methods have seen increasing use in machining process design and improvement in automotive, aerospace, construction equipment and drilling tool industries. Some have been fairly successful in describing the process, but none can be fully substantiated and definitely stated to be the correct solution. Thus, while none of the analysis can precisely predict conditions in a practical drilling situation, the analyses are worth examining because they can qualitatively explain the phenomena observed and indicate the direction in which conditions should be changed to improve drilling performance.

In this chapter, some of previous studies to the current research will be raised for discussion. In the next section 2, discussions will be introduced regarding the theoretical analysis on the drilling mechanisms. Section 3 will focus on the micro-drilling. Section 4 will investigate the issues arising in the micro-drilling process. Section 5, which consists of experimental tool and parameter setting, will be about the drilling tool, rotation speed and feed rate. Section 6 introduces the background knowledge regarding surface quality of composite material. In the section 7, a brief introduction is given on software modelling, simulation and experimental methods used in this research.

2.2 Theoretical analysis on the manufacturing machining

Machining is the most versatile and accurate of all manufacturing processes with capability to produce a diversity of part geometries and geometric features. In terms of machining process mode, drilling is one of the three known processing methods.

Literature review

Drilling process has been investigated in detail by many researchers, such as Aronson (2004), Ashley (1995), Bonston (1951), DeGarmo (2003) and Drozda (1983). Industrial Press Inc. (1949) gives a definition: A rotary end cutting tool having one or more cutting lips, and having one or more helical or straight flutes for the passage of chips and the admission of a cutting fluid.

A drilling machine comes in many shapes and sizes, from small hand-held power drills to bench-mounted and finally floor-mounted models. There are various types of drill process, including upright machines, radial machines, and various specialized machines (David, 2005), with a typical accuracy level at low millimetres and high micrometres. Such as aerospace, precision engineering, medical engineering, biotechnology, electronics and communication optics. Figure 2-1 shows the dimensional size and the accuracy with other manufacturing methods.

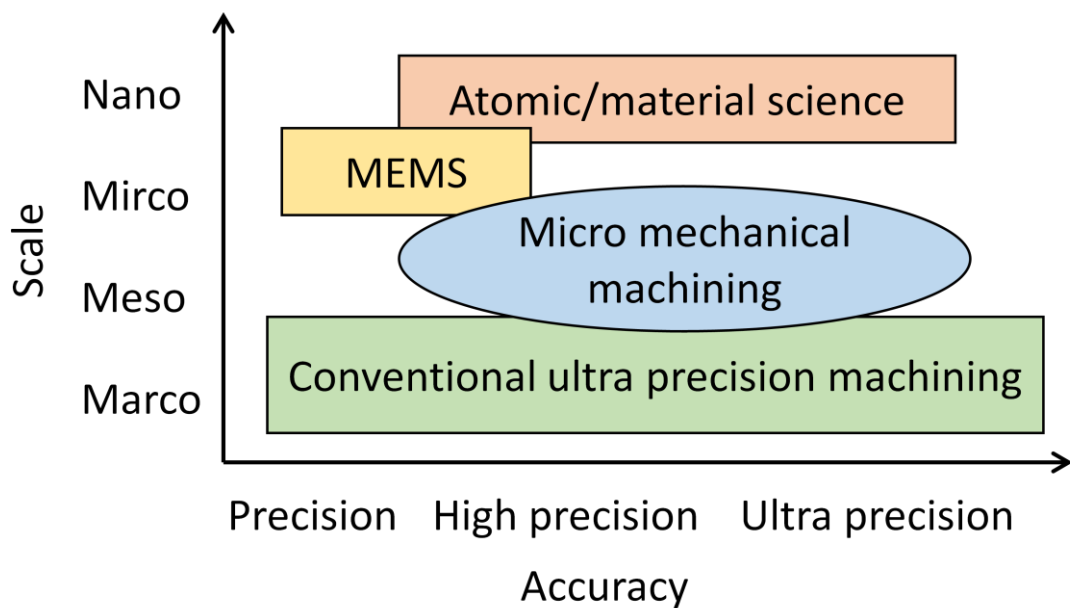


Figure 2-1: Dimensional size for the micro-mechanical machining (Chae, 2006)

The relative accuracies of MEMS-based methods are of the order of 10^{-1} to 10^{-2} mm, whereas the needs of many mechanical miniaturized components require relative accuracies in the order of 10^{-3} to 10^{-4} mm (Ehmann, K., 2007). As an added benefit of such high level of accuracy, micro-drilling also provides low surface roughness, which is an important feature of precision components.

Literature review

Geometrically, drilling is a complex process. There are many factors that can affect the outcome of drilling process. The drilling process depends on the materials involved, the drill geometry, the spindle speed and the feed rate (David, 2005).

Researcher Marinov (2008) gives a very good modelling of drill process: Cutting velocity in drilling is not a constant along the major cutting edge as opposed to the other machining operations. It is zero at the centre of the twist drill, and has a maximum value at the drill corner. The maximum cutting speed is given by

$$V = \pi DN \quad (2-1)$$

where

V = cutting velocity.

D = drill diameter.

N = rotational speed of the drill.

And two types of feed in drilling can be identified:

- a. Feed per tooth(f_z): has the same meaning as in the other multi-tooth cutting tools. Feeds per tooth are roughly proportional to drill diameter, higher feeds for larger diameter drills.
- b. Feed per minute (f_m): feed per minute is calculated taking into account the rotational speed N ,

Feed per minute is used to adjust the feed change gears:

$$f_m = 2f_z N \quad (2-2)$$

Feed per revolution: the depth of the drill penetrates into the material in one revolution.

$$f = \frac{f_m \times 1000}{N} \quad (2-3)$$

In drilling, depth of cut (d) is equal to the half of drill diameter:

$$d = \frac{1}{2} D \quad (2-4)$$

Literature review

In core drilling, a drilling operation used to enlarge an existing hole of diameter D_{hole} , depth of cut is given by

$$d = \frac{1}{2}(D_{drill} - D_{hole}) \quad (2-5)$$

where

D_{drill} = drill diameter.

D_{hole} = diameter of the hole being enlarged.

2.3 Theoretical analyses on the micro-drilling mechanics

To date, several methods are available for micro-drilling; this includes electrical discharge machining, ultrasonic machining, laser beam machining, electrochemical machining and mechanical micro-drilling (Qin, et al., 2010). A good definition of Micro-drilling can be extracted from Micro Machining Universal: a technology that combines tiny electronic and mechanical parts to create system with moving parts on a scale ranging from microns to a millimetre, typically using silicon or silicon-based fabrication methods. Mechanical micro-drilling is widely used in the printed circuit boards (PCB) and IC masking.

Especially numerous micro-through-holes have to be drilled in the modern industry. Even the alternative methods of laser or Electrical Discharge Machining (EDM) cannot replace mechanical micro-drilling sometimes. This is because micro-drilling includes many desirable features such as good roundness, straightness, and surface roughness achieved in a short processing time (Wiley, 2010). The alternatives to mechanical micro-drilling, for example, laser or EDM, are not acceptable in hole quality and accuracy with PCB manufacture (Lee, 2003).

In short, drilling size is the biggest difference between traditional drilling and micro-drilling. Because of the drilling size of micro-drilling is less than 1mm, to control the location, spacing between each other, depth and drilling speed of each hole must be very precise. Figure 2-2 is a simple diagram of micro-drilling system.

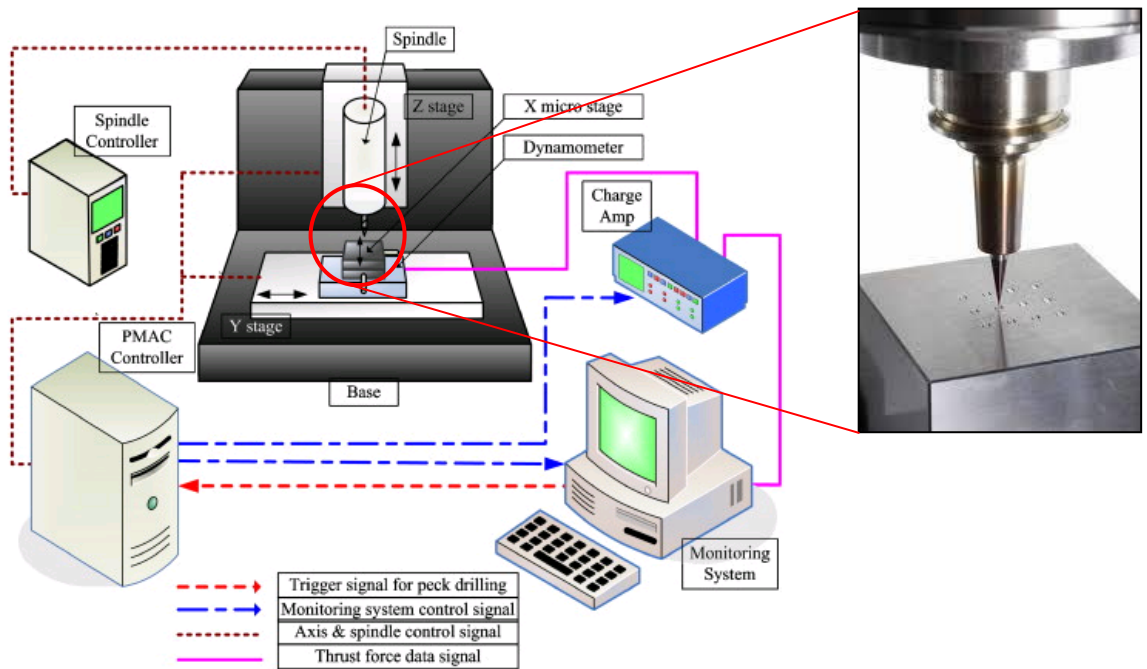


Figure 2-2: Micro-drilling machine (Qin, et al. 2010)

Micro-drilling can be defined as a traditional drilling process that has been scaled down to micron level. However, the tool size of micro-drilling is different to the normal drill in a variety of factors. Typical micro-drills are made of tungsten carbide and have diameters $d < 0.5$ mm and flute lengths $L < 10$ mm (Abouridouane, 2012). In the description of the modelling of micro-drilling, a very important factor in the drilling process is the metal removal rate (MRR), because higher MRR can effectively reduce the chip clogging produced. Pathak (2003) shows the formula of metal removal rate as:

$$MRR = D \times f \times V \quad (2-6)$$

Also,

Cutting speed is $V = \pi DN$,

Feed per revolution is $f = \frac{f_m \times 1000}{N}$

As we can get

$$MRR = D \times \frac{f_m \times 1000}{N} \times \pi \times D \times N \quad (2-7)$$

Literature review

To consider a macro-scale part and associated tooling that one wishes to homogeneously scale in size by a scaling factor, k . If the spindle speed is constant for both operations, the axial and radial depths of cut will scale by K , and thus the feed rate must be scaled by a factor of K to maintain a constant bending stress in the tool. Therefore

$$MRR = K \times \pi \times 1000 \times D^2 \times f_m \quad (2-8)$$

The cutting force can be followed

$$F = K \times \frac{k' \times k_c \times f \times D}{2} \quad (2-9)$$

Where

V = cutting velocity.

f_m = Feed per minute

F = cutting force

k_c = Specific cutting force ($\frac{N}{mm^2}$), which is depend on the material of item being machined.

f = Feed per revolution

D = drill diameter

k' = coefficient of the tip of the drill tool geometry.

However, the commercially available cutting tool edge radius typically is 2 to 3 μ m. To avoid the cutting tool edge radius and spindle run-out effect, the chip thickness is typically less than 1 μ m. So the tool edge effectively has a large negative rake angle.

In the equation, $F = K \times \frac{k' \times k_c \times f \times D}{2}$, the poor cutting geometry due to the effective cutting stiffness increase, k_c , will result in higher force. Therefore, in the drilling process that requires smaller chip thickness, slowing the feed rate and increasing the processing time are necessary.

Most of micro machining experimental research was built by two types of machines: traditional (ultra) precision machine and micro machining centre. The basic

Literature review

requirement of the industrial precision machine with micro drilling capability must include few components: high dimensional precision, typically better than a few microns; accurate geometrical form, typically better than 100nm departure from flatness or roundness; and good surface finish, in the range of 10 – 100nm Ra. At the same time, these requirements of high static stiffness, low thermal distortion, low motion errors and high damping or dynamics stiffness are also indispensable parts (Kai, 2013). Table 2-1 shows a clear comparison table to better understand the differences between micro machining and traditional ultra-precision machining process.

	Micro machining	Ultra-precision machining
Processes	Micro turning, milling drilling and grinding	Single point diamond turning, fly cutting
Tooling	Various tooling materials: tungsten carbide, CVD, CBN, diamond tools	Natural diamond tools
Component size	1 - 1000 μ m	1 mm
Shape	3D shape with high aspect ratios and geometric complexity	Rotational parts, both spherical and aspheric surface, normally low aspect ratios
Accuracy	Absolute: < 10 μ m Relative: $10^{-2} - 10^{-5}$	Absolute: < 1 μ m Relative: $10^{-5} - 10^{-6}$
Surface finish	< 100nm Ra	Typically < 20nm Ra
Machines	Precision machining centres, precision micro machines	Ultra-precision turning machines
Applications	Various applications requiring micro components	Electro-optics
Depth of cut	1 – 10 μ m	0.1 μ m – 10 μ m

Table 2-1: Comparison between micro machining and typical ultra-precision machining (Kai, 2013)

Figure 2-3 shows some industrial ultra-precision machines with micro drilling capability. A typical example is the KERN micro machine (Figure 2-3a). These machines are extensively used for manufacturing of components of high accuracy level or providing specific surface finishing results.



Figure 2-3: Industrial precision machine with micro drilling capability: (a) Copyright KERN Microtechnik GmbH; (b) Makino Releases iQ300 Precision Micromachining Centre; (c) Haas Super Mini Mill Vertical Machining Centre; (d) Makino's UPJ-2 Horizontal Wire EDM Machine; (e) 701S - 3-Axis Machining Centre with Parallekinematics; (f) F5 Vertical machining centre

2.4 Challenges with mechanical micro-drilling

Three important problems associated to micro-drilling are cutting force increase, wandering motion of the drills and tool breakage (Kim, 2009).

2.4.1 Cutting force

As drilling goes into operation on a work piece, the cutting force increase significantly, especially machining works at high cutting rates. Also the chip produced with cutting is the primary reason of force increase. Due to the friction between the flute and the

Literature review

cut surface of the work piece, most of the cutting energy is transferred into heat and absorbed by the work piece (Konig, 1990).

A conventional basic cutting force model from Armarego's unified mechanics of cutting model, which is through a proportional relation of the instantaneous cutting process with uncut chip cross section models:

$$F = k_m b h \quad (2-10)$$

At the same time, chip thickness h can be expressed as the tool rotation angle θ of the function model from Tlustý and MacNeil conventional cutting force model:

$$h = f_t \sin \theta \quad (2-11)$$

As we can get:

$$F = k_m b f_t \sin \theta \quad (2-12)$$

Where

h = the instantaneous uncut chip thickness variation,

b = the width of cut

k_m = the cutting coefficient

f_t = feed per tooth (mm/tooth)

θ = tool rotation angle

According to the model, cutting force could be affected by shear plane area, the flow stress, shear angle, rake angle, friction and prowl angle. If the cutting conditions are not appropriate, the drilling tool would be easily damaged or failed. Therefore, how to set the cutting conditions is becoming very important.

2.4.2 Wandering motion

The second problem is wandering motion of the drill. Figure 2-4 shows the boundary conditions tend to change in the sequence during the micro-drilling process.

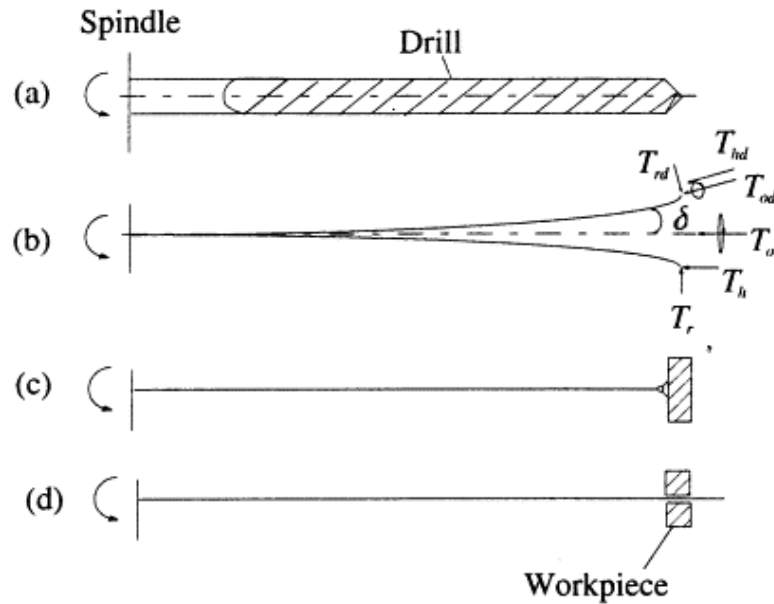


Figure 2-4: Boundary conditions changes of micro-drilling process (Cheong, 1999)

In first stage (a), the main feature is the drill remains in a free rotation state before the drill point contacts the work piece. During the second stage (b) the drill point touches the work piece but does not maintain a stable, continues contact. The motion of the drill called skidding. It is a phenomenon random in nature dictated by the state of the work-piece surface and the drill's chisel edge. After a few revolutions of skidding (c), the drill point stabilizes to penetrate at a new position on the work piece surface.

The third stage of skidding was stabilized and drills the hole for full diameter. The fourth stage (D) is usually accompanied by drill wandering of a major contributor to the hole's formation and out-of-roundness. Because of the initial skidding and subsequent wandering, both are associated with the drill's initial penetration. It will also lead to the drilled holes with non-circular, non-straight shape and spiral lines (Cheong, 1999). These problems are associated with the drill's initial penetration, particularly due to initial skidding and subsequent wandering of the drill point.

2.4.3 Tool breakage

Another serious problem of mechanical micro-drilling is tool breakage, especially drilling for the deep hole. When the drill size becomes smaller, the relative rigidity of

Literature review

drill decreases, and chip clogging the hole inside seriously (Wiley, 2010). For instance, Tansel I. (1997), if the same material loss (0.00375 in. × 0.005 in.) would eliminate the half of one cutting edge of a micro-tool with 0.015 in. diameter and it would easily double the cutting force on the other edge. The stress on the tiny shaft of the cutting tool will increase in proportion to the force increase.

Also during chip clogging, the cutting force increases continuously as long as the chip stays at the critical point and obstructs the movement of the cutting edge. These factors will lead to the reason of tool breakage.

2.4.4 Size effect of mechanical micro-drilling

For the micro-drilling size effect, Dolinsek (2006) reported: when the uncut chip thickness is on the same order as the material grain size, the work-piece material cannot any more is assumed as homogeneous and isotropic. Furthermore, the tool edge radius influences the cutting mechanism in micro machining significantly with regard to the effective rake angle and the plugging effect. The research of size effect has been studied by Abouridouane (2012). He proposed the related feed force can be increased by decreasing of the drill diameter in the micro range. The related feed force data can be attributed the size effect of the chisel edge length $d_{c,e}$ of the drill diameter.

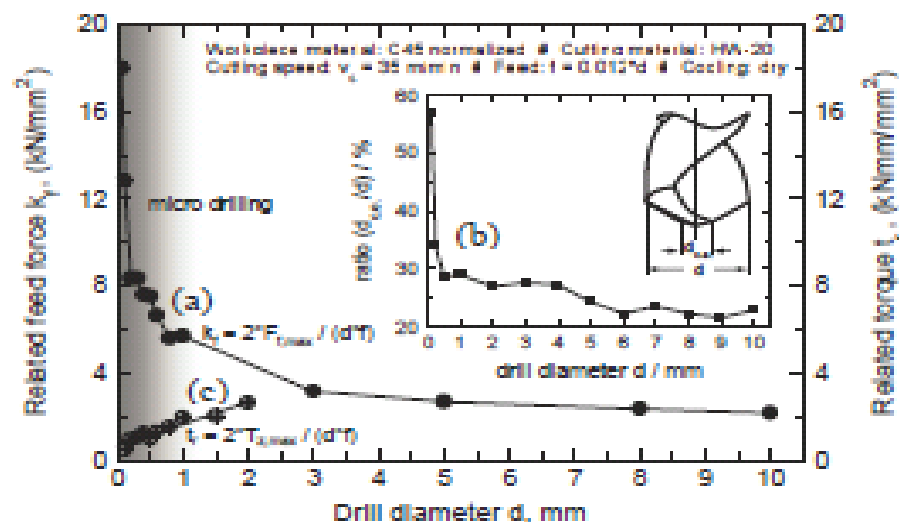


Figure 2-5: Size effect the feed force (Abouridouane, 2012)

2.5 Experimental measurements

2.5.1 Cutting parameters for micro-drilling

The micro-drilling tool geometry undoubtedly affects the whole drilling process, especially at beginning of drilling. They are classified as follows: flat drill, straight-fluted drill and twist drill. Twist drill, as shown in Figure 2-6 and 2-7, both are the most common geometry produced for micro-drilling today. It was to observe the reduction of the maximum thrust force achieved and to quantify the decrease in delaminating around the hole when this alternative drilling strategy is used. The diameters are ranging from 0.15 mm (0.006 in) to 75 mm (3.0 in). (Mikell, 2007)



Figure 2-6: PCB Twist drill

Figure 2-7 is clearly to show the elements of twist drill. It mainly consists of two parts: body and shank. Both are separated by a neck, and two long and diametrically opposite helical grooves called flutes run throughout the length of the drill (Rajput, 2007). Each element will be described in the following (Industrial Press, 1989, Rajput, 2007, Astakhov, 2014):

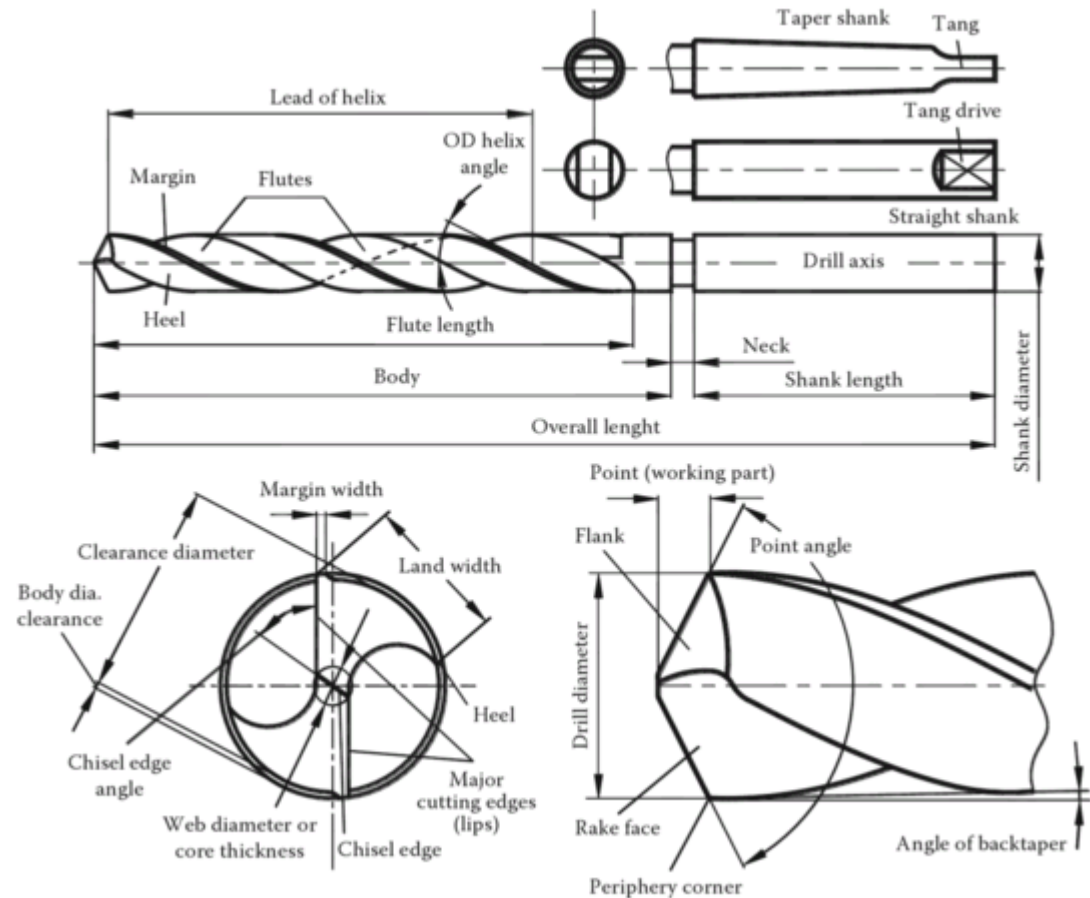


Figure 2-7: Twist drill elements (Astakhov, 2014)

- a. Axis: The drill axis is the centreline of the tool. It goes through the web and is perpendicular to the diameter.
- b. Body: The body of the drill extends from the shank to the point or the neck to the periphery corners of the flutes.
- c. Body Diameter Clearance: The portion of the land that has been cut away to prevent its rubbing against the walls of the hole being drilled.
- d. Chisel Edge: The edge ground on the tool point along the web that connects the major cutting lips.
- e. Chisel Edge Angle: The angle included between the chisel edge and the cutting lip, as viewed from the end of the drill.

Literature review

- f. Clearance: The space provided to eliminate undesirable contact between the drill and the work piece.
- g. Clearance Diameter: The diameter over the cut away portion of the drill lands.
- h. Drill Diameter: The diameter over the margins of the drill measured at the periphery corner.
- i. Flutes: Helical or straight grooves cut or formed in the body of the drill to provide cutting lips, to permit removal of chips, and to allow cutting fluid to reach the cutting lips.
- j. Flute Length: The length from the periphery corners of the cutting lips to the extreme back end of the flutes. It includes the sweep of the tool used to generate the flutes and, therefore, does not indicate the usable length of the flutes.
- k. Helix Angle: The angle made by the leading edge of the land with a plane containing the axis of the drill.
- l. Land: The peripheral portion of the cutting tooth and drill body between adjacent flutes.
- m. Length: Along with its outside diameter, the axial length of a drill is listed when the drill size is given. In addition, shank length, flute length and neck length are often used.
- n. Lips: The cutting edges of a two flute drill extending from the chisel edge to the periphery.
- o. Lip Relief Angle: The axial relief angle at the outer corner of the lip; it is measured by projection into a plane tangent to the periphery corner of the lip. – Obsolete term for the lip clearance angle.
- p. Margin: The cylindrical portion of the land which is not cut away to provide clearance.
- q. Neck: The section of reduced diameter between the body and the shank of a drill.
- r. Overall Length: The length from the extreme end of the shank to the outer corners of the cutting lips; it does not include the conical shank end often used on straight shank drills, nor does it include the conical cutting point used on both straight and taper shank drills.

Literature review

- s. Point: The point is the cutting end of the drill.
- t. Point Angle: The angle included between the cutting lips projected upon a plane parallel to the drill axis and parallel to the two cutting lips.
- u. Relief: The result of the removal of tool material behind or adjacent to the cutting lip and leading edge of the land to provide clearance and prevent interference between the cutting tooth and the bottom of the hole being drilled.
- v. Relative Lip Height: The difference in indicator reading on the cutting lip of the drill; it is measured at a right angle to the cutting lip at a specific distance from the axis of the tool.
- w. Shank: The part of the drill by which it is held and driven.
- x. Straight Flutes: Flutes which form lands lying in an axial plane.
- y. Tang: The flattened end of a taper shank, intended to fit into a driving slot in a socket.
- z. Taper Drill: A drill with part or all of its cutting flute length ground with a specific taper to produce tapered holes; they are used for drilling the original hole or enlarging an existing hole.
- aa. Web: The central portion of the body that joins the lands. The extreme end of the web forms the chisel edge on a two-flute drill.
- bb. Web Thickness: The thickness of the web at the point, unless another specific locations is indicated.

The twist drill is a complex tool that usually has two cutting edges designed to produce identical chips. There are three major actions during the drilling at the point of drill:

1. A small hole is pierced by the rotating web.
2. The chips are formed by rotating cutting edges.
3. A screw conveyor in the form of the helical flutes provides chips convey out of the hole.

Literature review

According to the three above actions, the more important parameter points of drill tool are:

1. Helix angle, δ .
2. Point angle, $2p$.
3. Web thickness, w .
4. Clearance angle, θ .
5. Drill diameter, d .

According to Milton Clayton (1915), the radius (r) of the helix angle can be varied in any particular point on the cutting edge. A helix angle without specification refers to the helix angle at the circumference of the drill. The pitch length of the helix (L) is constant for all points along the cutting edge, and the helix angle at any point may therefore be determined by use of the following equation. The helix angle may be easily determined by rolling a drill across a piece of carbon paper that rests on a sheet of white paper.

$$\delta = \tan^{-1}\left(\frac{2\pi r}{L}\right) \quad (2-13)$$

The feed angle (ϵ) that is generated by any point on the cutting edge at radius r may be obtained from the following expression in terms of the feed per revolution of the drill (f).

$$\epsilon = \tan^{-1}\left(\frac{f}{2\pi r}\right) \quad (2-14)$$

The clearance angle (θ) at any radius must provide this much clearance before there is anything left to take care of elastic recovery. The drill clearance that corresponds to that of a conventional tool is $(\theta - \epsilon)$. The quantity ϵ is seen to increase as the point of the drill is approached.

Literature review

2.5.2 Rotation speed and feed rate

Material	Recommended Speed, V [surface ft/min]
Aluminum and its alloys	250
Bronze (high tensile)	100
Cast Iron (soft)	100
Cast Iron (medium hard)	80
Cast Iron (hard chilled)	20
Hastelloy	20
Inconel	25
Magnesium and its alloys	300
Monel	25
High nickel steel	50
Mild steel (.2-.3 C)	100
Steel (.4-.5 C)	60
Tool steel	40
Forgings	40
Steel alloys (300-400 Brinell)	30
Heat Treated Steels	
35-40 Rockwell C	20
40-45 Rockwell C	20
45-50 Rockwell C	15
50-55 Rockwell C	15
stainless steel free machining	40
stainless work hardened	20
Titanium alloys	20

* Multiply surface speeds in table by 2.5 for carbide cutting tools. *

Figure 2-8: The drilling speed used in different material (Machinery Handbook, 2008)

Most machinery handbooks have tables or lists of spindle speeds and feed rate for different material work piece. Furthermore, the manufacturer would give a similar available table of cutter used.

In the most of machining cases, a cylindrical object such as a drilling cutter or turning work piece in a lathe need to determine the tool speed of object. The drilling speed

Literature review

is usually measured in the terms of rate of the tool outside. This velocity of term is called SFM (surface feet per minute). General SFM is commonly found by resources of Machinery Handbook (2008), as shown in Figure 2-8.

From the drilling modelling above, the peripheral and rotational velocities of the tool are related as shown in the following equation:

$$V = \pi DN \quad (2-15)$$

N is the rotational speed of the drill. Since the peripheral velocity is commonly expressed in units of ft/min, and tool diameter is typically measured in unit of inch. The N in the following manner

$$N(\text{rpm}) = \frac{12 \frac{\text{inch}}{\text{feet}} \times V(\text{SFM}(\frac{\text{feet}}{\text{mins}}))}{\pi \times D(\frac{\text{inch}}{\text{rev}})} \quad (2-16)$$

The handbook of Mikell P. (2007) gives some descriptions about drilling that is specified in mm/rev or in/rev. Most recently, the feeds are recommended roughly proportional to drill diameter. Simply said, larger diameter drill use higher feeds. Usually there are two cutting edges at the drill point. The feed rate equation can be converted by

$$f_r = Nf \quad (2.17)$$

where

f = feed-rate (in/min)

N = spindle speed (rpm)

f_r = feed per revolution (in/rev)

General the recommended average feed rates for various drill diameters as shown as Figure 2-9.

Drill Diameter [in.]	Recommended Feed, f_r [in./rev]
under 1/8"	up to 0.002
1/8" to 1/4"	0.002 to 0.004
1/4" to 1/2"	0.004 to 0.008
1/2" to 1"	0.008 to 0.012
1" and over	0.012 to 0.020

Figure 2-9: Feed rates used in drill diameter (Machinery Handbook, 2008)

2.6 Surface quality in drilling composite

The Surface finishing plays a vital function in many areas like dimensional accuracy. Also in the processing, the accuracy of dimensions greatly affects the performance of the product, especially in high-strength products. In the drilling process industry, the surface quality of FRP (Fibre-reinforced plastic) machining is based on two main aspects; surface topography and machining damage (Ho-Cheng, 1990).

In general, the drilling quality mainly depends on the mechanical properties of the reinforcing fibres. Abrate (1992) reported the surface roughness was mostly influenced by feed rate, depth of tool engagement and work-piece thickness. Also, there is a strong correlation between the surface roughness parameters and surface speed. Therefore, high thrust force, feed rate, rotation speed, depth of tool engagement and work-piece thickness are the major reasons responsible for delamination damage.

2.6.1 Mechanisms of composite delamination

Delamination is a mode of failure for composite materials and steel. The multilayer composite material is formed by many stacking layers material stack from each other. The delamination occurs at both of the entry and the exit points during the drilling process. At the entry point of delamination is called peel up, and the push out happened at the exit point of delamination occurs when the drill bit tries to push through the material. (Astakhov, 2014)

a. Peel-up delamination

Entry peel-up delamination occurs at the entrance side of the hole, as shown in the Figure 2-10; when the cutting edge of the drill abrades the top layer of the laminate, the inner layer will be generated in the circumferential direction of the cutting force.

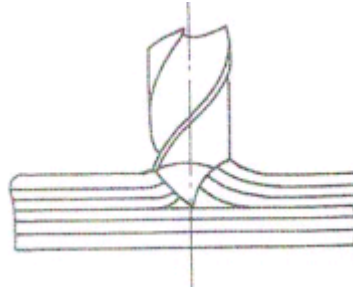


Figure 2-10: Peel up at delamination entry point (Astakhov, 2014)

This circumferential force in the face of the helix angle hole on the tool will produce an axial force component upward, when this component is over between laminates layer bond strength of 90° . It will make the inlet side of the upper substrate material peeling occurs, and forming the entrance defects.

b. Push-out delamination

Exit push out delamination occurs in the drilling tool reaches the exit side of the work-piece as shown in the Figure 2-11. With the downwards of delamination, the thickness of laminate becomes smaller at the exit of uncut material.

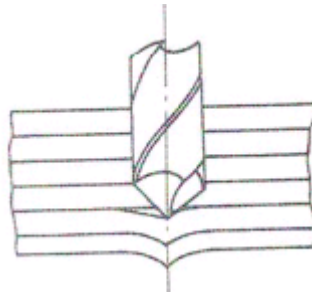


Figure 2-11: Push out at delamination exit point (Astakhov, 2014)

The composite remaining materials layers gradually become less, the composite material resists the axial forces and ability to deform the sheet thickness direction will be getting worse. Push-out occurs upon the reaching 90° inter-layer bond strength of laminates.

Push-out delamination generally occurs before the exit hole is not fully penetrated the work-piece material, push-out layered directly related to the axial force, and surface damage is much more sensitive than peel-up delamination.

2.6.2 Damage criteria on composite delamination

Currently, the most common estimation of delamination damage is to take the measure of maximum diameter of the delamination pattern ratio as the drill hole diameter (Shyha, 2010)& (Durao, 2014), as seen in Figure 2.12.

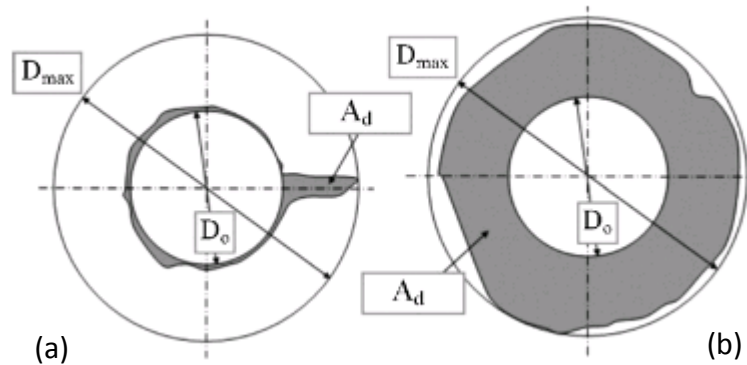


Figure 2-12: Examples of extreme delamination patterns when drilling FRP laminates (a) fine cracks and (b) uniform damage area (Shyha, 2010 and Durao, 2014)

F_d is used to characterize delamination, it is represented as follows

$$F_d = \frac{D_{max}}{D_0} \quad (2-18)$$

Where: D_{max} is the maximum diameter of delamination damage; D_0 is the diameter of the hole.

Damage delamination pattern F_d is a relatively straightforward one-dimensional evaluation index. Sometimes this calculating way will get problem. For example, in some damage delamination, it only occurs one long length bundle of FRP fibre but there is not a significant damage in other regions of the entire space, as shown in Figure 2-12 (a).

In such case, F_d evaluation is not appropriate for delamination damage estimation. When F_d was used to damage delamination pattern to evaluate in Figure 2-12 (b), the D_{max} is the same diameter of Figure 2-12 (a), but the difference in damage

Literature review

delamination pattern (a) and (b) is significant.

Area Damage delamination pattern F_a , also called the two-dimensional damage delamination evaluation index. F_a considers a very uneven layer around the holes and takes the actual area of damage substituted into the evaluation of delamination pattern. Through the ratio of the actual area of damage and the hole area to evaluate the degree of damage delamination evaluation index. It is represented as:

$$F_a = \frac{A_d}{A_0} \quad (2-19)$$

Where: A_d is the actual area of delamination damage; A_0 is the area of the hole.

Therefore, Davim (2003) presented a new damage delamination evaluation index, F_{da} . It does not only include the one-dimensional evaluation index of Damage delamination pattern, F_d , but also the total damaged area F_a . It is represented as:

$$F_d = F_d + \left(\frac{A_d}{A_{max} - A_0} \right) (F_d^2 - F_d) \quad (2-20)$$

Where, A_d is the damaged area, A_{max} is the area corresponding to D_{max} , and A_0 is the nominal area.

2.7 Modelling and simulation

Modelling of simulation shows how the models operating situation evolve over time in a particular environment. Simulation is a simple form of design analysis. The target is more readily analysed piece to understand deeper into the design properties and to enable a system through dissection, even partitioning into smaller tool. This analysis specifies why or what a system does or fails, and show a model what it would be in the real.

Modelling simulation has a central role in modern design process. To be effective of the design, the models must follow physical principles and laws. If the model

Literature review

simulation would be understandable and analysable, it needs to have a clear meaning of semantics.

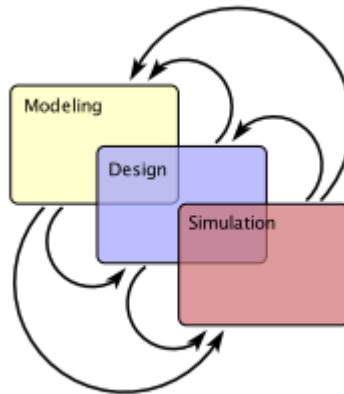


Figure 2-13: Simulation analysis process

Most models of computation have a notion of time. Specifically this means that communication between actors and computation performed by actors occurs on a logical time line. More specifically, this means that there is a notion of two actions, communication or computation, being either ordered in time, one occurs before the other, or being simultaneous. A notion of time may also have a metric meaning loosely that the time gap between two actions may be measured.

In today's industrial development, computer simulation software includes simulation of finite element software more than 50 kinds. For example: ANSYS, COMSEL Multiphysics, HyperSizer, Quickfield etc.

2.7.1 Cero parametric 2.0

In industry terms, Cero Parametric 2.0 is highly respected graphics software. In addition to the powerful graphics capabilities of Cero Parametric itself, the export file has quite extensive compatibility in other simulation software. In this research, all the structures use to be a geometry creation model in simulation analysis or to be a sketch drawing in manufacturing.

2.7.2 FEA simulation in ANSYS

ANSYS Mechanical is a finite element analysis tool for structural analysis, including linear, nonlinear and dynamic studies. This simulation product provides finite elements to model behaviour, and supports material models and equation solvers for a wide range of mechanical design problems. The advantage of ANSYS is not only they are often used in academic and industry, but also the user interface is clean, clear setting steps and rich built-in databases. Therefore, this thesis uses the finite element software ANSYS. According to the ANSYS Workbench User's Guide (2009), there are three stages of cells available in ANSYS Workbench:

- a. Pre-processing: defining the problem
 - Define dimensions
 - Define element type and material properties
 - Define mesh
- b. Solutions: assigning loads, constraints and solving
- c. Post-processing: viewing and results

ANSYS is used for finite element analysis of model structure to simulate the structure operating status. In this research ANSYS will help to solve the problem of modal analysis, and static analysis micro-drilling process.

2.7.3 LabVIEW 2014

LabVIEW is short for 'laboratory virtual instrument engineering workbench'. It supports a development environment based on the graphical programming language G-code. The LabVIEW software is not only provide for acquiring, analysis and presenting data but also available for measurement and automation applications. (Bishop, 2006 and Bitter, 2006)

In the LabVIEW programming, the graphical interface provides a series of virtual measurement program to define and control the data acquisition. The operating set of the various sampling rates and recording durations, as shown in Figure 2-14.

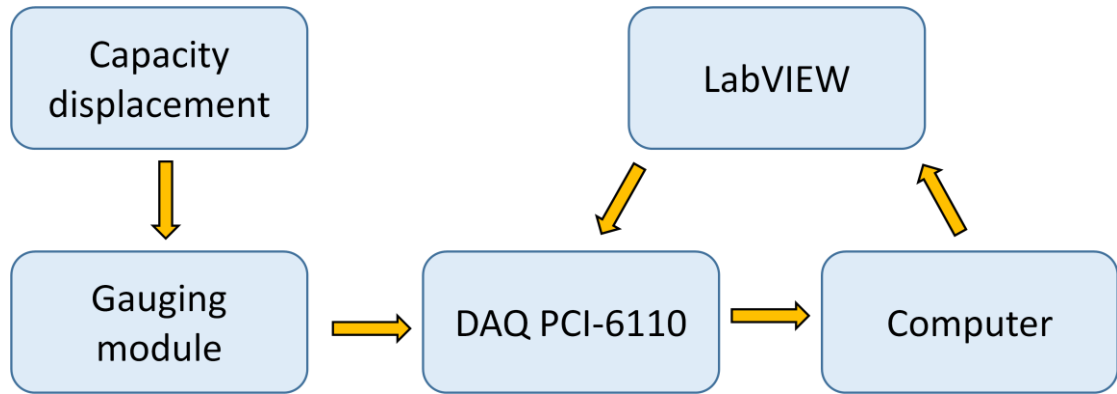


Figure 2-14: Details of connection for transferring signal to user interface

2.7.4 MATLAB R2014a

MATLAB (Matrix Laboratory) is a numerical computing environment and fourth generation programming language. Developed by Math Works, it allows matrix manipulation, plotting functions and data, implementation of algorithms, creation of user interfaces and interfacing with programs written in other languages (Math Works, 2015).

Image Processing Toolbox, it is one of many MATLAB Toolbox programming. It provides a comprehensive set of reference-standard algorithms, functions, and apps for image processing, analysis, visualization and algorithm development. It can perform image analysis, image segmentation, image enhancement, noise reduction, geometric transformations, and image registration (Math Works, 2015).

The MATLAB Toolbox programming supports a wide range of image processing operations, including:

- Geometric operations
- Linear filtering and filter design
- Image analysis and enhancement
- Binary image operations
- Region of interest operations
- Fourier Transforms

2.8 Summary

This chapter presents a number of relevant background knowledge in the regard of micro-drilling. While less information and established research were found in terms of mathematical drilling model, processing machine, tool configuration and parameter-induced influences, the importance of these aspects are clearly demonstrated. Although drilling in general is a well established industry practice, most of the research and technical description were done based on specific operation in reality and physical, post operation measurements. Although they provide valuable details and insights toward the drilling processes, it lacks the capability in predicting and modelling the drilling process, which is a key aspect FEA can significantly enhance.

The need for combining experiences gained through conventional drilling process and mathematical modelling becomes even more significant when the advancement of manufacturing is considered, especially in terms of size scale, level of accuracy and precision requirements. As drilling process shifts from traditional scales to millimetre and micrometre, an accurate but flexible mathematical model that can describe drilling process at such scale has now become necessary.

Therefore, in the subsequent chapters, this research will focus on the validation of drilling force data to express the stages of micro-drilling through FEA simulation, mathematical modelling and experimental measurement. Various operation conditions and parameters such as drill tool size, diameter, tool angle, coolant application, spot drill, rotation speed and feed rate will be investigated. Findings above will also be cross-examined with different work piece materials ranging from metal to polymer based composites in order to extend model feasibility. Interactions and correlations between all parameters will also be analysed so the extent of influence of individual factors can be further established.

Chapter 3: Modelling and simulation of micro-drilling

3.1 Introduction

Mechanical engineers routinely use the Finite Element Analysis (FEA) to solve the physical structure problems of stress, deformation, heat transfer, fluid flow and electromagnetic, etc. This research used ANSYS Mechanical APDL, one of the most versatile and widely used of commercial finite element programs to simulate the micro-drilling process. To match the realistic situation, this research used Explicit Dynamics module, one of the module functions in the ANSYS workbench version 16.2 to present the simulation result, as Figure 3-1 shown. Also, each parameter setting at the Explicit Dynamics module was strongly dependent on the experimental settings.

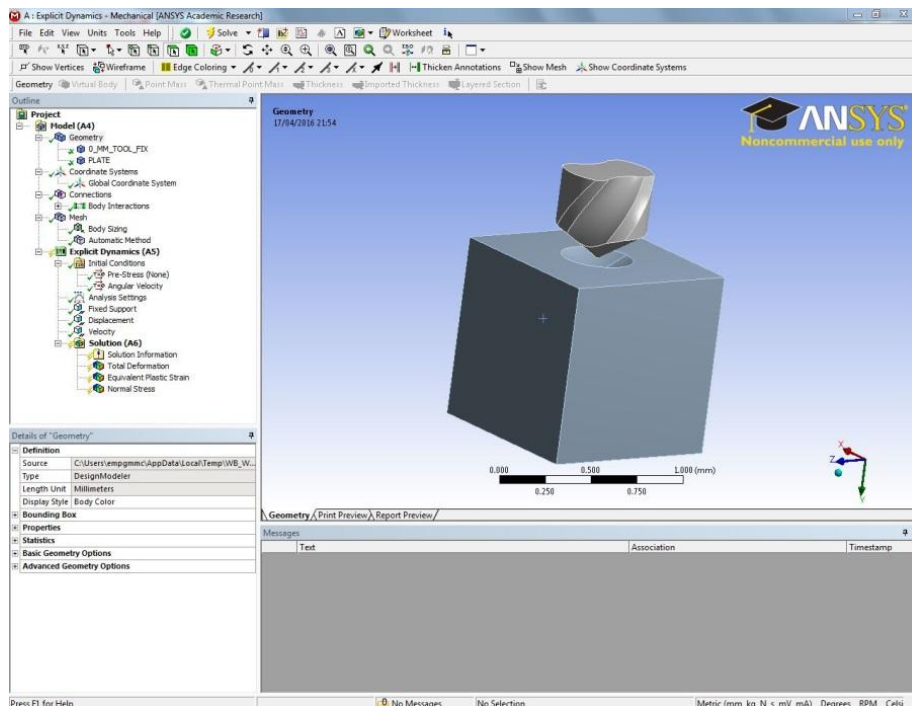


Figure 3-1: ANSYS workbench explicit dynamics simulation

Experimental methods

Explicit Dynamics analysis system is one operational Module of ANSYS Mechanical APDL workbench 16.2. The Explicit Dynamics also deals with transient structure dynamics; however, it uses an explicit integration method for calculation in ANSYS workbench. The explicit method is very efficient for each time step. It allows a large number of time steps to be calculated within an acceptable time. Each integration time steps must be very small (about $2E^{-10}$) in order to achieve stable solution. Finally, millions of time steps are required to complete the dynamic simulation.

This chapter will present respectively the setting steps of the Explicit Dynamics module for three major parts: geometry creation, mesh generation and boundary conditions. These three parts will have more detailed description in the next sections. Figure 3-2 is the simulation flow diagram of this research.

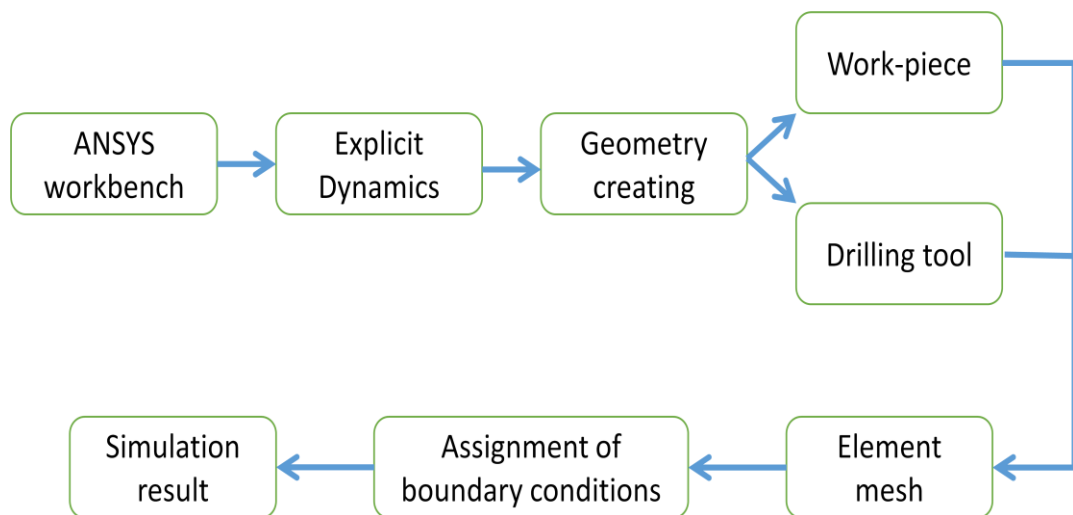


Figure 3-2: Process steps for FEA analysis on micro-drilling

3.2 Geometry creation

During the dynamic simulation of micro-drilling process, the geometry model creation is the first step of the simulation. In the process of geometry creation, in order to make the desired simulation results closer to the real situation, all geometry solids are designed in reference to the size of experimental used in the research. All geometry solid was firstly created by the software of Cero Parametric 2.0, and then imported for Dynamics simulation by ANSYS Mechanical APDL workbench 14.0. The

Experimental methods

solid creation was divided into two parts: Geometry solid of tool and Geometry solid of work-piece.

3.2.1 Drill tool geometry

The drill diameter was set at 0.5mm and body length at 10mm, as Figure 3-3 and 3-4 shown.

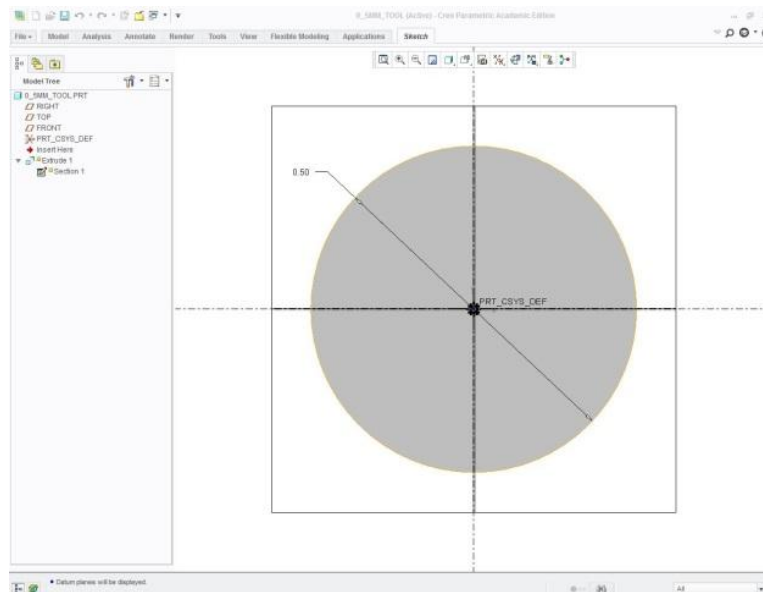


Figure 3-3: Drill diameter: 0.5mm

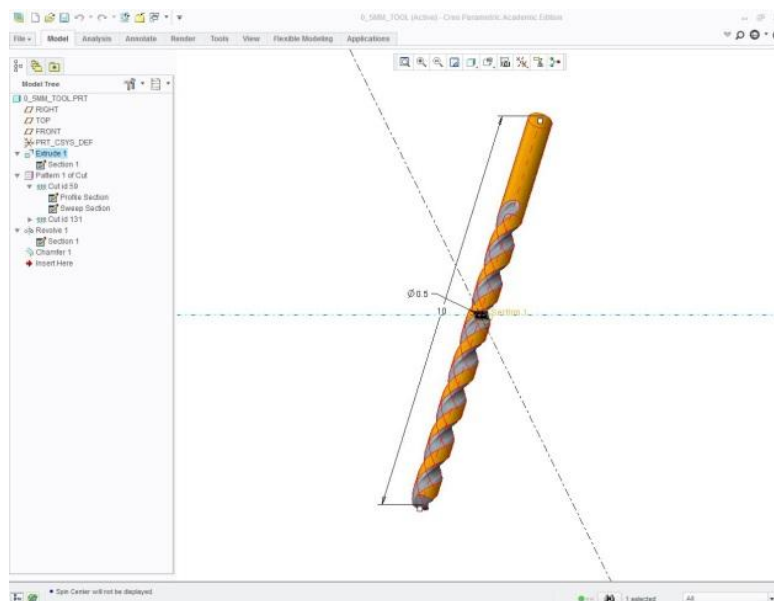


Figure 3-4: Body length: 10mm

Experimental methods

The flute diameter was set at 0.25mm and flute length at 7.5mm, as shown in Figures 3-5 and 3-6.

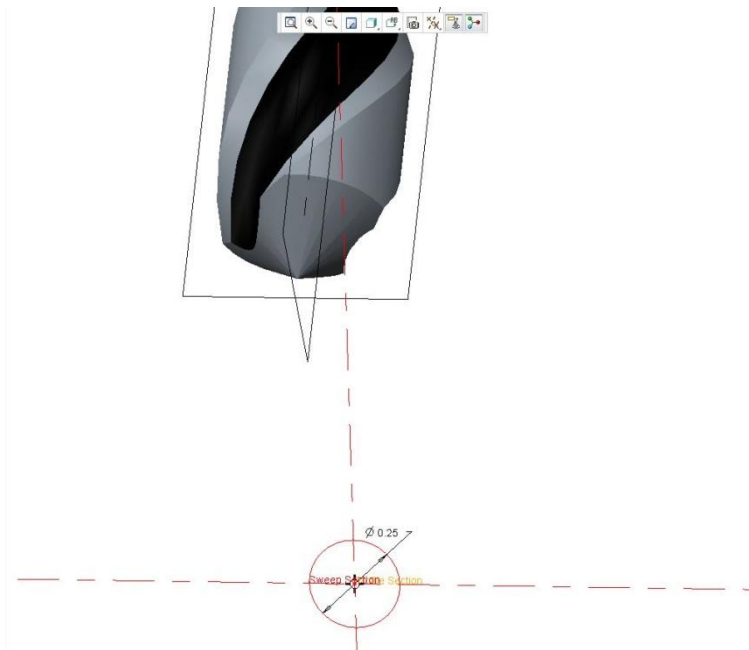


Figure 3-5: Flute: Φ 0.25mm setting

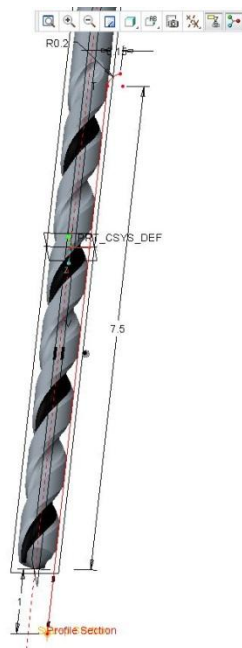


Figure 3-6: Flute length: 7.5mm

The degree setting of point angle will affect the result of micro-drilling simulation. Although point angle varies with different tool sizes, for this research the value was

Experimental methods

set at 110 degrees for a 0.5mm diameter tool as shown in Figure 3-7.

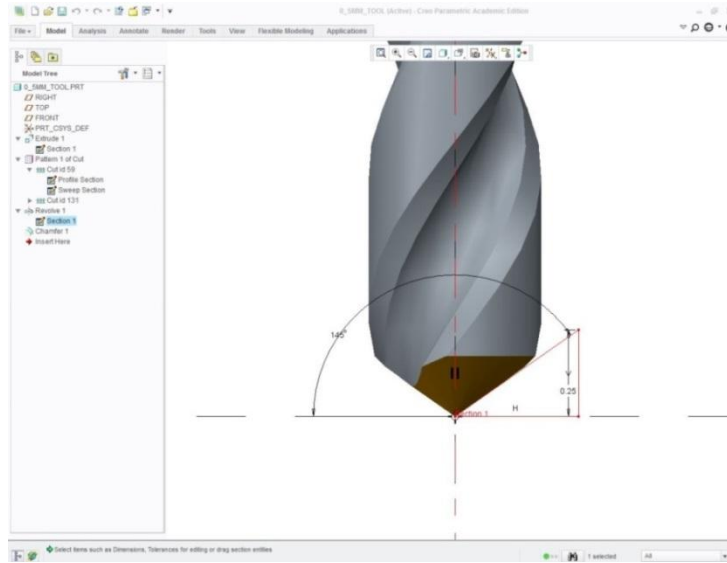


Figure 3-7: Tool point angle drawing

The simulation process focuses on the tip portion of tool since only the tip portion comes into contact with the work-piece. The geometry length was set at 1mm since through preliminary experiments 1mm was found to be sufficient for drilling process description. This mainly due to the small size of drill tools and drill length more than 1mm only adds more information of the shaft friction instead of the actual drill tip, at the price of much longer simulation time. It is therefore all subsequent simulations are carried out at 1mm length, as Figure 3-8 shows, in order to maintain best balance between data accuracy and cost of time.

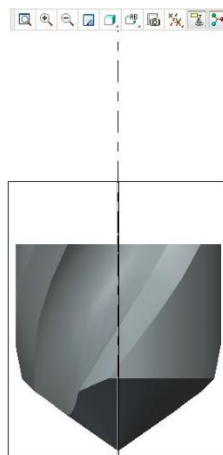


Figure 3-8: Φ 0.5 mm tool solid

Experimental methods

3.2.2 Geometry of the work-piece

Although a 100mm diameter aluminium plate was used as the work-piece, considering the tool diameter is only 0.5mm the simulation focuses on the changes around the drilling hole instead of the entire plated.

To reduce the time of the simulation, the solid geometry of work-piece was represented by a 1mm cube, with a conical recess on the top of solid work-piece to represent the pre-drilled hole. The depth and diameter of recess was set at 0.1mm and 0.4mm, as Figure 3-9 shows.

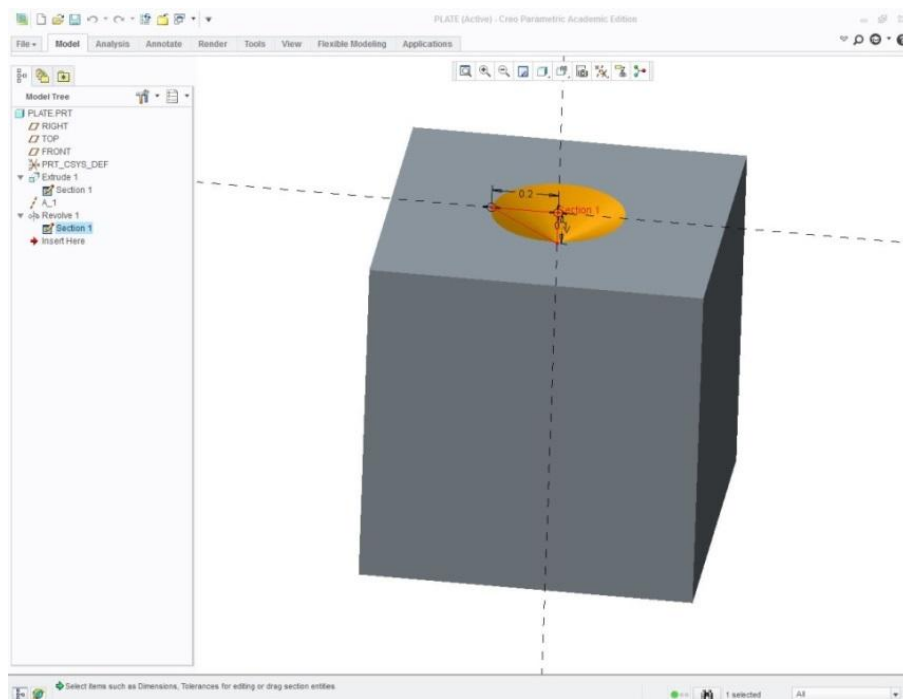


Figure 3-9: Geometry solid of work-piece

Finally, the function of Assemble can combine the geometry of tool and solid of work-piece together, and then export the geometry files in ANSYS format to complete geometry creation. It is noteworthy that, in the assemble process, the central axis of tool should be aligned to the central axis of the pre-drilled hole, as Figure 3-10 shows.

Experimental methods

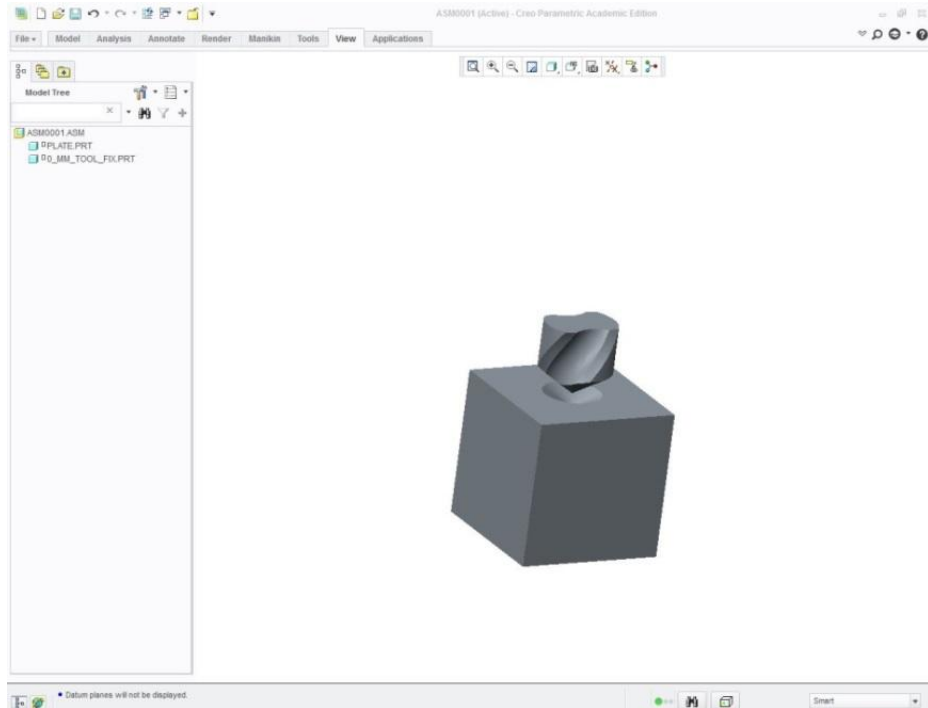


Figure 3-10: Assemble of geometry of tool and solid of work-piece

3.3 Mesh generation

Mesh generation is an integral part process in ANSYS, as Figure 3-11 shows. The target of meshing is to provide the computational elements for physical simulation such as finite elemental analysis. In general, mesh generation in ANSYS provides a pure hex mesh for subsequent highly detailed hybrid meshes.

In short, adequate setting for mesh generation would result in better representation of physical model, as well as improving the accuracy of the simulation results. On the other hands, the smaller element size leads to greater number of mesh elements and increase the time of simulation.

Therefore, the mesh boundary setting is not only affecting the simulation speed but also influences the accuracy of simulation result, convergence and solution speed.

Experimental methods

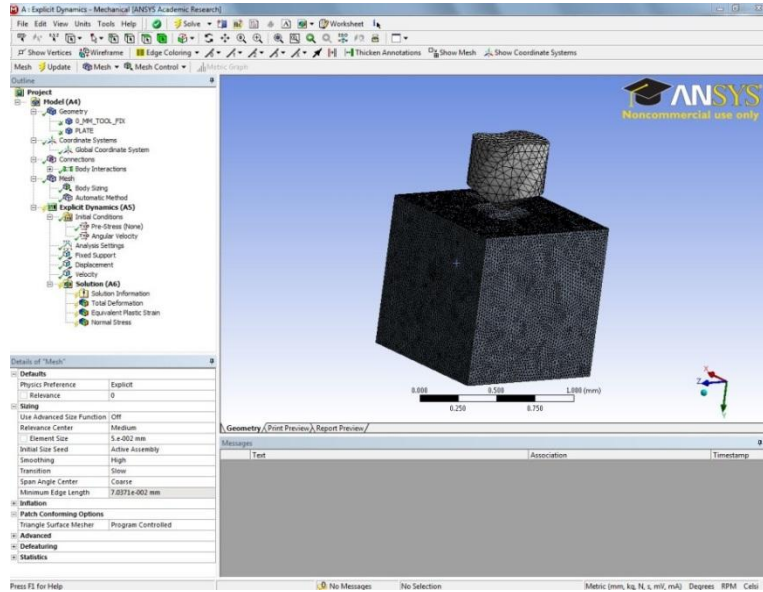
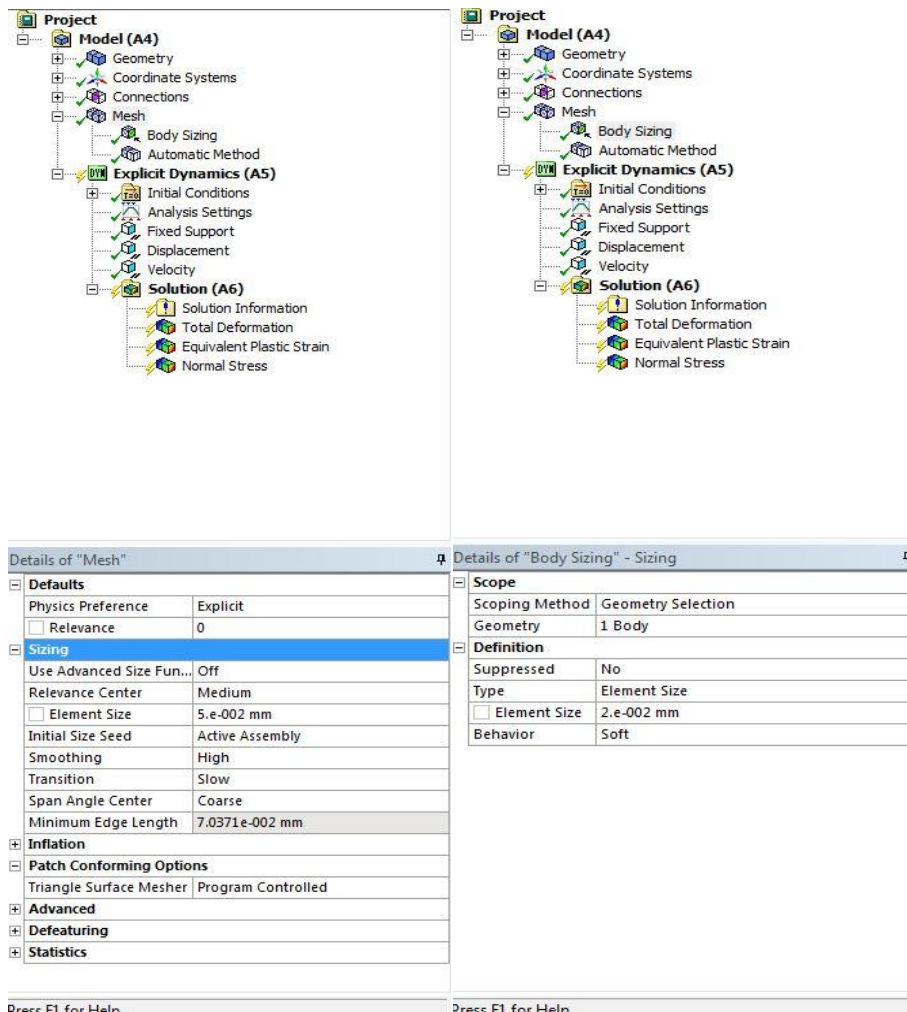


Figure 3-11: Mesh generation



(a)

(b)

Figure 3-12: Element size

Experimental methods

In this simulation, due to the small size of solid geometry, the mesh elements size was set at 0.005 mm, as Figure 3-12(a) shows. Also, the simulation result of this study focuses on the work-piece. Additional increase in body sizing function of the work-piece was carried out in order to improve accuracy, especially for a highly detail mesh generation. Therefore the element size of mesh generation was set at 0.002mm for the work-piece, as Figure 3-12 (b) shows.

3.4 Boundary conditions

After geometry creation and mesh generation, the boundary conditions have to be decided for subsequent simulation. Boundary conditions define a specific problem that allows respective solutions to be found. It must have specific information on the dependent variables at the domain boundaries. This can be easily achieved by accessing the user interface of ANSYS workbench. The user can freely define the conditions on the point, edge, face or the entire solid model. The following are the descriptions for each boundary conditions used in this simulation.

3.4.1 Engineering data

ANSYS provides a practical computational approach that enables physical simulation for each mesh element. Computational physics is the study and implementation of numerical analysis to solve problems in physics for which a quantitative theory already exists. As different materials have different physical properties, different dynamic simulation settings can be selected via the drop list of “engineering data”, as Figure 3-13 shows.

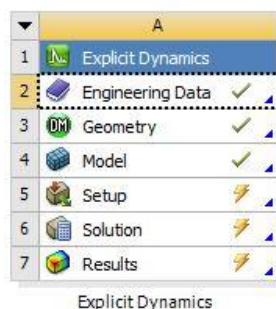


Figure 3-13: Function of engineering Data

Experimental methods

In order to carry out direct comparison between experimental data and simulation, Aluminium 6061T was chosen as the work-piece material for dynamic simulation. Tables 3-1 and 3-2 show the material properties of the work-piece and drilling tool.

Aluminium 6061T	
Density	2703kg/m ³
Initial Yield Stress	2.9e ⁸ Pa
Maximum Yield Stress	6.8 e ⁸ Pa
Shear Modules	2.76 e ¹⁰ Pa

Table 3-1: Material property of aluminium 6061T for the work-piece

Structure Steel	
Density	7850kg/m ³
Young's Modules	2e ¹¹ Pa
Poisson's Ratio	0.3
Tensile Yield Stress	2.5e ⁸ Pa
Compressive Yield Strength	2.5e ⁸ Pa
Ultimate Tensile Strength	4.6 e ⁸ Pa

Table 3-2: Material property of structure steel for the drilling tool

In order to perform FEA simulation of drilling process, an accurate and reliable flow stress model is highly necessary to represent work material constitutive behaviour under large deformation due to cutting conditions. In this simulation Johnson-Cook constitutive material model (1983) and related damage model is used for Aluminium 6061-T6. The flow stress is calculated according to equation as:

$$\sigma = [A + B(\varepsilon)^n] \left[1 + C \ln \left(\frac{\dot{\varepsilon}}{\dot{\varepsilon}_0} \right) \right] \left[1 - \left(\frac{T - T_{room}}{T_{melt} - T_{room}} \right)^m \right]$$

$$\bar{\varepsilon}_D^{pl} = \left[d_1 + d_{2exp} \left(d_3 \frac{p}{q} \right) \right] \left[1 + d_4 \ln \left(\frac{\bar{\varepsilon}^{pl}}{\dot{\varepsilon}_0} \right) \right] \left(1 + d_s \frac{T - T_{room}}{T_{melt} - T_{room}} \right) \quad (3-1)$$

Experimental methods

3.4.2 Fixed support

In order to secure relative work-piece position for simulation, the “Fixed support” function was selected as one of the boundary conditions. It prevents one or more flat or curved faces from moving or deforming. Here the “Fixed support” was selected for all four sides of the work-piece but not the upper and lower surfaces since they are in direct contact with the drill bit during the simulation, as Figure 3-14 shows.

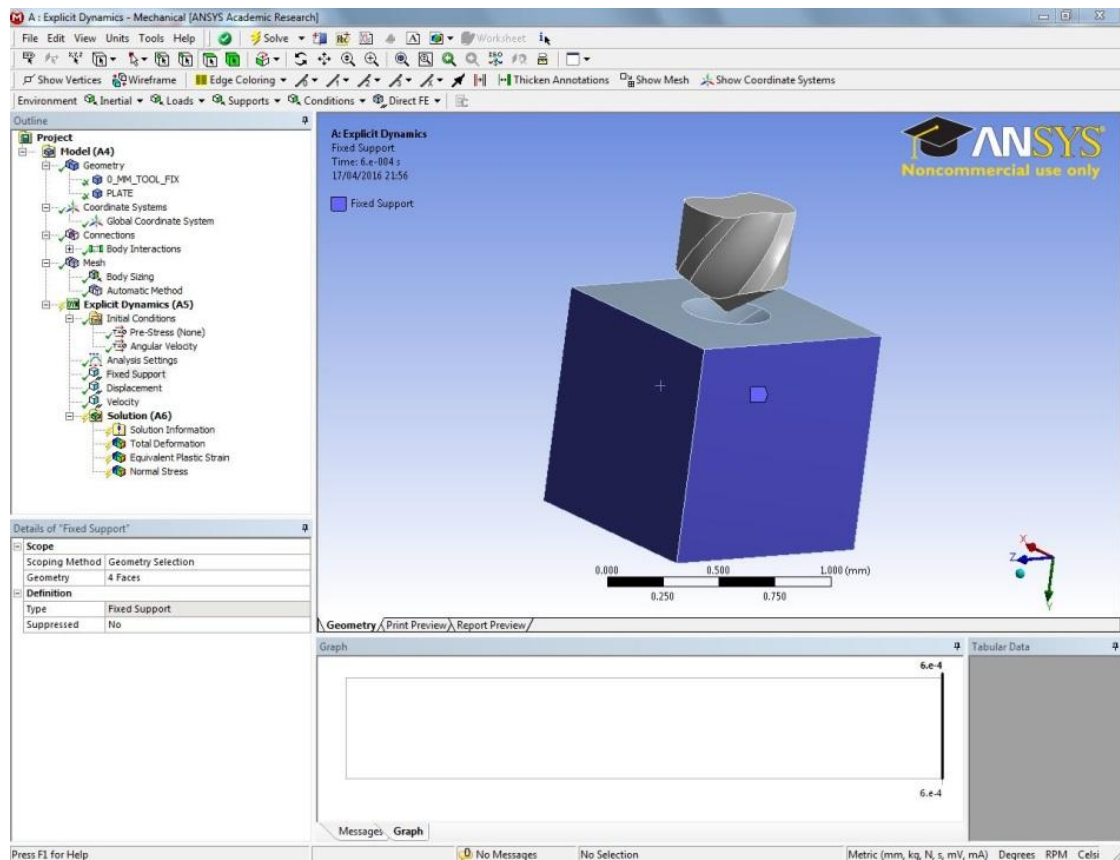


Figure 3-14: Fixed support

In this simulation the sides of work piece is defined by the boundary condition of fixed support. This not only provide clear definition of the geometry of work piece but also helps to avoid possible interference caused by the movement of work piece and spindle. A further benefit of such setup is to achieve good representation of how the work piece is secured in actual operation.

Experimental methods

3.4.3 Displacement support

In the setting of boundary condition, displacement support and fixed support (section 3.4.2) belong to a complementary relationship. In the case of fix support it does not allow movement regardless the change of external force, displacement and geometry variation.

A displacement support is applied at the geometry level and requires that one or more flat or curved faces or edges or one or more vertices to displace relative to their original location by one or more components of a displacement vector in the world coordinate system. The space beneath the drill spot and work piece is empty so the stress variation on both tool and work piece can be observed without obstruction.

The simulation of displacement support was selected for the bottom surface of the work-piece, where X and Z-axis are not movable and Y-axis is free to move, as Figure 3-15 show. This setup also helps to express the stress variation of drill tip when it moves along Y axis, which is the drilling process from the initial contact the exit of work piece.

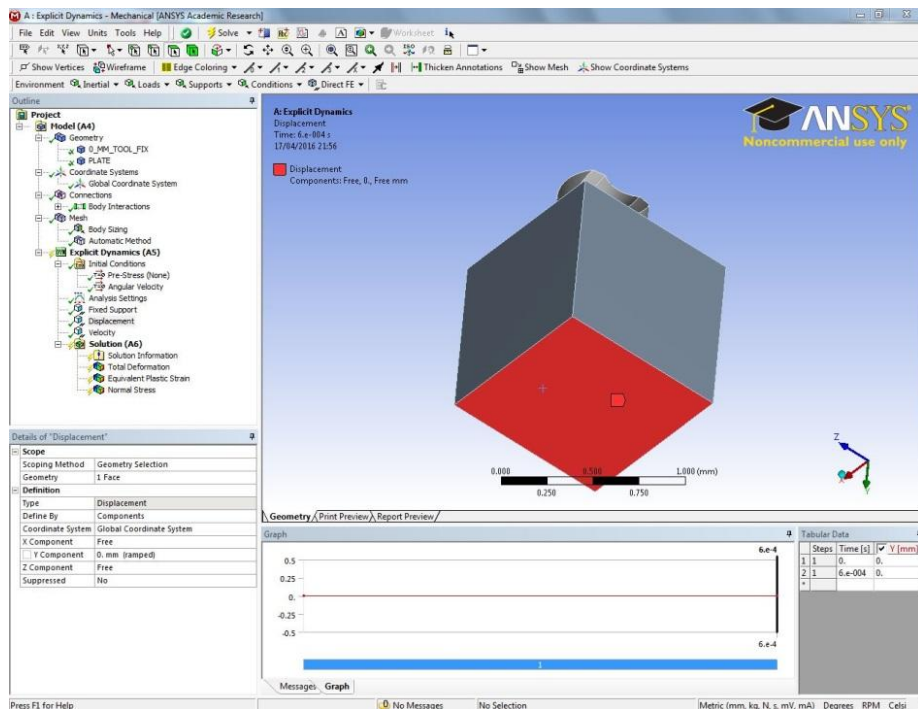


Figure 3-15: Displacement support

Experimental methods

3.4.4 Velocity

The function “Velocity” is to apply a velocity to faces, edges, vertices, or bodies considered as one of boundary conditions in FEA simulation. In this research “Velocity” was defined as the movement of the entire drill bit, and can be separated into two parts: rotation and moving with the vector.

In the setting process of rotation part, the first stage is to select and define the whole solid tool as the rotation geometry. Then to define the direction of rotation and enter 60,000rpm as the rotation speed, as Figure 3-16 show.

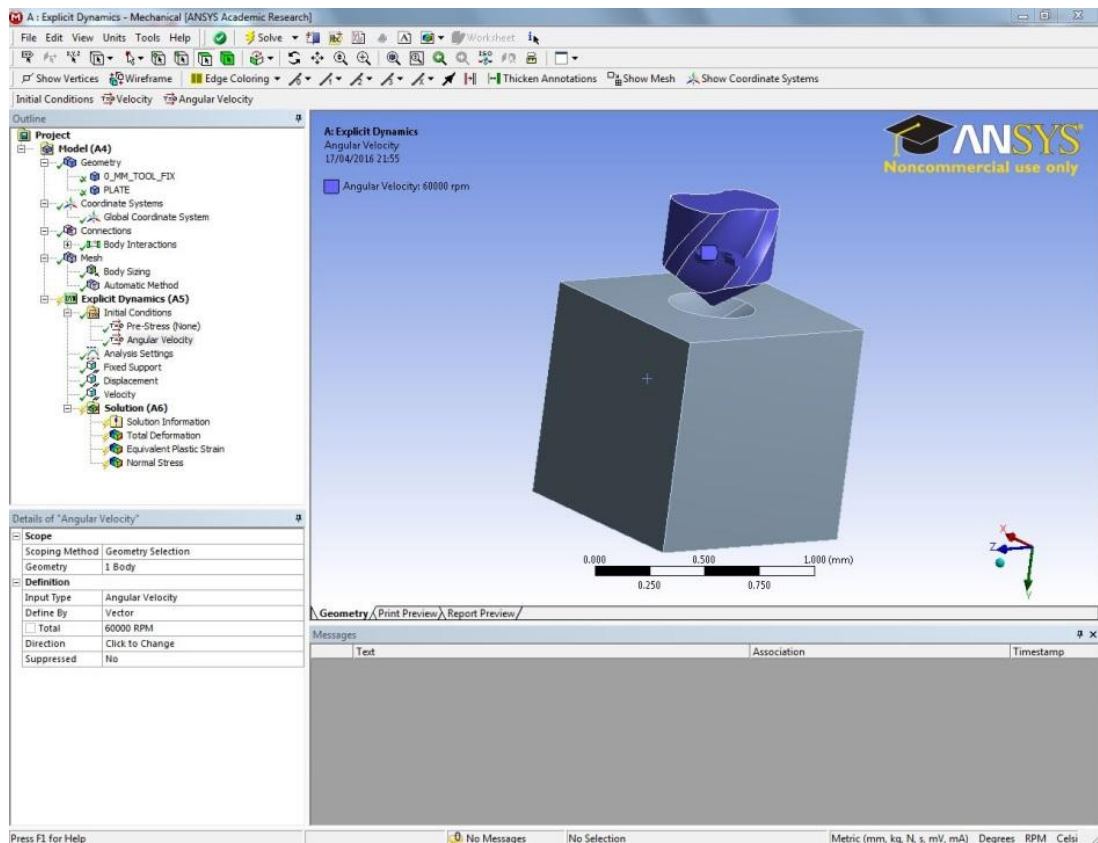


Figure 3-16: Tool rotational speed setting

In the velocity function, the setting stages are similar as rotation setting. The whole solid tool was selected and defined the moving geometry and second stage was defined the moving direction and speed. Here the velocity was set at 2400mm/min along the Y-axis, as shown in Figure 3-17.

Experimental methods

Here, the rotation speed and feed rate were change to 60000rpm and 2400 mm/min. The main reason is the Dynamic simulation of the ANSYS software which calculating cycle time is very small. If the study uses the feed rate of 12 mm/min feed rate for distance 1.5 mm, the time will be taken 7.5 seconds to finish the process. But total time of 7.5 seconds is over the calculation cycling of 10 million.

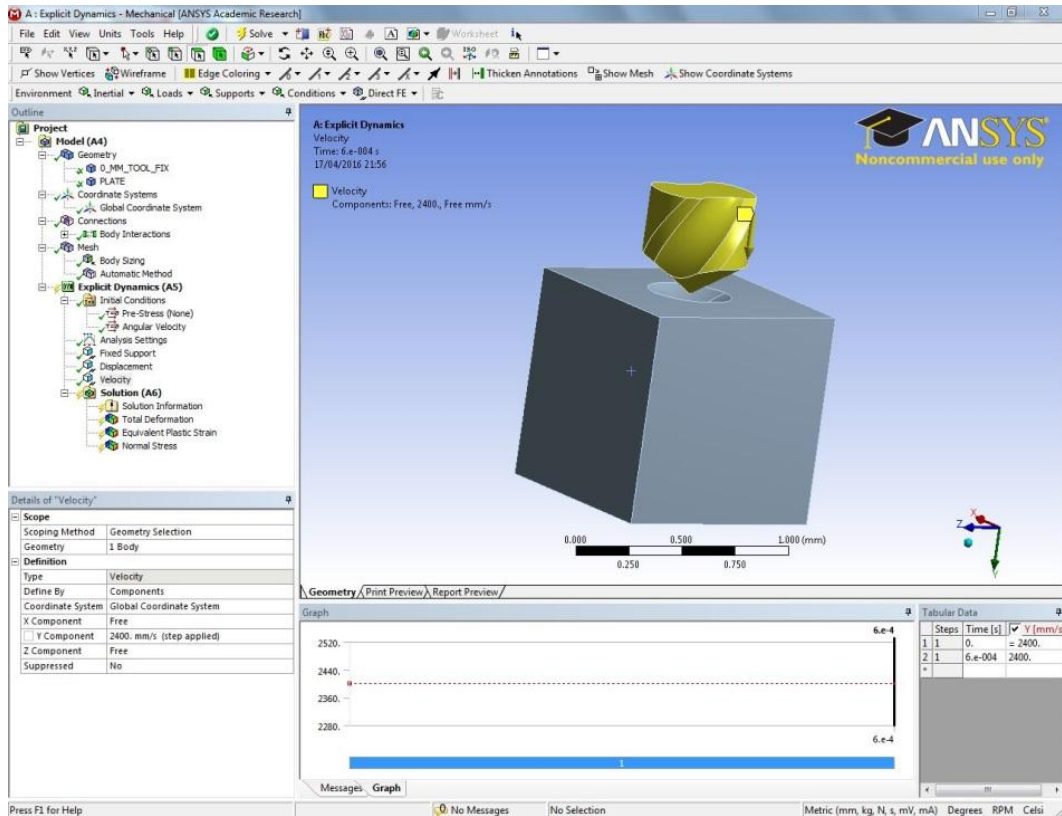


Figure 3-17: Tool velocity setting

3.4.5 End time

The End time is determined by calculating the speed and moving distance. In this simulation, the velocity of solid tool was 2400 mm/min and the thickness of solid work-piece was 1mm. But the total moving distance of the tool must be coupled with the gap of work-piece and tool. So the total moving distance is about 1.5 mm. After calculation, the drill tool would take 0.0006 second to drill through the Aluminium work-piece.

Experimental methods

To ensure the drilling tool can completely drill through the Aluminium work-piece the End time is set to be 0.0006 second, as Figure 3-18 shows.

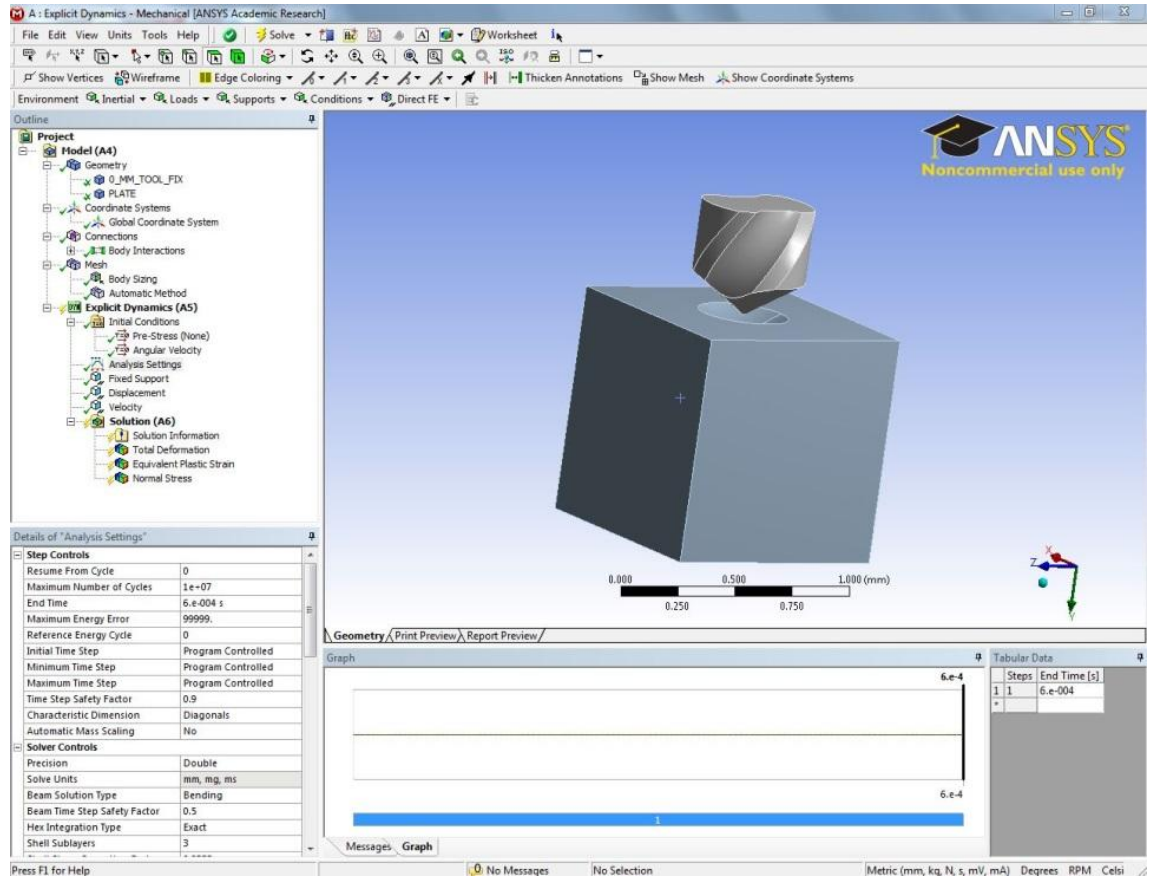


Figure 3-18: Action end time

3.5 Results and discussion

Figure 3-19 shows the entire drilling process from the drill tool starting the position of 100um above the work-piece to the final position of 0.5mm depth into the work-piece. Figure 3-19(a) shows the beginning point of drill tool still above the work-piece, and drill tool continued to move in the direction to the work-piece. After about 6×10^{-4} second, drill tool just touches the top surface of work-piece as shown in Figure 3-19(b). Figure 3-19 (c) and (d) show that the drill tool is continuously keep drilling process into the work-piece, and the position of drill tool was located in the different depth of work-piece at the corresponding times.

Experimental methods

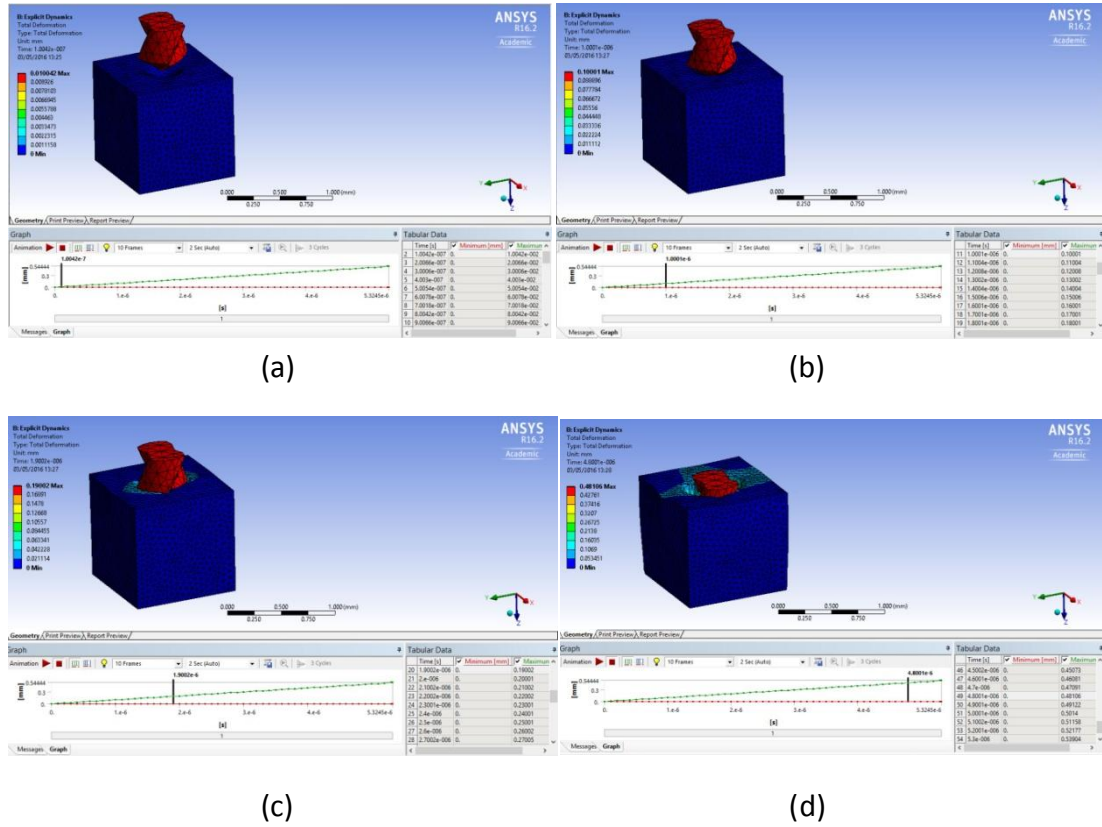


Figure 3-19: Drilling action with time

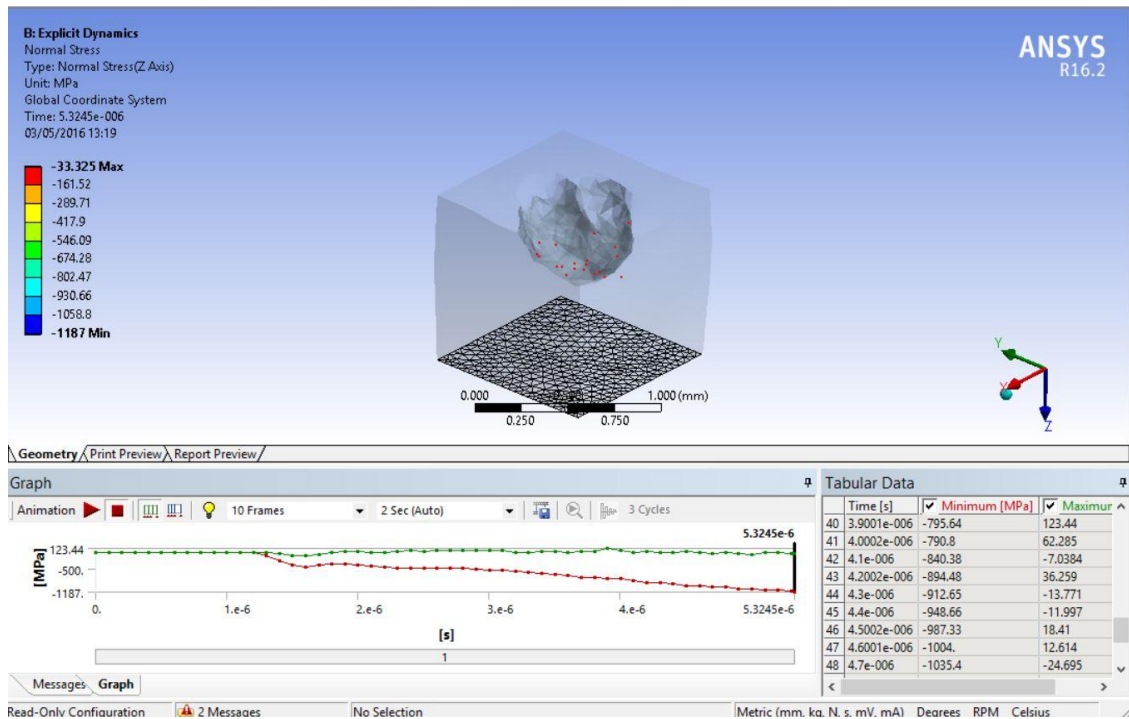


Figure 3-20: The deformation of the Al work-piece during drilling process

Experimental methods

Figure 3-20 shows the deformation of the aluminium work-piece during the drilling process. Figure 3-20 is hidden the part of the drilling tool, it can more clearly observe the drilling situation in the work-piece.

After drilling process, the middle of work-piece has an obvious signs of drilling, there are some of the angular portion of the drilling because of the size value of mesh is not enough.

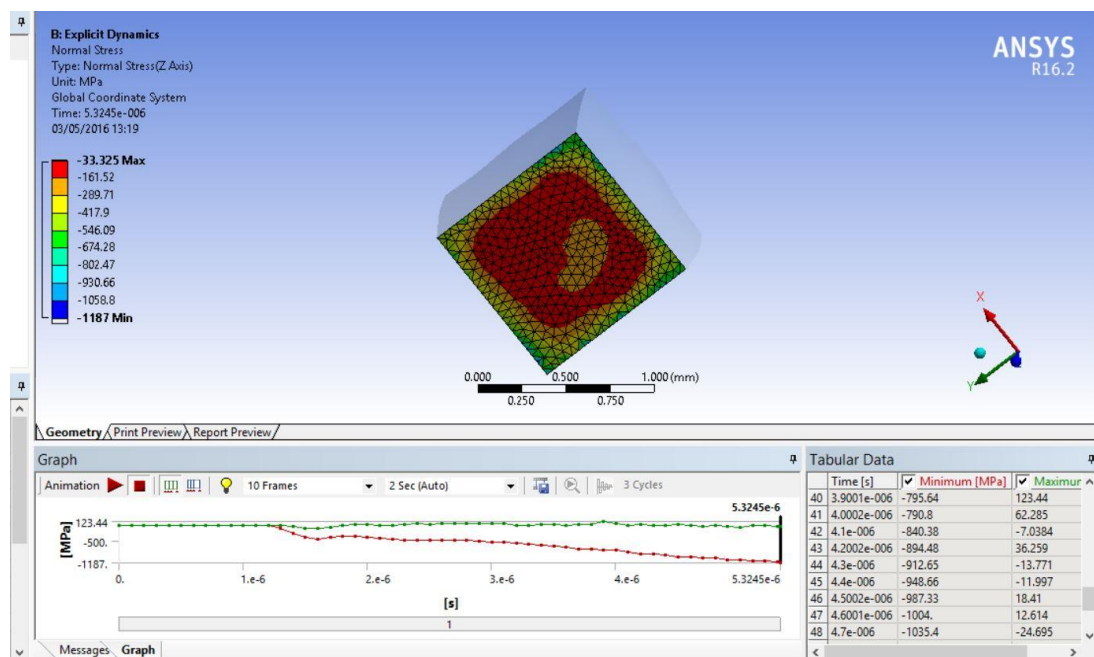


Figure 3-21: The normal stress of the bottom surface of the Al work-piece during drilling process

Figure 3-21 shows the normal stress of the bottom surface of the Al work-piece during drilling process. Figure 3.21 can clearly see the maximum normal stress will keep increasing to 1187 Mpa into 0.0006 second in the drilling process.

Here the drilling tool dimension is 0.5 mm; therefore the thrust force can get 931.8 N. In this simulation model, the value of the feed rate is 200 x corrections in order to obtain the experimental value. In this case, if the result of simulation is calculated in terms of equal proportions, the force can get 4.67 N in the feed rate of 12 mm/min.

Experimental methods

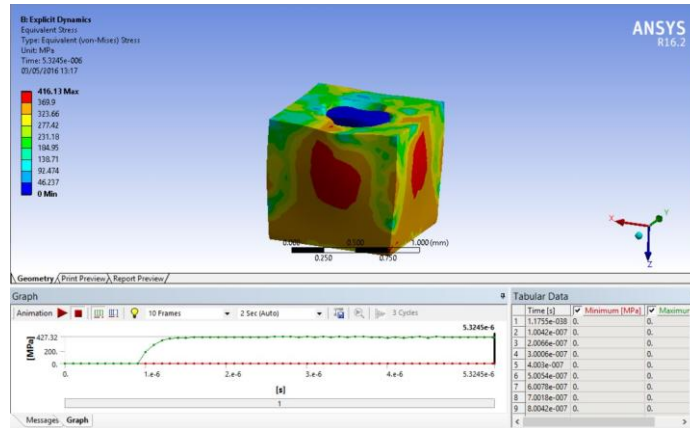


Figure 3-22: Von-Mises stress of the work-piece during drilling process

Figure 3-22 shows the stress level during the drilling process. The drilling tool fully drills into the Al work-piece and the maximum Von-Mises stress of 416 MPa is induced as shown in Figure 3-22. The result chart at the bottom indicates the stress induced at different drilling positions. The initial stress of the work-piece is to be 0 MPa when the drilling tool is not yet touching to the top surface the work-piece, and then the stress increases when the chisel edge of the drilling tool is pushing down and eventually the stress reaches to its maximum level when cutting into the work-piece.

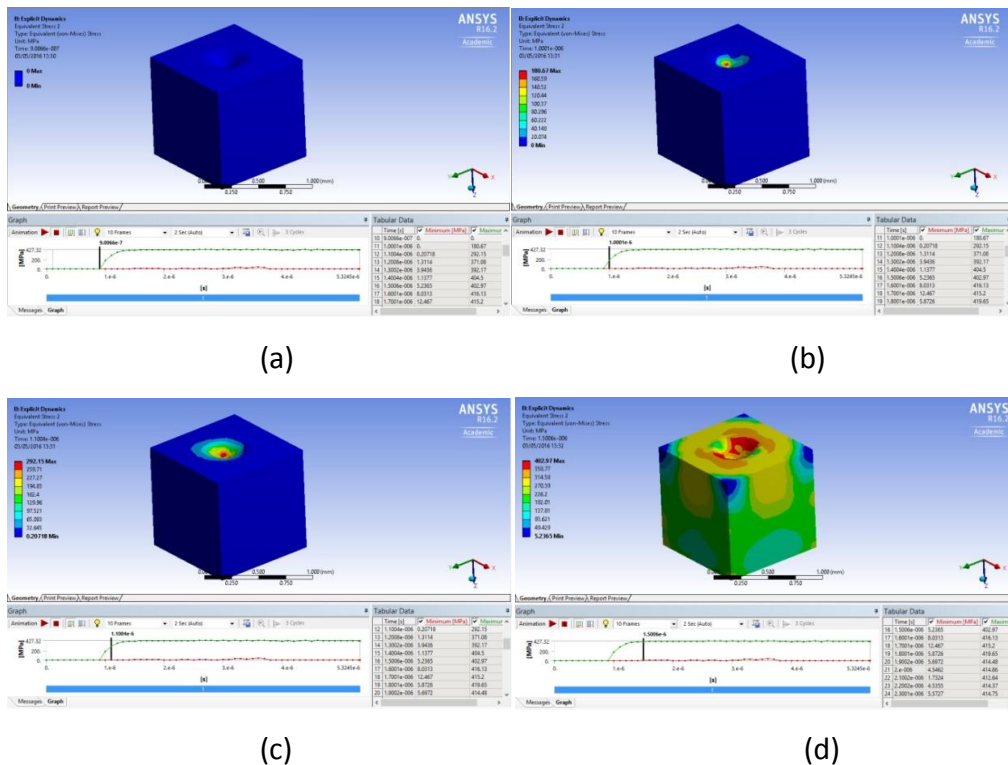


Figure 3-23: Von-Mises stress change with time

Experimental methods

Figure 3-23(a), (b), (c), and (d) show that the drill tool with Von-Mises stress change is continuously keep drilling process into the work-piece, and the position of drill tool was located in the different depth of work-piece at the corresponding times.

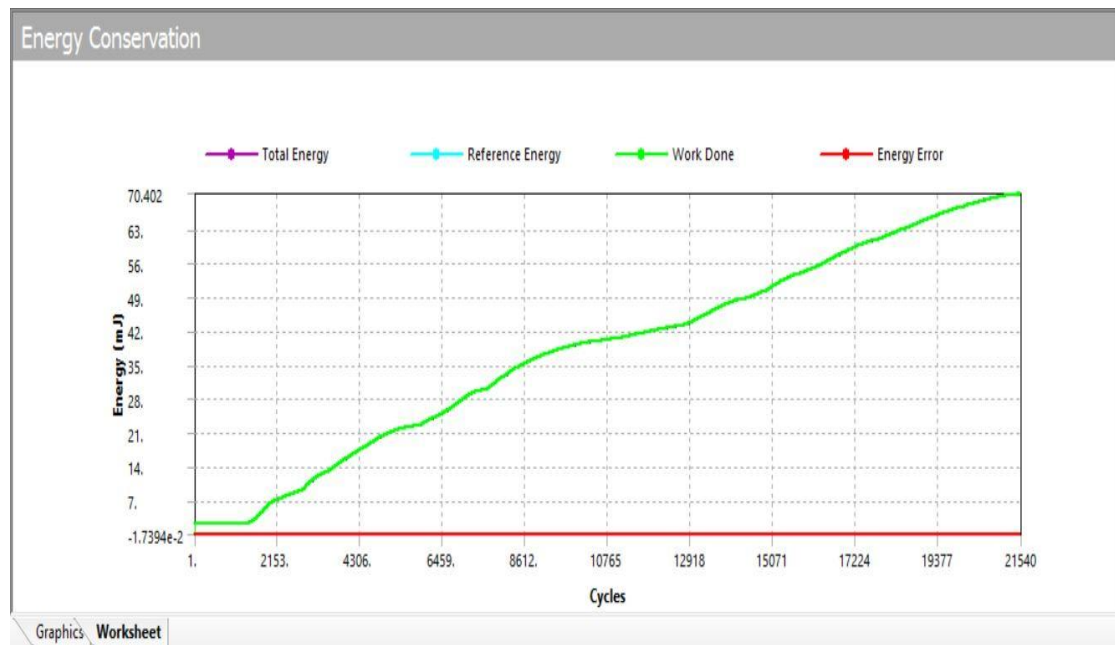


Figure 3-24: Energy conservation in drilling simulation

Figure 3-24 shows the simulation result of energy conservation changing during the drilling process. As the previously end time set, in the 0.0006 second the drilling process will finish 21540 cycles calculation. Here, the energy conservation was started record before the drilling tool touch the work-piece, and after 21540 cycles calculating the drilling process produces maximum 70.4 J in the end. Since the Figure 3-24 shows the energy conservation generally exhibits a linear growth with time. Meanwhile, the energy error represented in red line as shown in Figure 3-24 is almost zero, which indicates the simulation results are very accurate.

3.6 Summary

Due to limitations of the software, ANSYS simulation cannot match the drilling parameter needs of this research exactly. But the thrust force of simulation result can still get 4.67 N by equal proportions. The energy conservation produces maximum 70.4 J in the drilling process. Findings above agree well to the results obtained from

Experimental methods

actual measurement, which is 4.08 N.

It was also found the accuracy of simulation can be further improved by utilizing computer with better processing performance. The direct impact would be increased resolution of simulation, meaning smaller steps that reflect actual operation better than the current setup, which is at a bigger step interval setting so the computer performance issue can be compensated.

Apart from the computer performance issue above, heat generated by the friction between tool and work piece is treated as a fixed condition considering in practice coolant is always present and no significant, prolonged temperature variation is expected.

Chapter 4: Experimental methods

4.1 Introduction

In the field of engineering research, experimental step is an integral part of a systematic study and subsequent verification. This research, without exception, also used systematic experimental approaches to verify the findings. With the help from the university's department and technicians, it was successful to obtain the materials and equipment this research required. This chapter describes in detail all the equipment involved as well as the experimental considerations. In the process of introducing the experimental methods, they will be discussed individually in two aspects: experimental set-up and the respective parameters.

4.2 Experimental set-up

The experimental equipment of this research was provided by the department of Mechanical of Aerospace and Civil Engineering in Brunel University. In order to achieve the accuracy of the experiment, all the experiments were done in a constant temperature and humidity laboratory. The laboratory was keeping at 20 °C temperature and humidity of 40 degrees. During the manufacturing test, all the instruments and equipment operation methods were in accordance to the manufacturer specified standard process of operation, and the instrument will be reset to zero before the test start.

Here is the main experimental setup consists of the following equipment: processing machinery (KERN milling machine), force dynamometer (Kistler Dynamometer), Aluminium work-piece fixture, products image acquisition (SMART JCM-6000), drilling tool and work-piece. These pieces of equipment and their respective specifications will be introduced according to the flow of experimental work.

Experimental methods

The following diagram is shown in Figure 4-1 illustrates the general process of this research experimental study:

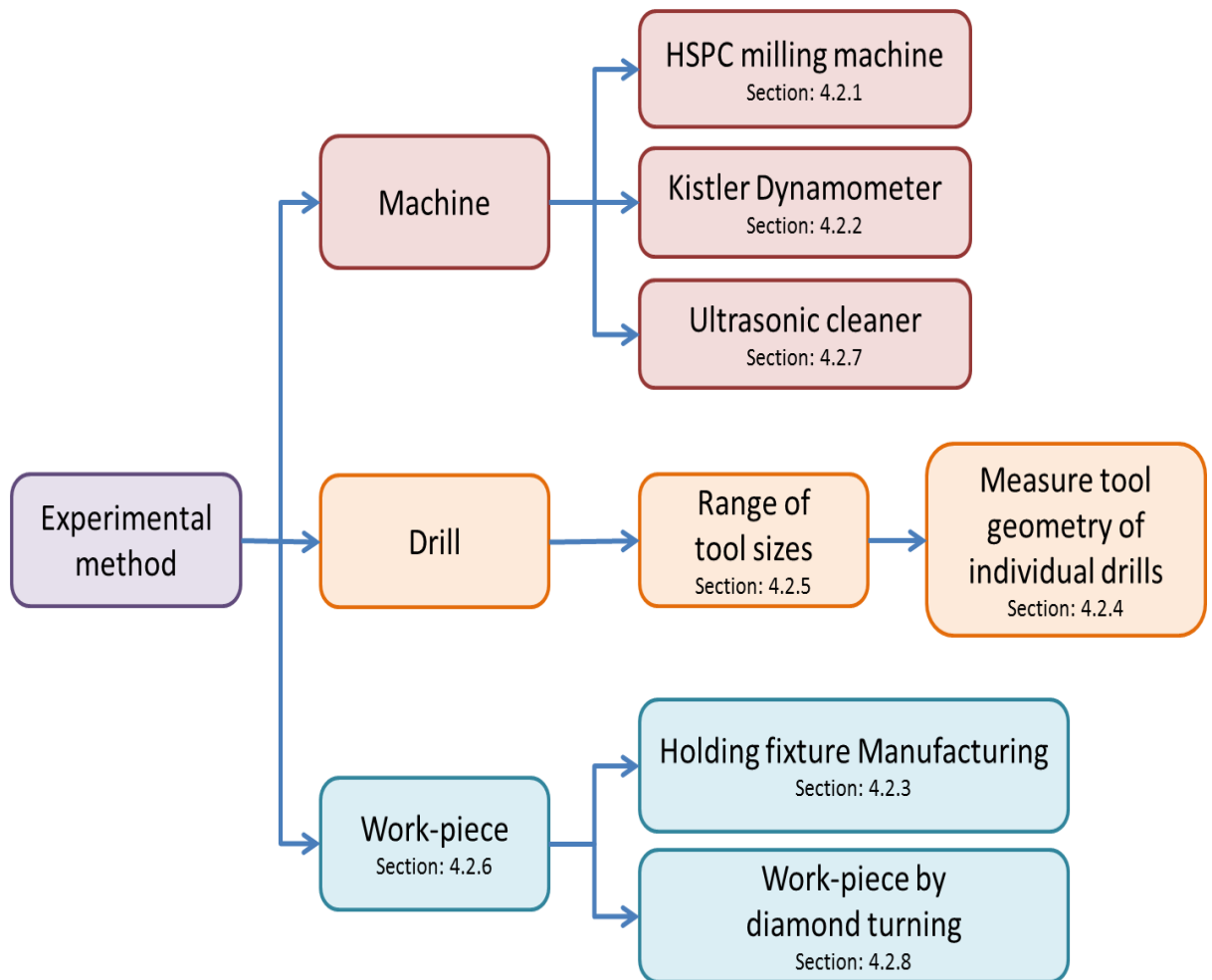


Figure 4-1 Experimental process

All of the experimental equipment required for this study will be divided into three main projects: machine, drill, and work-piece. The first part would be focus on the machine equipment. Machine equipment consists of six main equipment as this research used: Manufacturing machine, HSPC milling machine, Force measurement, Kistler Dynamometer; Tool and Work-piece cleaner, Ultrasonic cleaner. At the second part, drill will describe more details and compare list for the range of testing drill tool sizes and individual drills geometry measurement. The third part, in addition to the testing work-piece itself, it includes the special holding/manufacturing fixture and pre-treatment with the work-piece diamond turning.

Experimental methods

4.2.1 KERN CNC milling machine tool

Figure 4-2 shows the main machine tool used in this research: KERN CNC High precision Micro Milling and Drilling machine (Type HSPC). This manufacturing machine provides 3-axis ultra-precision micro-milling capability. The machining volume can be up to 280mm × 280mm × 250mm. Processing accuracy is at 1 μ m on each translational axis and a ceramic bearing-supported spindle delivers machining operation, which can reach a maximum rotation speed of 33,000rpm.



Figure 4-2: KERN milling machine

For the operation of KERN milling machine, the first step is to check whether the Aluminium fixture is parallel to the moving platform mounted on the KERN machine. Also this calibration needs to keep the work-piece and tool in vertical alignment since any misalignment will seriously affect the quality of drilling and tool life.

Experimental methods

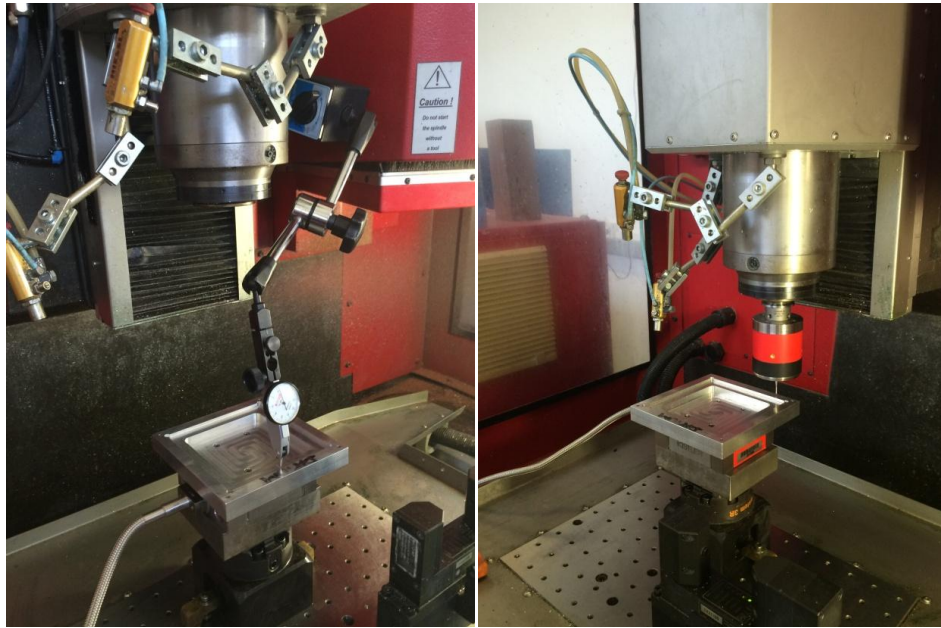


Figure 4-3: Calibration of the aluminium fixture

The second step is the use of Infrared Probe 32.00-MINI to measure the relative position of Aluminium fixture and work-piece. This step will ensure the drilling is carried out at the best precision. The Infrared Probe 32.00-MINI is designed for KERN HSPC milling machine to measure the length, width, and height of work-piece.

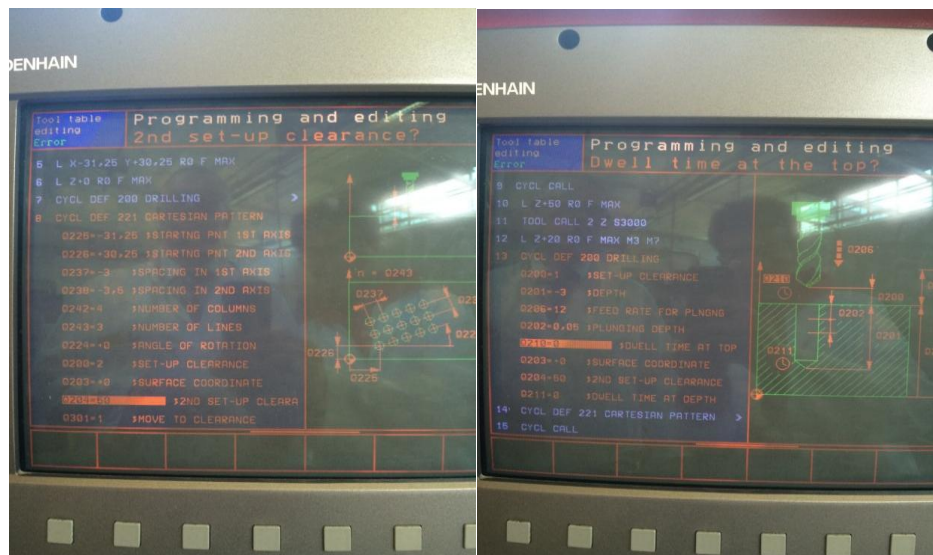


Figure 4-4: Set up the drilling parameter

The third step is the selection of drilling parameters. These parameters include tool code, drilling location, drilling depth, rotation speed, feed rate and plunging value or non-plunge. The operation screen is shown in Figure 4-4.

Experimental methods

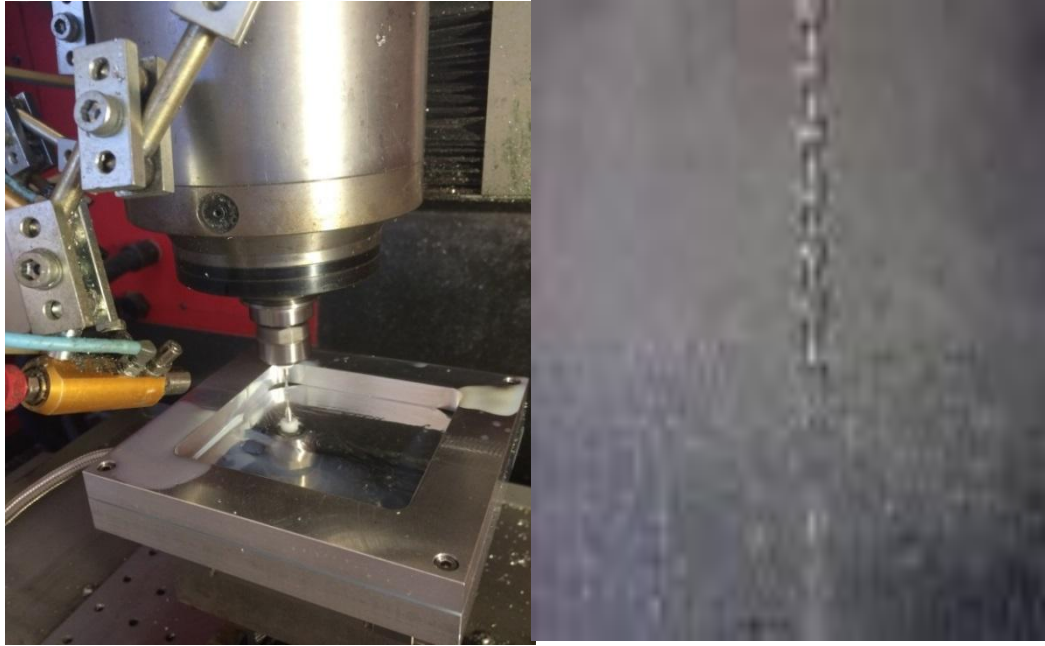


Figure 4-5: The experiment test of micro-drilling

Figure 4-5 and 4-6 show the micro-drilling process in action. A camera was set to record the micro-drilling process and the operation was monitored with real time data on the screen.



Figure 4-6: Drilling and monitor control

The KERN milling machine is the main processing equipment in this research, its operation procedure is as follows:

Experimental methods

- a. Set up the drilling tool in the tool changer.
- b. Set various drilling parameters in the KERN machine computer, including the tool code, drilling location, drilling depth, rotation speed, feed rate and plunging value or non-plunge.
- c. Set the spindle at the rotation operation for 20-30 minutes to warm-up.
- d. Start the Infrared Probe 32.00-MINI to measure the work-piece position and do the initialization.
- e. Load the spot drill from the tool changer and calibrate the tool diameter and shank length.
- f. Start to rotate the spindle with the spot drill for the pre-drill action.
- g. Set spindle movement in Z-axis for 0.1mm pre-drill depth.
- h. Sent back the spot drill to tool changer and load the twist drill for the experiment.
- i. Set the desired period of time (second) for Kistler Dynamometer data recording.
- j. Check the twist drill tool diameter and shank length.
- k. Switch on the cooling/lubricating liquid to avoid the tool failing by friction.
- l. Start to rotate the spindle with the twist drill and use the Z-axis with spindle movement for drilling process.
- m. Before the drill touches the work-piece, start the recording of drilling force data by Kistler dynamometer.
- n. Stop the spindle rotation once the drilling is finished. Switch off the liquid and send back the twist drill to tool changer.
- o. Load the next twist drill from tool changer and repeat the step i – n.
- p. Finish all micro-drilling process, remove the work-piece from the Aluminium fixture and clean the work-piece by compressed air.

Experimental methods

The following tables 4-1, 4-2 and 4-3 show the various experimental parameters used in this research.

Material	Aluminium 6061T			
Spot drill diameter (mm)	Φ0.15			
Depth of pre-drill hole (mm)	0.1			
Drill type	Twist drill			
Drilling process No.	Diameter Φ(mm)	Spindle speed (rpm)	Feed rate (mm/min)	Pecking (μm/each)
1	0.2	6,000	12	50
2	0.4			100
3	0.6			None
4	0.8			None
5	1.0			None
6	0.2		24	50
7	0.4			100
8	0.6			None
9	0.8			None
10	1.0			None
11	0.2		36	50
12	0.4			100
13	0.6			None
14	0.8			None
15	1.0			None

Table 4-1: Drilling parameters for drilling aluminium 6061T

Experimental methods

Material	Aluminium/ Copper metal alloy board		
Spot drill diameter (mm)	Φ 0.15		
Depth of pre-drill hole (mm)	0.1		
Drill type	Twist drill		
Drilling process No.	Diameter (mm)	Spindle speed (rpm)	Feed rate (mm/min)
1	Φ 0.5	6,000	12
2			24
3			36
4		9,000	12
5			24
6			36
7		12,000	12
8			24
9			36

Table 4-2: Drilling parameter at aluminium/ copper metal alloy board

Material	Carbon Fibre reinforced plastic		
Drill type	Twist drill		
Drilling process No.	Diameter (mm)	Spindle speed (rpm)	Feed rate (m/min)
1	Φ0.5	20,000	0.4
2			0.6
3			0.8
4		40,000	0.4
5			0.6
6			0.8
7		60,000	0.4
8			0.6
9			0.8

Table 4-3: Drilling parameter at carbon fibre reinforced plastics

Experimental methods

4.2.2 Force dynamometer

Dynamometer is an extensively used instrument, which can faithfully record the tool of throughout the drilling process. Kistler Dynamometer 9256C is the tool force measurement instrument used in this research.

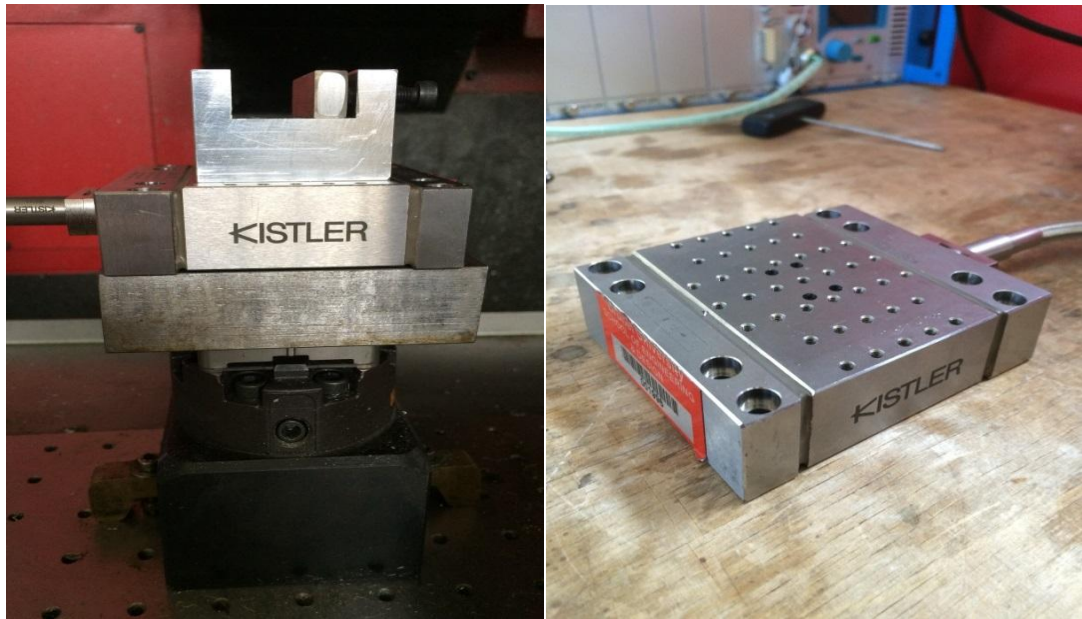


Figure 4-7: The Kistler dynamometer



Figure 4-8: The data collection and multichannel charge amplifier

Experimental methods

As shown in Figure 4-7, the Kistler Dynamometer with two lateral base plates was mounted on the X, Y-axis movement plate of KERN milling machine. Additional fixture is applied to the work piece to eliminate bending deformation caused by stress thus maintaining the force measurement accuracy in the testing process. All the work-pieces have a special made Aluminium fixture to fix. The top surface of Kistler Dynamometer cover plate was secured by the Aluminium fixture. In the measurement of the testing, the Kistler Dynamometer transmits the measured force values by electrical signals.

Therefore, the Kistler Dynamometer would be connected to a multichannel change amplifier by cable and three separate-channel signals (X, Y, Z-axis) are sent to data collector by multichannel change amplifier, as shown in Figure 4-8. The data collector uses USB cable to link with computer and controlled by LabView 2013 software to record the drilling force data, as shown in Figure 4-9.

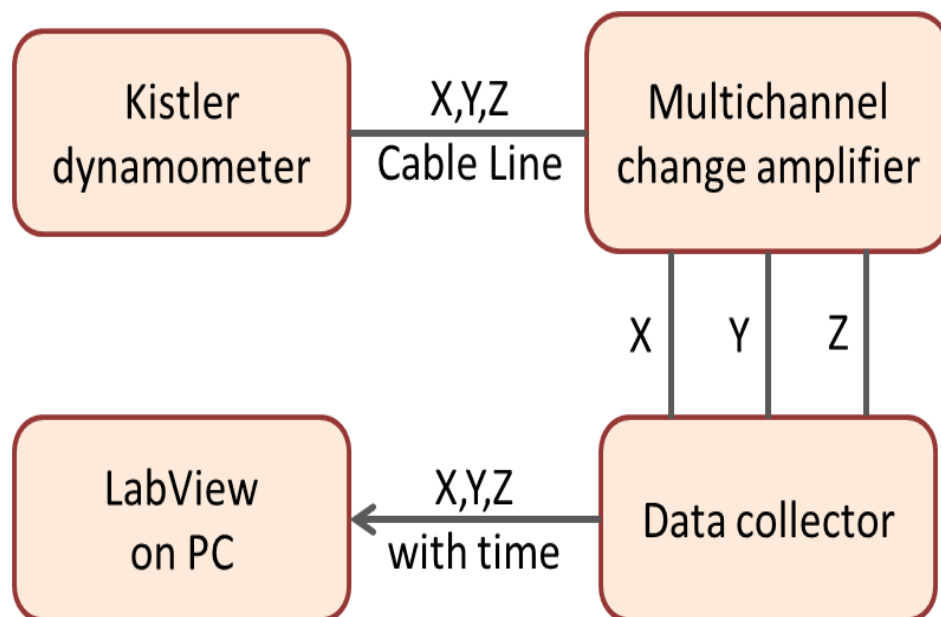


Figure 4-9: Force signal data collect

This multi-component Kistler 9256C dynamometer can measure three orthogonal components of a given force. It consists of four 3-component force sensors mounted under high preload between the cover plate and the two lateral base plates. The applicable measuring range is ± 250 N. According to the tutorial manual, the measurement accuracy is 0.001N within the operating temperature range 0 - 70 ° C.

Experimental methods

Standard weights are also used prior to each measurement for calibration purpose so all data collected are in good accuracy.

4.2.3 Aluminium work-piece fixture

Two Aluminium work-piece fixtures were manufactured to the specifications as described in the engineering drawing in Appendix A.

In order to receive work-piece of different sizes, the small size fixture is 70mm × 70mm × 30mm, as shown in Figure 4.10; large fixture is 120mm × 120mm × 30mm, as shown in Figure 4-11. The testing volume can be up to 40mm × 40mm × 10mm for smaller one and bigger fixture testing volume is 80mm × 80mm × 10mm.

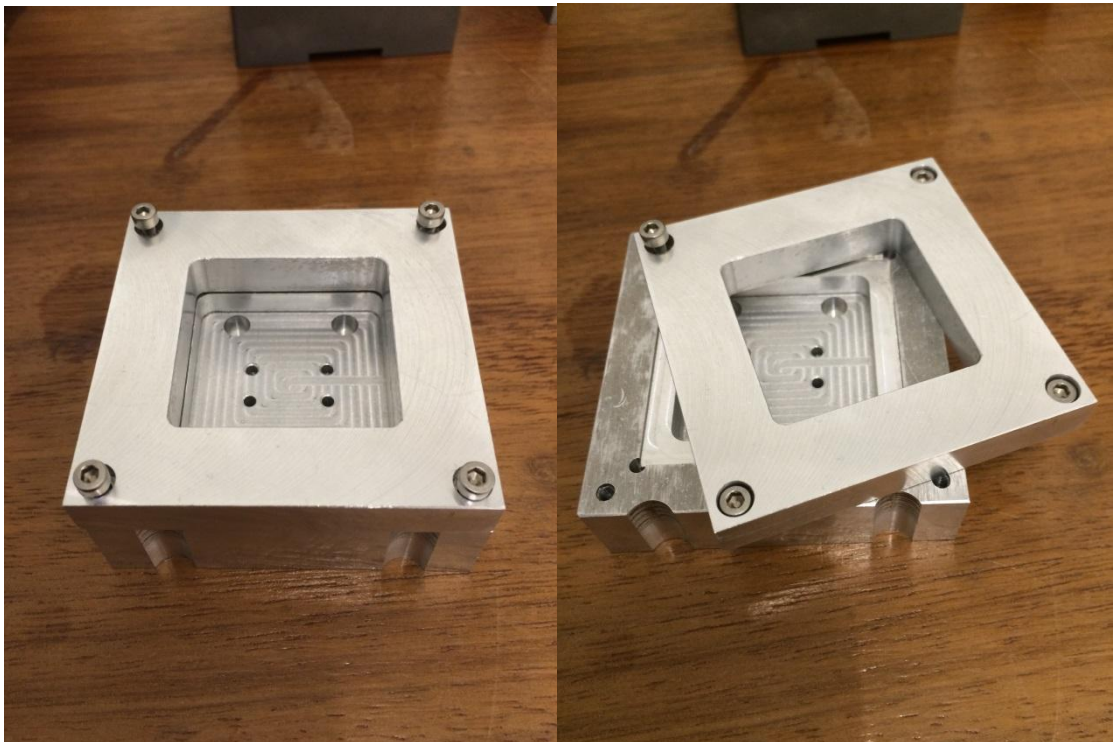


Figure 4-10: Smaller aluminium fixture

The Aluminium fixture consists of central recess base and hollow cover, as shown as Figures 4-10 and 4-11. The central recessed part uses the two-stepped design. While the testing work-piece sits on the higher step, the lower step is design to leave enough empty space under the work-piece. This design helps to avoid the tool

Experimental methods

touching the base during the drilling process. Also the base part of the fixture must be connected with Kistler Dynamometer for the recording of the load data.

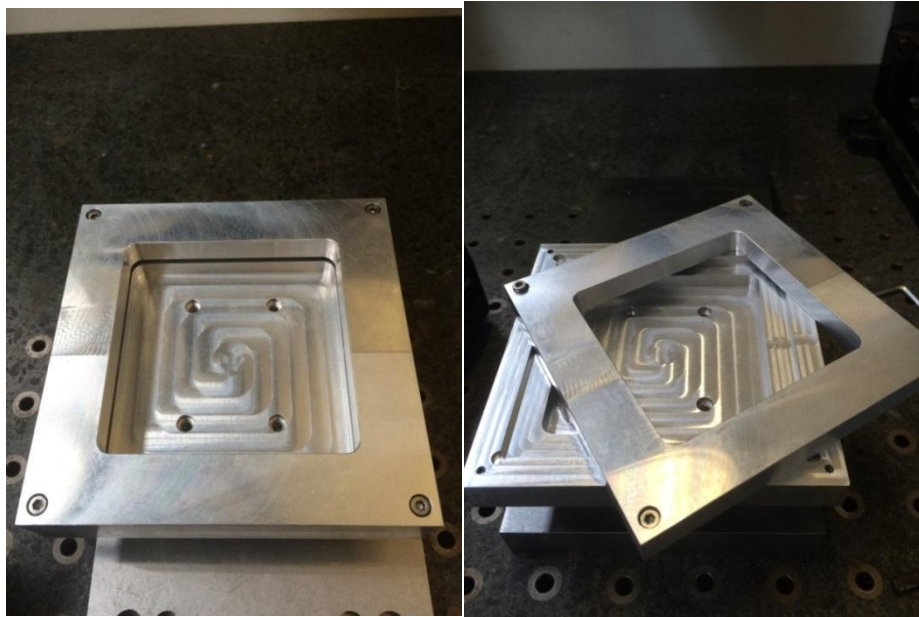


Figure 4-11: Bigger aluminium fixture

4.2.4 Image acquisition

Since the diameter of the twist tool used in this research is relatively small, it is difficult to observe fine features with the naked eye. Therefore, magnified images of both drill tool and work-piece were recorded by the JCM-6000 Benchtop SEM (SCANNING ELECTRON MICROSCOPE). Figure 4-12 and 4-13 are the JCM-6000 Benchtop SEM during sample observation.



Figure 4-12: JCM-6000 Benchtop SEM

Experimental methods

The JCM-6000 Benchtop SEM offers high and low vacuum modes (HV, LV) and is capable to capture image between X10 and X60000.

High vacuum mode (HV) and secondary electron imaging were used for SEM sample observation in order to achieve best image quality with magnifications between X60 and X110.

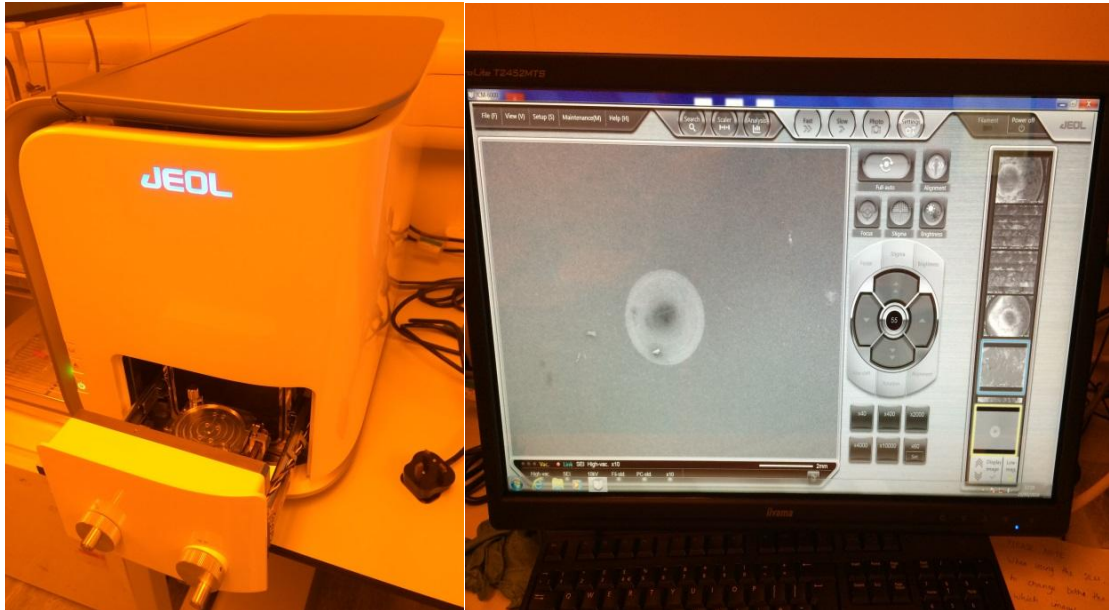


Figure 4-13: The operating of JCM-6000 Benchtop SEM

Prior to the SEM session each sample, tool or work-piece has to be secured to the specimen holder and reset to the centre of the C circle, as shown in Figure 4-14.

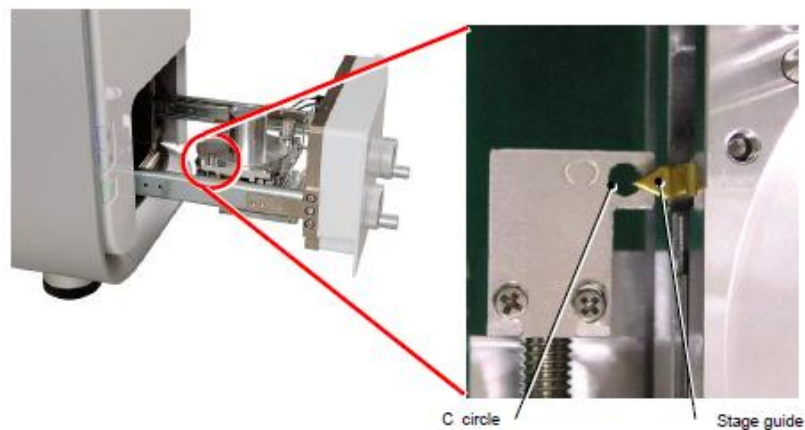


Figure 4-14: Specimen holder of JCM-6000 Benchtop SEM

Experimental methods

4.2.5 Drilling tools

In this research, all twist drilling tools were selected from the UNION TOOL product range, as shown in Figure 4-15. Table 4-4 and 4-5 show the drilling tool specifications.

Drill type	Drill material	Drill diameter	Flute length	Overall length	Shank diameter	Point angle	Helix angle
Twist drill	Tungsten carbide	0.1 to 1.0 mm	7.5 mm	38 mm	3.175 mm	110°	30°

Table 4-4: Drilling tool specification

Drill type	Drill material	Drill diameter	Flute length	Overall length	Shank diameter	Point angle	Helix angle
Spot drill	Tungsten carbide	0.4 mm	7.5 mm	38 mm	3.175 mm	130°	30°

Table 4-5: Spot drill tool specification



Figure 4-15: PCB Tungsten carbide drill tool

Experimental methods

4.2.6 Work-pieces

This research used two different materials for experimental work-piece: full Aluminium disc and Aluminium/Copper metal matrix composite panel. The first work-piece was 100 mm in diameter and 3mm thick Aluminium disc, as shown in Figure 4-16. The chemical composition and microstructure of Aluminium details are shown in Table 4-6.

Element (%)				Al-6061T			
				97.5			
Density (g/cm ³)	Tensile modulus (GPa)	Tensile strength (Mpa)	Yield strength (Mpa)	Poisson's ratio	Thermal conductivity (W/(m×K))	Thermal expansion (1/K)	Heat capacity (J/(kg×K))
2.7	69	241	214	0.33	200	23.5e ⁻⁶	900

Table 4-6: The material element of aluminium 6061T

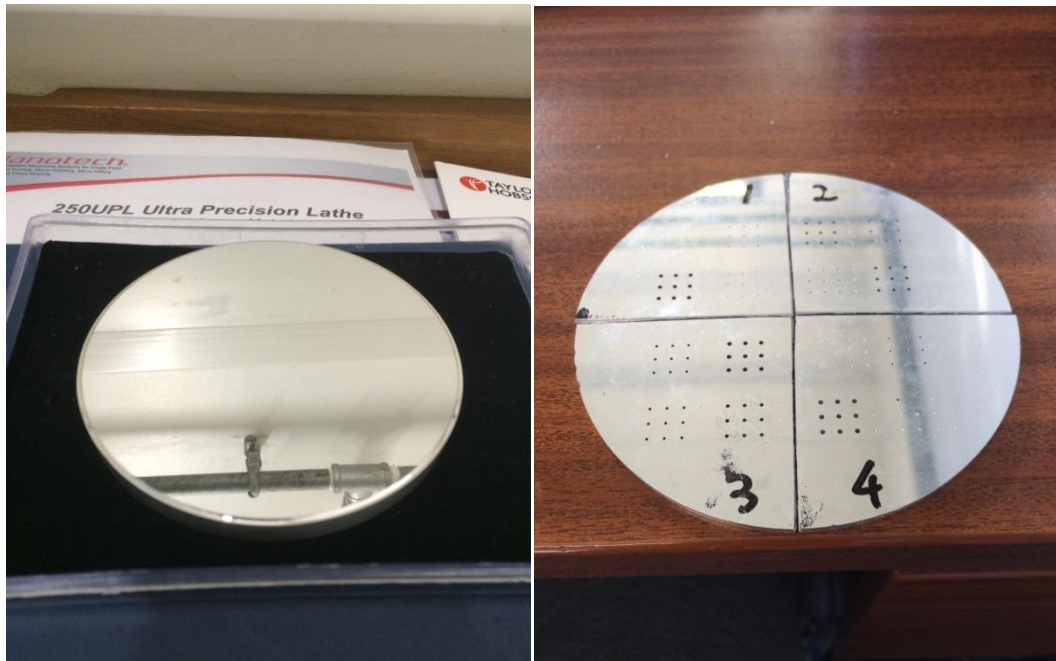


Figure 4-16: Aluminium work-piece

Experimental methods

The second experimental work-piece was the Al/Cu metal matrix composite and the dimension was 50mm × 50mm × 2mm as shown in 4-17. The chemical composition and microstructure of Al/Cu metal matrix composite element details are shown in Table 4-7.

Element (%)				Al		Cu	
				96.7		3.3	
Density (g/cm ³)	Tensile modulus (GPa)	Tensile strength (Mpa)	Yield strength (Mpa)	Poisson's ratio	Thermal conductivity (W/(m×K))	Thermal expansion (1/K)	Heat capacity (J/(kg×K))
2.85	100	610	400	0.32	247	23e ⁻⁶	897

Table 4-7: The material element of Al/Cu metal matrix composite



Figure 4-17: Al/Cu metal matrix composite

4.2.7 Ultrasonic cleaner

If the work-piece or drilled tool was observed by JCM-6000 Benchtop SEM at high magnification, sometimes impurities can be found on the specimen. Therefore in this research all tool and work-piece were cleaned by ultrasonic cleaner for minimum 60 second, before drilling process as well as SEM observations. In order to maintain cleanliness and water quality, each time distil water will be replaced before cleaning starts, as shown in Figure 4-18.



Figure 4-18: Ultrasonic cleaner

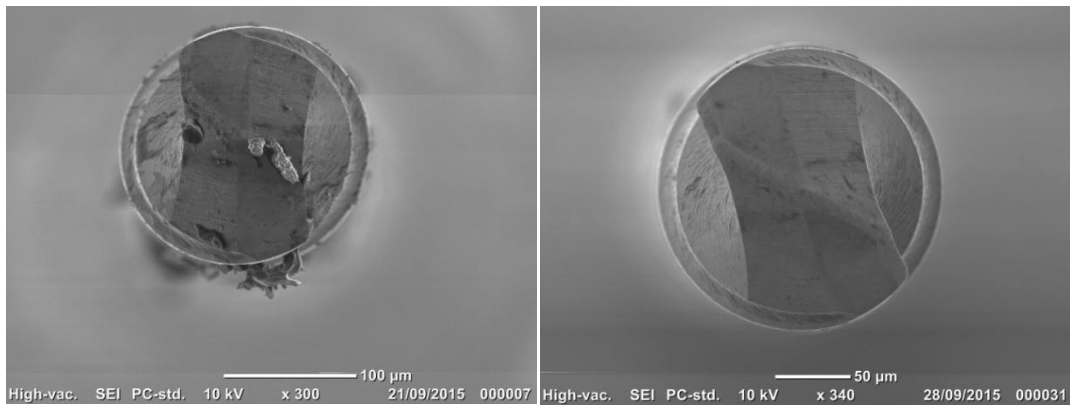


Figure 4-19: Drill tool before clean and after

4.2.8 Mirror surface finishing process

In order to avoid surface irregularity, which will result in drilling bit offset or incline, the work-piece has to go through a mirror surface finishing process for best surface smoothness. This was achieved by carrying out diamond turning on a NANOTECH 250UPL Ultra-precision Lathe, as shown in Figure 4-20.

In the mirror surface finishing process, the diamond turning feed rate was set at 20 mm/min and each depth of cut is 3μm. Such diamond turning was repeated 5-10 times until all the area of turning surface was a mirror finished, as shown in Figure 4.20.



Figure 4-20: NANOTECH 250UPL Ultra-precision Lathe

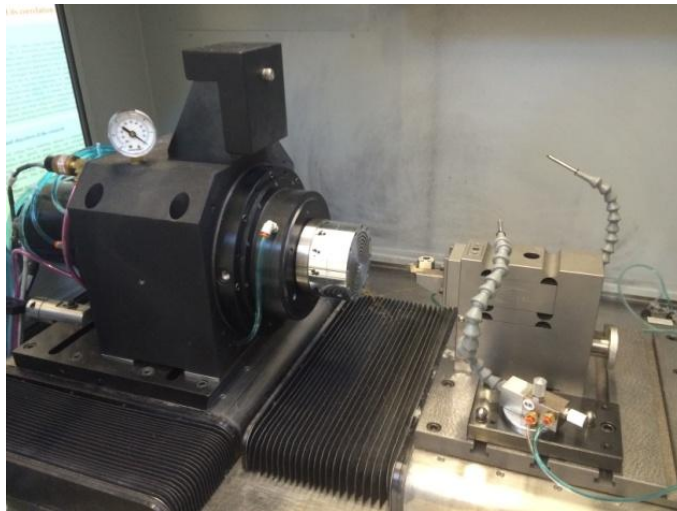


Figure 4-21: The spindle of NANOTECH 250UPL Ultra-precision Lathe

4.3 Checking on the setting

Despite the setup was done in laboratory environment, it is possible that slight variations could be induced due to changes in ambient temperature, equipment vibration and manual access. This could result in experimental error considering the delicate nature of the tool used in this research.

Therefore, before each drilling process the tool must undergo a close inspection, as well as checking the work-piece horizontal position with a gauge indicator, as shown in Figure 4-22.

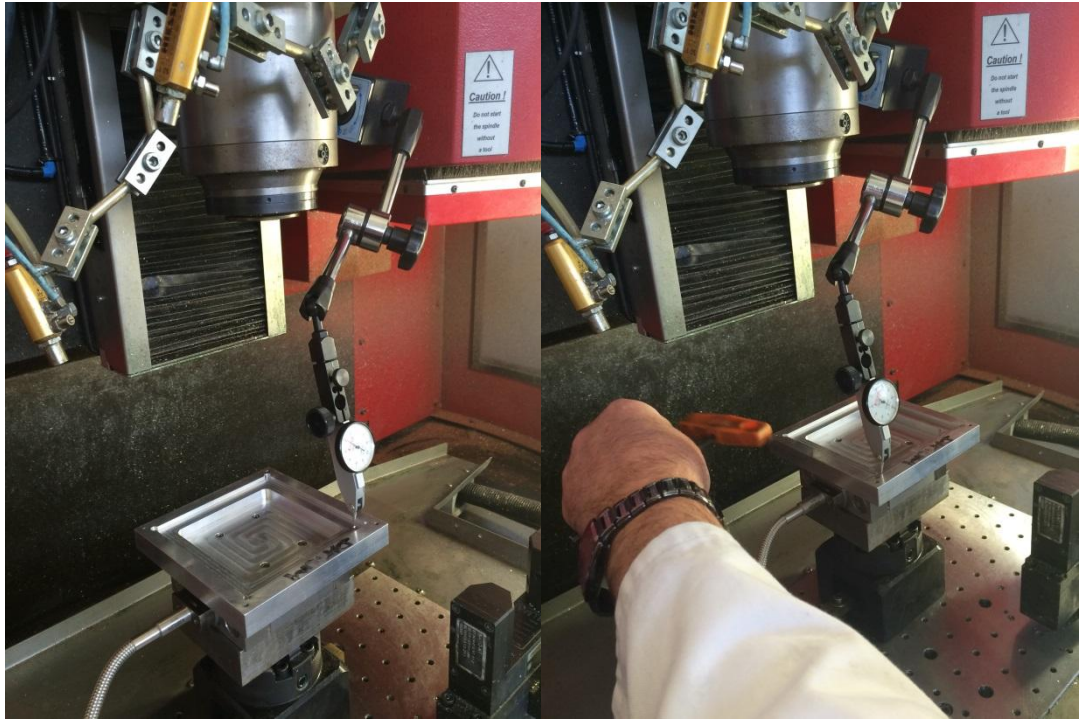


Figure 4-22: To calibrate the Aluminium fixture remains parallel to the moving direction of the base plate

4.3.1 Laser tool measuring system

In this research, before each micro-drilling process, the length of drill tool must be verified by the laser tool measuring system. As different size tools swapped and installed to the tool holder manually, it is well possible that each setup results in slightly different positions.

Laser tool position measuring system can help to avoid the negative effects caused by external environment factors such as temperature and the possible variation in tool position. In addition to the length of drill tool, this laser tool position measuring system can also verify tool diameter and tool point position. By carrying out such verification the overall quality of each drilling can be kept at the best possible level. Figure 4-23 is the photo of laser tool measuring system in action.

Experimental methods



Figure 4-23: Laser tool position measuring system

Before start using the laser position measurement system, the spindle runs continuously for 30 minutes to do a warm-up action. This action can not only keep the spindle in the stable processing, but also it can accurately obtain the tool tip position in the spindle running operation. This laser tool position measuring system would function in conjunction with infrared touch probe system (see section 4.3.2) to set the spindle location in the manufacturing processing starting point.

4.3.2 Infrared touch probe system

The Infrared Probe 32.00-MINI is specifically designed for KERN milling machine. The function is to check the spindle working area and measure the location of the work-piece device. Since all the drillings cannot be completed in one day, and each micro-drilling process may cause the position of work-piece moving slightly, it is therefore before each micro-drilling process Infrared Probe 32.00-MINI was used to verify the relative position of spindle and the work-piece.

Its power is supplied by 4×1.5V, type of AAA battery (1175mAh) and the measurement signal is sent/collected via wireless network. The applicable operating temperature range is 10°-50°C, and the accuracy was up to $\pm 1\mu\text{m}$. Figure 4-24 is the photo of Infrared Probe 32.00-MINI.

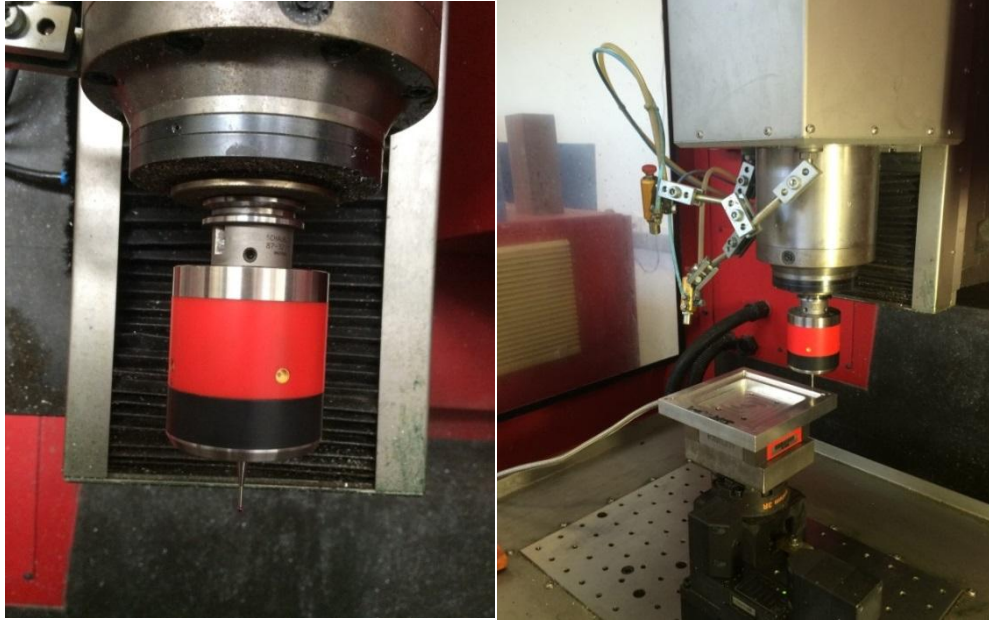


Figure 4-24: Infrared probe 32.00-MINI

4.3.3 Non-contact tachometer

For the setup of drilling parameters for KERN HSPC milling machine, one of most important parameters is the spindle rotation speed. This rotation speed is directly linked to the stress stability throughout the drilling process. It is therefore all modern drilling machines are equipped with dedicated user interface for defining spindle rotation speed. Although the user can directly enter the value experiment requires, it is possible to find variation in the real speed since all parts are driven mechanically.



Figure 4-25: RS163-5348 Non-contact tachometer

Experimental methods

This research uses RS163-5348 Non-contact tachometer to measure the true rotation speed. RS163-5348 Non-contact tachometer measures rotational speed via infrared reflection. Result is taken as an average of ten consecutive measurements and only after a 30-minute pre-rotation so stability and accuracy can be ensured.

Therefore this research uses RS163-5348 Non-contact tachometer to determine the difference from the true rotation speed and UI information board to make the adjustment accordingly, as shown in 4-25.

4.3.4 Point angle and diameter of the drilling tool

It is known that the chisel edge extrudes into the work-piece material and contributes substantially to the thrust force. Also, during a drilling process, the chips are formed along the cutting lip and move upward following the drill helix. Such chips could get attached to the drill geometry and result in complicated effect on the cutting forces. Therefore, before the experiments of this research started, all the geometric values of drill tools must be checked before use. With the help of JCM-6000 Benchtop SEM, important geometric values such as: point angle, diameter and helix angle etc. can be measured and checked through SEM photos, as shown in Figure 4-26 and Table 4-8. Such inspection not only can confirm the consistency of each individual measurement but also help the subsequent investigation on the correlation between drill tip angle and stress variation.

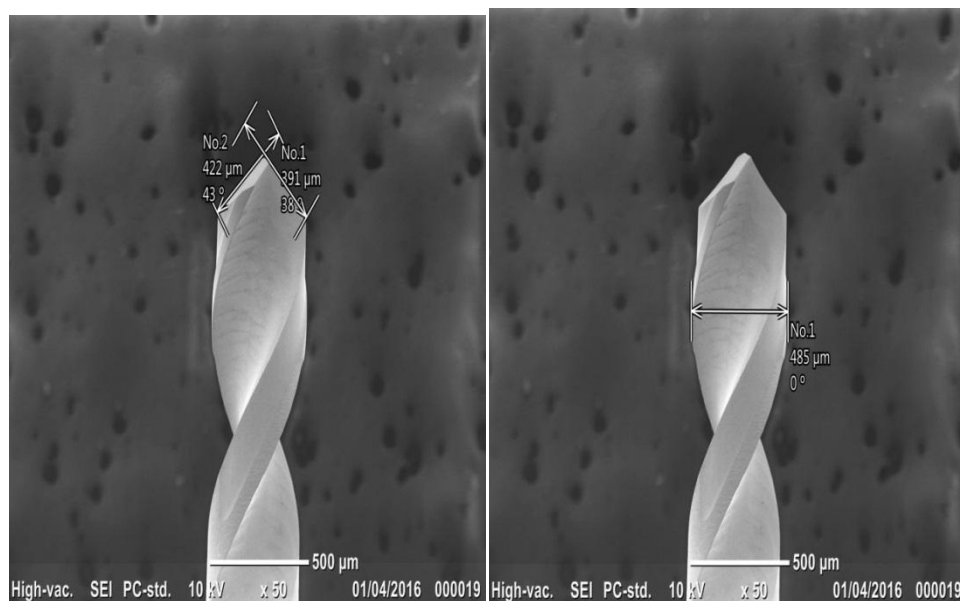


Figure 4-26: Measured by the SEM photo

Experimental methods

	Twist drill										Spot drill
Nominal diameter (mm)	0.1	0.2	0.3	0.4	0.5	0.6	0.7	0.8	0.9	1.0	0.5
Measured diameter (mm)	0.106	0.189	0.295	0.395	0.448	0.545	0.682	0.786	0.887	1.013	0.483
Web half width (mm)	0.0241	0.0483	0.0601	0.0576	0.0699	0.0729	0.1149	0.0617	0.0605	0.0702	0.0315
Point angle	112°	107°	127°	127°	110°	128°	122°	110°	107°	126°	130°

Table 4-8: Each tool measured diameter and point angle

4.4 Summary

The experimental described in detail all the equipment involved as well as the experimental considerations, and the process of introducing the experimental methods. Next chapter are concerned to represented drilling process by diagram and mathematical model.

Chapter 5:

Thrust force model for drilling

5.1 Introduction

In this chapter, the drilling process is represented by diagram and mathematical model. In the diagram, it uses different colour lines to indicate the various stages of drilling. Also, each mathematical model describes the meaning of symbols in detail. All simplifying processes for mathematical models were carried out by MATLAB (R2014a) software.

5.2 Thrust force model

The mathematical model developed in this section is for the case where the twist drill point angle is greater than that of the spot-drill used for producing the pre-drilled countersunk hole. This is because all cutting trials performed belong to this situation.

Figure 5-1 shows the side view of a twist drill tip as it moves into a work-piece, the surface of which aligns with the y -axis; the profile of a pre-drilled hole is shown in black. The twist drill tip is defined by a cutting lip (the angled line segment) and web (the vertical line segment).

The drill has a radius of R_1 and a web width of $2R_0$. The four positions of the moving tip are shown in red, yellow, green and purple respectively. These mark the boundaries between the different stages of drilling as will be explained shortly.

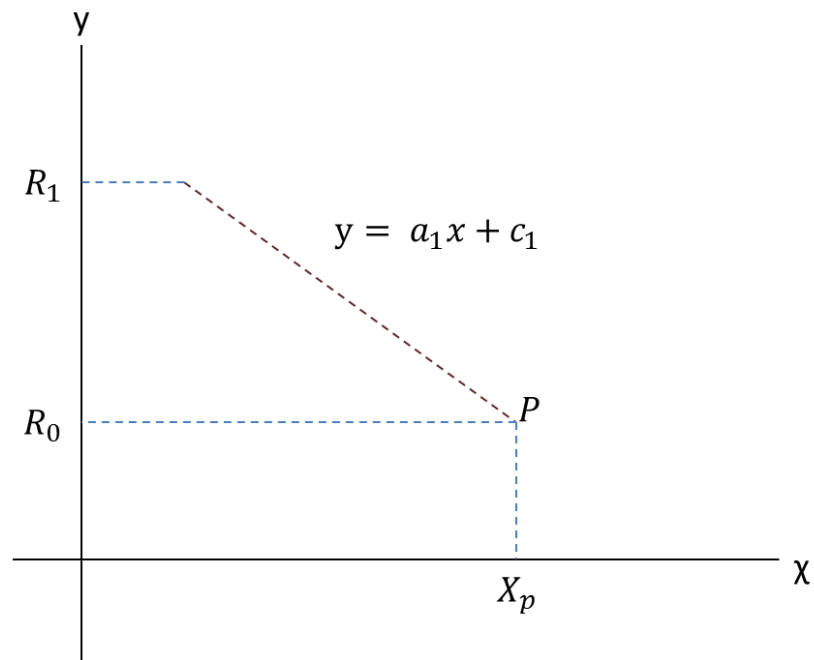


Figure 5-2: Cutting lip move with time

Let the cutting lip be represented by a straight line, $y = a_1x + c_1$ where a_1 and c_1 are the respective slope and y-intercept. This line passes through point $P(x_p, R_0)$ so that

$$R_0 = a_1x_p + c_1,$$

Giving

$$c_1 = R_0 - a_1x_p.$$

Hence, any point (x, y) on the cutting lip satisfies the equation

$$y = a_1x + R_0 - a_1x_p.$$

Rearranging this gives

$$y = a_1(x - x_p) + R_0. \quad (5-1)$$

It is noted that a_1 has a negative value and x_p increases with time.

Experimental and theoretical of micro-drilling manufacturing

The pre-drilled hole, shown as black in Figure 5-1, has a circular bottom at x_1 of radius r_0 and a bevel side C_0Q which can be represented by a straight line $r_0 = a_0x_1 + c_0$ with a_0 and c_0 as the slope and y-intercept.

From this equation, $c_0 = r_0 - a_0x_1$. Thus, any point (x, y) on C_0Q satisfies the equation $y = a_0x + r_0 - a_0x_1$ or

$$y = a_0(x - x_1) + r_0. \quad (5-2)$$

It is noted that a_0 is also negative and $a_0 < a_1$. In addition, x_1 , unlike x_p , stays constant for a given pre-drilled hole.

The volume of material removed from the work-piece will be considered in terms of the four stages of drilling in the following sections.

5.3 Stage 1: $x_0 < x_p \leq x_1$

In this stage, the drill tip moves from x_0 to x_1 , corresponding to the respective red and yellow outlines in Figure 5-3.

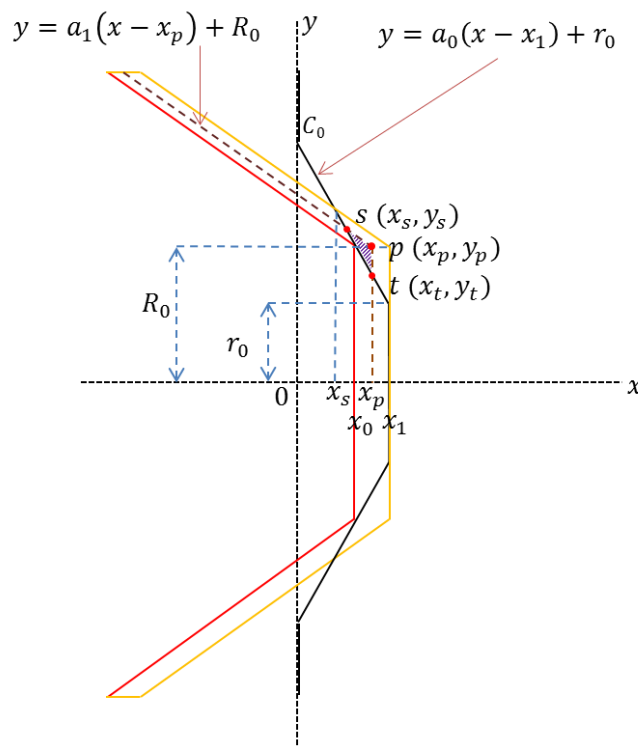


Figure 5-3: Material removal during Stage 1: $x_0 < x_p \leq x_1$

Experimental and theoretical of micro-drilling manufacturing

When the drill tip is at x_p , the cross-section of material removed is triangle SPT , where S is the point of intersection of the two straight lines given by equations 5-1 and 5-2. The coordinates of S can be obtained by solving equations 5-1 and 5-2 simultaneously for x and y , giving the point of intersection $S(x_s, y_s)$ as

$$x_s = \frac{a_1}{(a_1 - a_0)} x_p + \frac{(r_0 - R_0) - a_0 x_1}{(a_1 - a_0)} \quad (5-3)$$

and

$$y_s = \frac{a_0 a_1}{(a_1 - a_0)} x_p - \frac{a_0 a_1}{(a_1 - a_0)} x_1 + a_1 r_0 - a_0 R_0. \quad (5-4)$$

It is observed from the equations 5-3 and 5-4 that as the drill moves, that is x_p increasing, taking into account the fact that $a_0 < 0$, $a_1 < 0$ and $a_0 < a_1$, x_s decreases while y_s increases both linearly.

To find the coordinates of point t (Figure 5-3), it is noticed that $t(x_t, y_t)$ has the abscissa value of

$$x_t = x_p, \quad (5-5)$$

and is a point on the straight-line equation 5-2.

Accordingly,

$$y_t = a_0(x_p - x_1) + R_0. \quad (5-6)$$

It is assumed that workpiece material ahead of the web is removed by ploughing action whereas that ahead of the cutting lip by cutting action. Both actions contribute to the thrust force during drilling but are unlikely to the same extent. Consequently, the volumes of material removed by these two actions will be treated separately. These volumes are cylindrical or conical in shape.

For a conical frustum with the end radii r_1 and r_2 and height h , its volume V can be shown to be (reference to be added)

$$V = \frac{1}{3} \pi h (r_1^2 + r_1 r_2 + r_2^2). \quad (5-7)$$

Experimental and theoretical of micro-drilling manufacturing

In Figure 5-4, the volume, V_{1c} , swept out by the cross-sectional area A_c is due to the cutting action; the volume, V_{1p} , by A_p is from the ploughing action. Applying equation 5-7 to these two areas and simplifying,

$$V_{1c} = \frac{1}{3} \pi (x_p - x_0) (y_s^2 + R_0 y_s - 2R_0^2) \quad (5-8)$$

and

$$V_{1p} = \pi R_0^2 (x_p - x_0) - \frac{1}{3} \pi (x_p - x_0) (R_0^2 + y_t^2 + R_0 y_t). \quad (5-9)$$

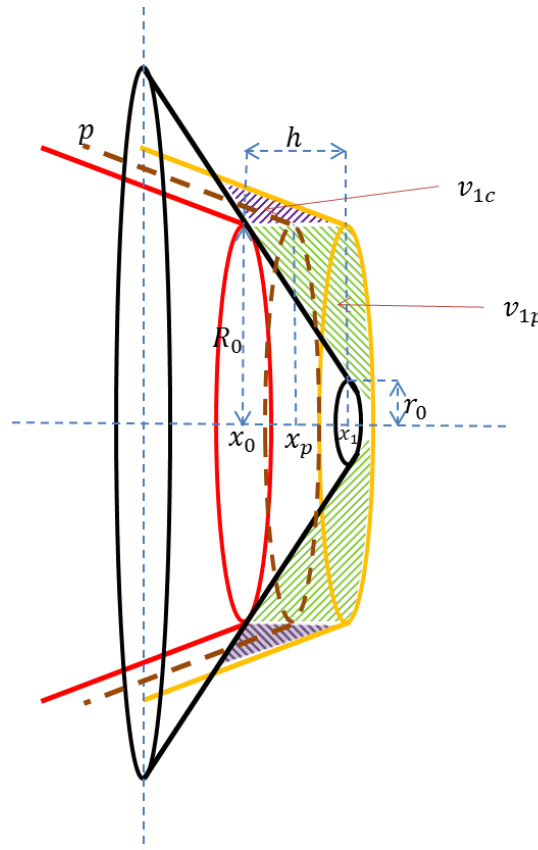


Figure 5-4: Volume removal during Stage 1

The total volume removed, after substituting in equations 5-8 and 5-9 and simplifying, is

$$V = V_{1c} + V_{1p} = \frac{1}{3} \pi (x_p - x_0) [y_s^2 - y_t^2 + R_0 (y_s - y_t)] \quad (5-10)$$

It should be noted that the volume equations 5-8, 5-9 and 5-10 are a function of the

Experimental and theoretical of micro-drilling manufacturing

variable x_p since, according to equations 5-3, 5-4, 5-5 and 5-6, x_s , y_s , x_t and y_t can be expressed solely in terms of x_p .

5.4 Stage 2: $x_1 < x_p \leq x_2$

This stage begins at the point where the drill web touches the bottom of the countersunk pre-drilled hole, $x_p = x_1$, and ends when the drill lip reaches the surface rim of the countersunk hole at y_u at which $x_p = x_2$, as shown in Figure 5-5.

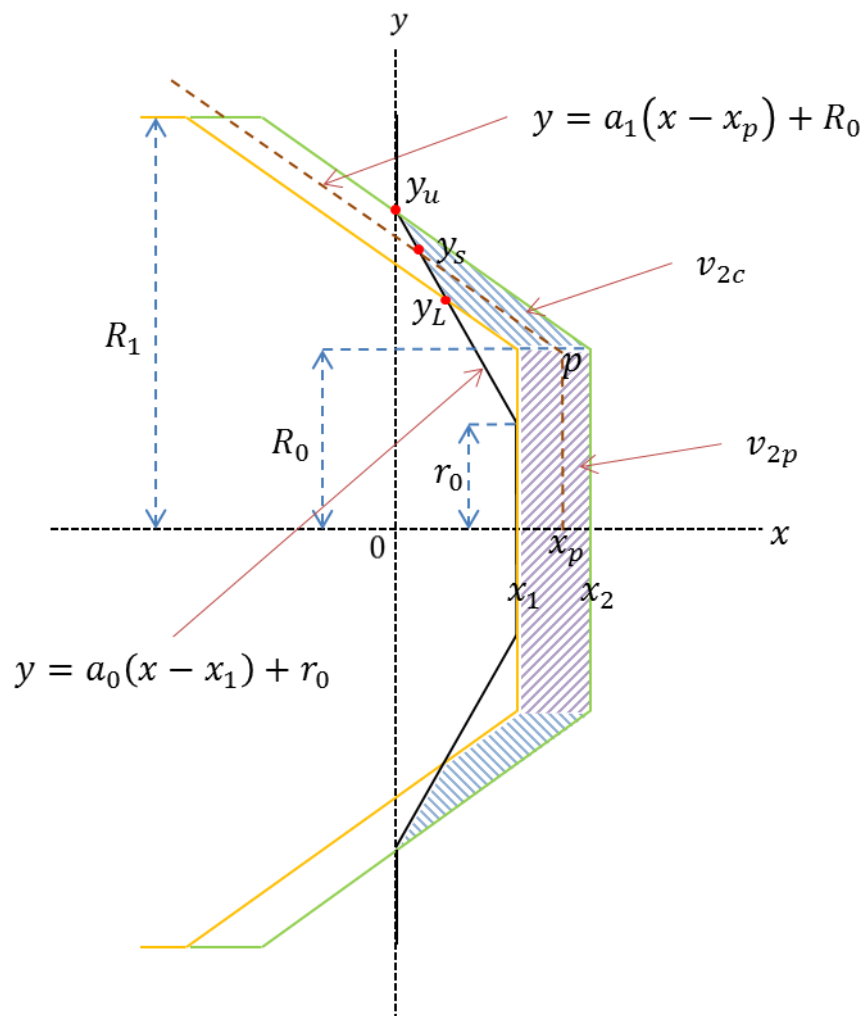


Figure 5-5: Material removal during Stage 2: $x_1 < x_p \leq x_2$

When the drill tip is at x_p , the cross-section of material removed is straight line $y_s p$, where y_s is the point of the straight line given by equation 5-1. The coordinates of y_s can be obtained by solving equation 5-1 simultaneously for x and y , giving the

Experimental and theoretical of micro-drilling manufacturing

point of intersection $y_s(x_{y_s}, y_{y_s})$.

When $y_s = y_L$, that y_L has the abscissa value of

$$x_p = x_1, \quad (5-11)$$

To find the coordinates of point y_L (Figure 5-5), it is the point of intersection of the straight line given by equation 5-1. Accordingly,

$$y_L = a_1 r_0 - a_0 R_0. \quad (5-12)$$

When $y_s = y_u$, that y_u has the abscissa value of

$$x_p = x_2, \quad (5-13)$$

To find the coordinates of point y_L (Figure 5-5), it is the point of intersection of the straight line given by equation 5-1. Accordingly,

$$y_u = \frac{a_0 a_1}{(a_1 - a_0)} (x_2 - x_1) + a_1 r_0 - a_0 R_0. \quad (5-14)$$

The cross-sectional area of material removed in this stage of drilling is shown hatched in Figure 5-5. In Figure 5-5, the volume, V_{2c} , swept out by the cross-sectional area A_c is due to the cutting action; the volume, V_{2p} , by A_p is from the ploughing action. Applying equation 5-7 to these two areas and simplifying,

$$V_{2c} = \frac{1}{3} \pi (x_p - x_1) (y_s^2 + y_L^2 + y_s y_L) - \pi (x_p - x_1) R_0^2 \quad (5-15)$$

and

$$V_{2p} = \pi (x_p - x_1) R_0^2 \quad (5-16)$$

The total volume removed, after substituting in equations 5-15 and 5-16 and simplifying, is

$$V = V_{2c} + V_{2p} = \frac{1}{3} \pi (x_p - x_1) (y_s^2 + y_L^2 + y_s y_L) \quad (5-17)$$

5.5 Stage 3: $x_2 < x_p \leq x_3$

This stage begins at the drill lip reaches the surface rim of the countersunk hole at y_u at which $x_p = x_2$, and ends at the point where the rim of the drill lip touches the surface of the work-piece at y_v at which $x_p = x_3$, as shown in Figure 5-6.

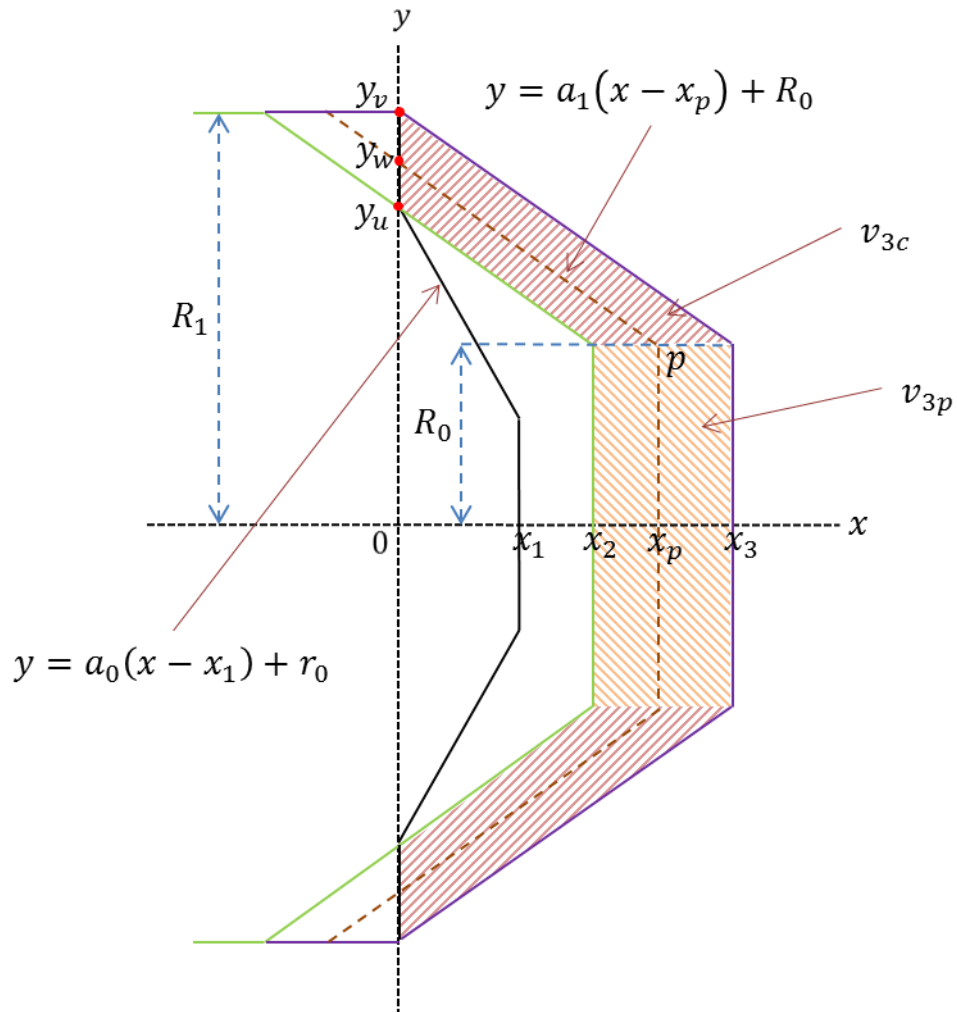


Figure 5-6: Material removal during Stage 3: $x_2 < x_p \leq x_3$

As same as stage 2, when the drill tip is at x_p , the cross-section of material removed is straight line $y_w p$, where y_w is the point of the straight line given by equation 5-1. The coordinates of y_w can be obtained by solving equation 5-1 simultaneously for y , giving the point of intersection $y_w(0, y_w)$.

Experimental and theoretical of micro-drilling manufacturing

When $y_w = y_v$, that y_w has the abscissa value of

$$x_p = x_3 , \quad (5-18)$$

To find the coordinates of point y_v (Figure 5-6), it is the point of intersection of the straight line given by equation 5-1. Accordingly,

$$y_v = -a_1 x_p + R_0 . \quad (5-19)$$

The cross-sectional area of material removed in this stage of drilling is shown hatched in Figure 5-6. The volume, V_{3c} , swept out by the cross-sectional area A_c is due to the cutting action; the volume, V_{3p} , by A_p is from the ploughing action. Applying equation 5-7 to these two areas and simplifying,

$$V_{3c} = \frac{1}{3} \pi (x_p - x_2) (y_w^2 + R_0^2 + y_w R_0) - \pi (x_p - x_2) R_0^2 - \pi (x_p - x_2) R_0^2 \quad (5-20)$$

and

$$V_{3p} = \pi (x_p - x_2) R_0^2 \quad (5-21)$$

The total volume removed, after substituting in equations 5-20 and 5-21 and simplifying, is

$$V = V_{3c} + V_{3p} = \frac{1}{3} \pi (x_p - x_2) (y_w^2 + R_0^2 + y_w R_0) - \pi (x_p - x_2) R_0^2 \quad (5-22)$$

5.6 Stage 4: $x_3 < x_p$

This stage begins at the rim of the drill lip reaches the work-piece surface at y_v which $x_p = x_3$, and keeps material removed until the drilling action ends, as shown in Figure 5-7.

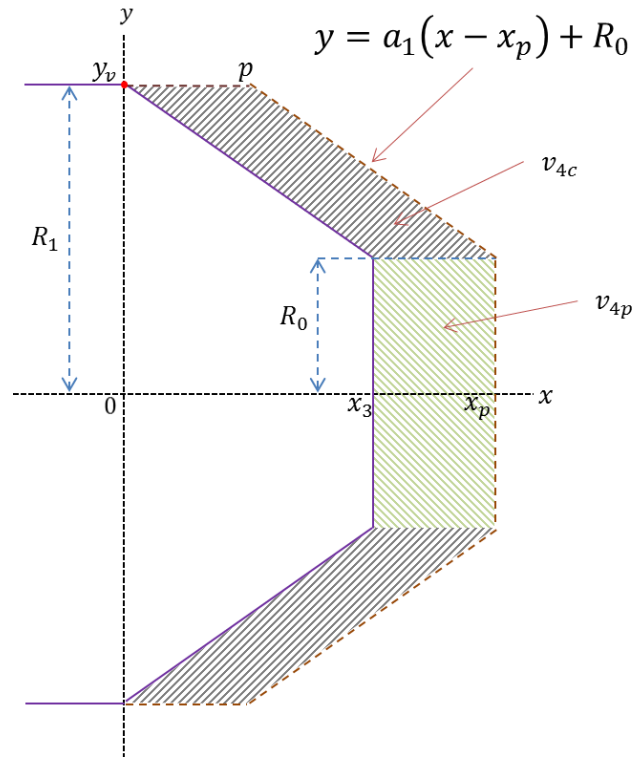


Figure 5-7: Material removal during Stage 4: $x_3 < x_p$

The cross-sectional area of material removed in this stage of drilling is shown hatched in Figure 5-7. The volume, V_{4c} , swept out by the cross-sectional area A_c is due to the cutting action; the volume, V_{4p} , by A_p is from the ploughing action. Applying equation 5-7 to these two areas and simplifying,

$$V_{4c} = \pi(x_p - x_3)(R_1^2 - R_0^2) \quad (5-23)$$

and

$$v_{4p} = \pi(x_p - x_3)R_0^2 \quad (5-24)$$

The total volume removed, after substituting in equations 5-23 and 5-24 and simplifying, is

$$V = V_{4c} + V_{4p} = \pi(x_p - x_3)R_1^2 \quad (5-25)$$

5.7 Summary

Drilling process has generally been considered as a continuous process and respective analysis were carried out accordingly; however, in the real world during the drilling process always uses spot-drill to produce a countersunk hole before start drilling, suggesting a step-wise process.

This significantly affects the thrust force tool experiences while going through the work-piece. Based on the multistep perspective this chapter develops the mathematic models for drilling process that describes thrust force variation not only the beginning but also the subsequent stages drilling tool goes through. On the other hand, parameters such as x_s , y_s , x_t and y_t were quantified as part of the construction of model, and could be adjusted individually for better process description.

Chapter 6:

Experimental and theoretical results of micro-drilling manufacturing

6.1 Introduction

In this chapter, experimental results are divided into few parts. Firstly, to study the characteristics of the thrust force signal from the drilling, it includes investigation on the different materials: Aluminium 6061T, Aluminium/Copper metal matrix alloy panel and Carbon Fibre reinforced plastic.

In each drilling analysis, the force signal is analyzed and compared with the driving units, such as drilling tool geometry (Table 4-4 and 4-5), cutting parameters (Table 4-1, 4-2 and 4-3) and drilling times. In this study, these results will be discussed particularly focusing on the early stages of drilling.

Furthermore, tool wear and drilling quality over different work-piece materials were analyzed using SEM images. Such SEM observation was focus on the tool cutting edge where the damage is thought to be more significant. Quality of the drilled work-piece was also analyzed based on the roundness and burr formation.

All the force data and diagram results are discussed in the following sections. Hopefully this would help to improve the understanding in drilling process, drilling tool life and product quality of micro-drilling manufacturing.

6.2 Force measurement

In this section drilling thrust force and force gradient were analyzed with three different materials: Aluminium 6061T, Aluminium/Copper metal matrix alloy panel and Carbon Fibre reinforced plastic. Due to the slight differences in cutting parameters, the discussion of results is also separated accordingly.

Experimental and theoretical of micro-drilling manufacturing

6.2.1 Aluminium 6061T work-piece

The drilling of Aluminium 6061T work-piece was conducted using high speed ball bearing spindle of KERN HSPC milling machine. As discussed in chapter 4, the cutting parameters can be found in Table 4-1. The force signal of each drilling process was recorded at a sampling rate of 25600 Hz and a 20X factor correction was applied in order to obtain the final thrust force value.

It should be mentioned that pecking actions of 50 μ m and 100 μ m were applied to Φ 0.2mm and 0.4mm drilling processes respectively. To reduce noise level, moving average of 3000 points was applied during the calculation of maximum thrust force and force gradient.

Figure 6-1 shows the thrust force data of 1st drilling with Φ 0.2mm drilling tool. The spindle feed rate and constant speed are 12 mm/min and 6000 rpm respectively. Short gap between each peak, seen in Figure 6-1, is thought to be caused by the applied pecking action.

The main reason of using the pecking action in the Φ 0.2 mm drilling process is to avoid the total failure of drilling tool, which was found likely to happen without pecking action.

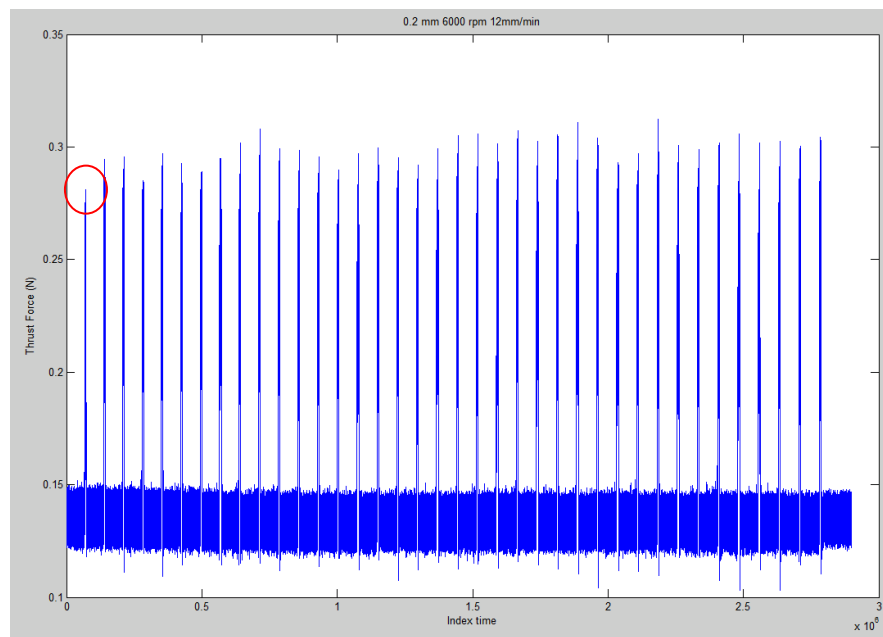


Figure 6-1: Force signal of the 1st drilling process of Φ 0.2mm drilling tool and Al work-piece

Experimental and theoretical of micro-drilling manufacturing

Figure 6-2 shows the signal of first pecking marked in Figure 6-1. It is clear to see the thrust force was increasing with index time since the drilling tool began to contact the Al work-piece until the first pecking action was finished.

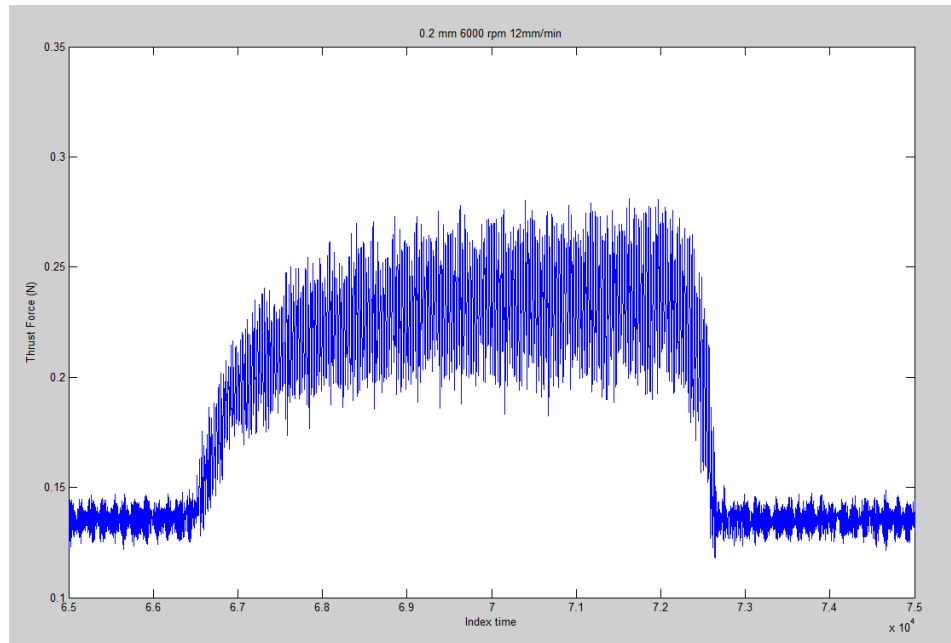


Figure 6-2: Force signal of 1st pecking action of Φ 0.2mm drilling

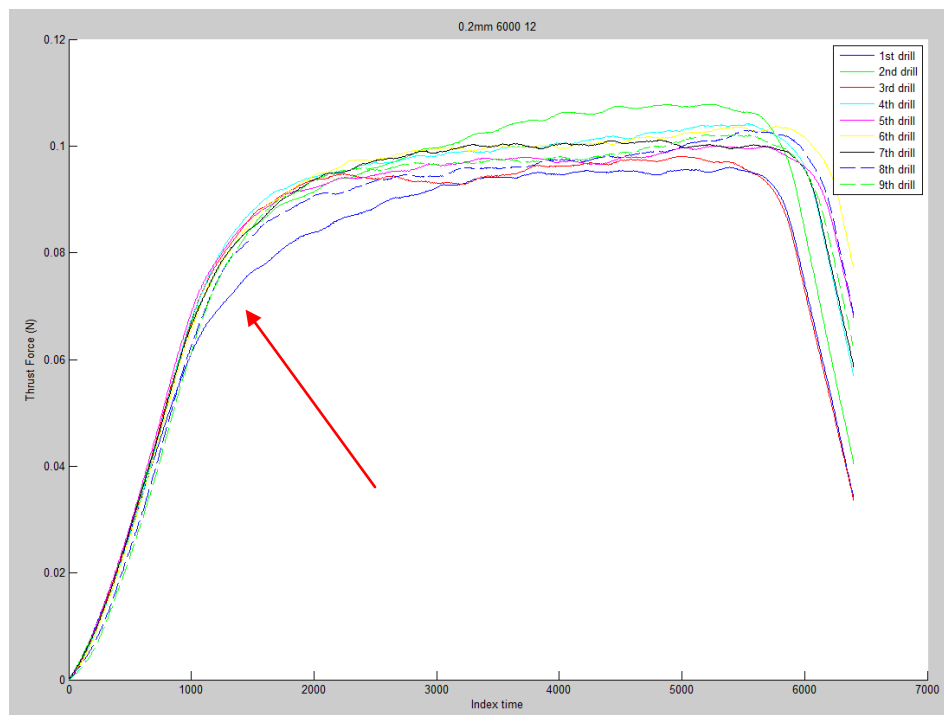


Figure 6-3: Thrust forces of all 1st pecking with Φ 0.2mm tool on Al work-piece

Experimental and theoretical of micro-drilling manufacturing

Figure 6-3 shows the comparison of the 1st pecking thrust force of the total 9 drilling processes on Al work-piece. In this test the thrust force was recorded at 12mm/min feed rate and 6,000 rpm using Φ 0.2mm drilling tool. After total 9 drilling processes, the each 1st pecking data was corrected by applying the moving average with 1,000 points.

From the Figure 6-3, it is clear to see the thrust force was increasing rapidly between the beginning and index time 1,000. After index time 1,000, the gradient of thrust force gradually decreased, then stabilized and finally declined rapidly at index time 5,500.

Note the force difference in Figure 6-3 between the marked signal (1st drill) and the rest. This is thought to be caused by the drilling tool sharpness at the beginning and the possible dulling effect due to the further use of drilling tool.

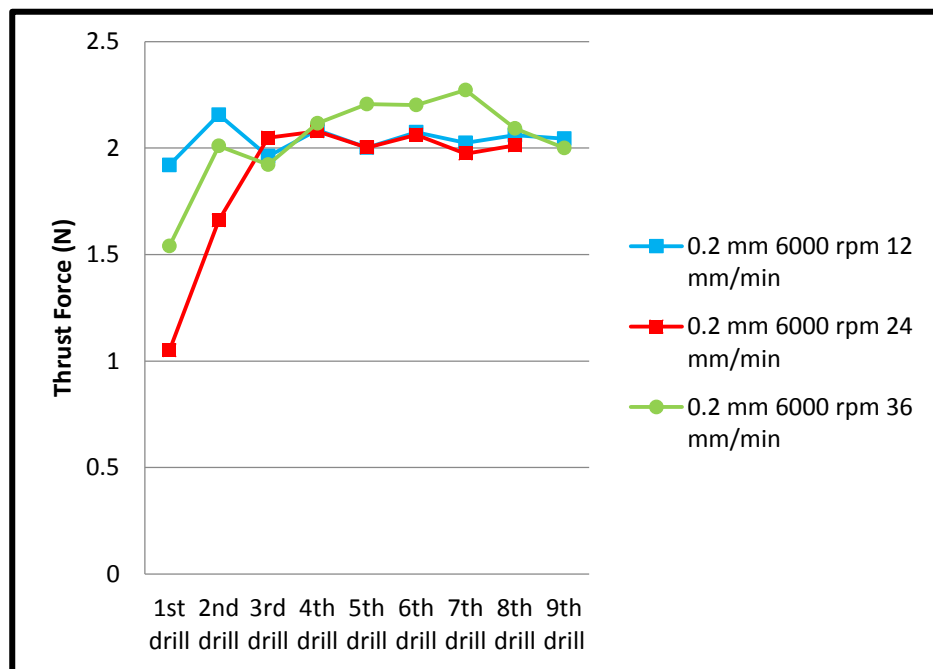


Figure 6-4: Thrust force comparison over different feed rates of 1st pecking with Φ 0.2mm tool on Al work-piece

Figure 6-4 shows the variation in average thrust force caused by different feed rates with 0.2mm drilling tool. It is interesting to see, in Figure 6-4, 12mm/min feed rate shows the highest thrust force during the first two drilling processes.

Experimental and theoretical of micro-drilling manufacturing

A possible reason is chips accumulated in the vicinity of tool lip and cutting edge of drilling tool may cause serious damage at the beginning of the 12mm/min feed rate drilling process. This leads to a higher maximum thrust force value than other two feed rate settings. As to the rest of the signals, it was found the maximum thrust force between 3rd and 9th drilling process maintained stable and no significant variation appears to be caused by different feed rates.

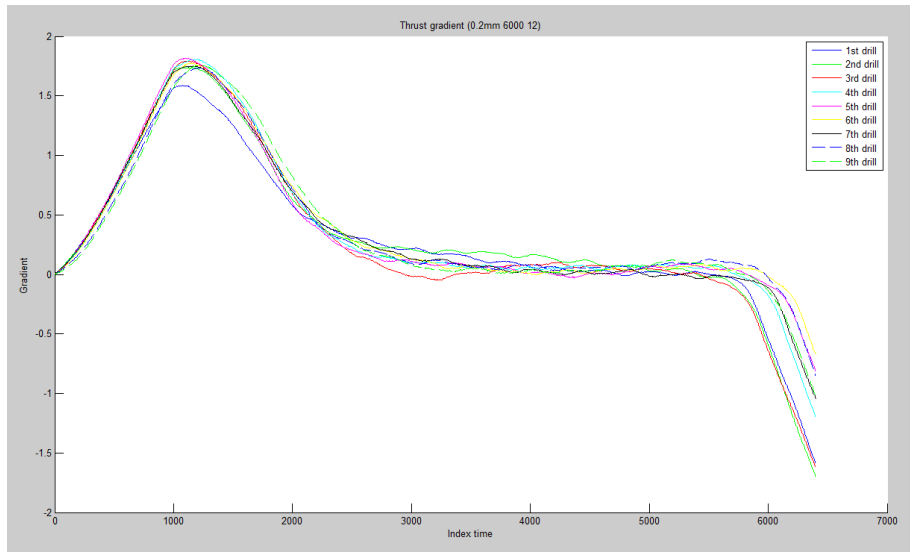


Figure 6-5: Force gradients of all 1st pecking with 0.2mm tool on Al work-piece

Figure 6-5 shows the force gradients of 1st pecking of total 9 drilling processes at 12mm/min feed rate, 6000 rpm speed and 0.2mm drilling tool. In Figure 6-5, the maximum gradient was found at index time 1000 and all 9 drilling processes share the similar trend, which is thought due to the 50 μ m pecking action.

Following the same difference seen in Figure 6-3, force gradients in Figure 6-5 also show similar behaviour that can be explained by the chip accumulation described earlier.

Figure 6-6 shows the effect of different feed rates on the force gradients of total 9 drilling processes on Al work-piece, showing a typical trend that is clearly influence by the various feed rates.

An interesting point found is the maximum gradient values of 12mm/min feed rate are quite similar throughout the total 9 drilling processes, and is not shared by the

Experimental and theoretical of micro-drilling manufacturing

drilling processes of 24 and 36 feed rates. This also means for the Φ 0.2 mm tool and 6000 rpm drilling process the force gradient of 12 mm/min feed rate is more stable than the rates of 24 or 36 mm/min.

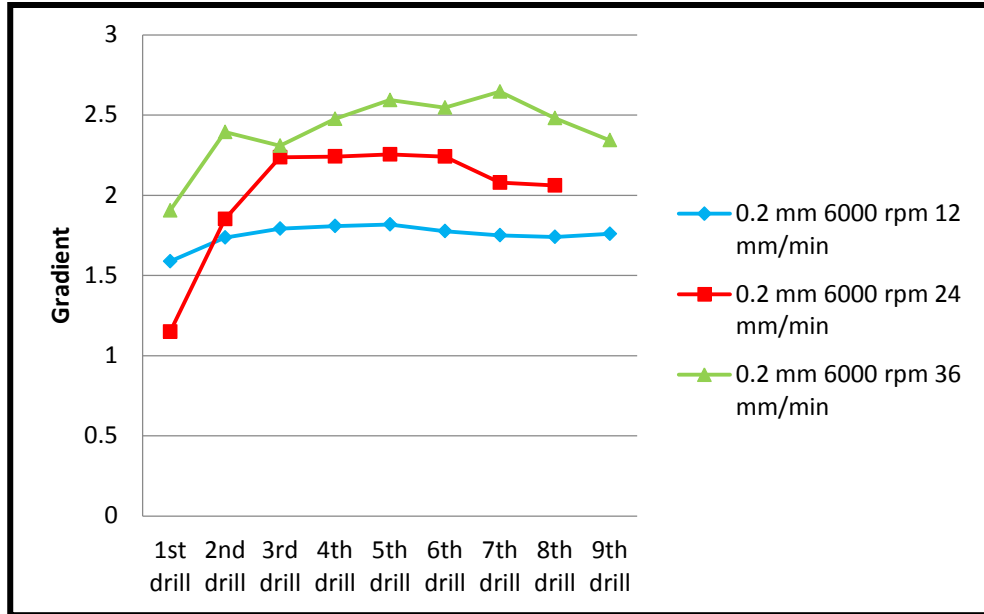


Figure 6-6: Force gradients comparison over different feed rates of 1st pecking with Φ 0.2mm tool on Al work-piece

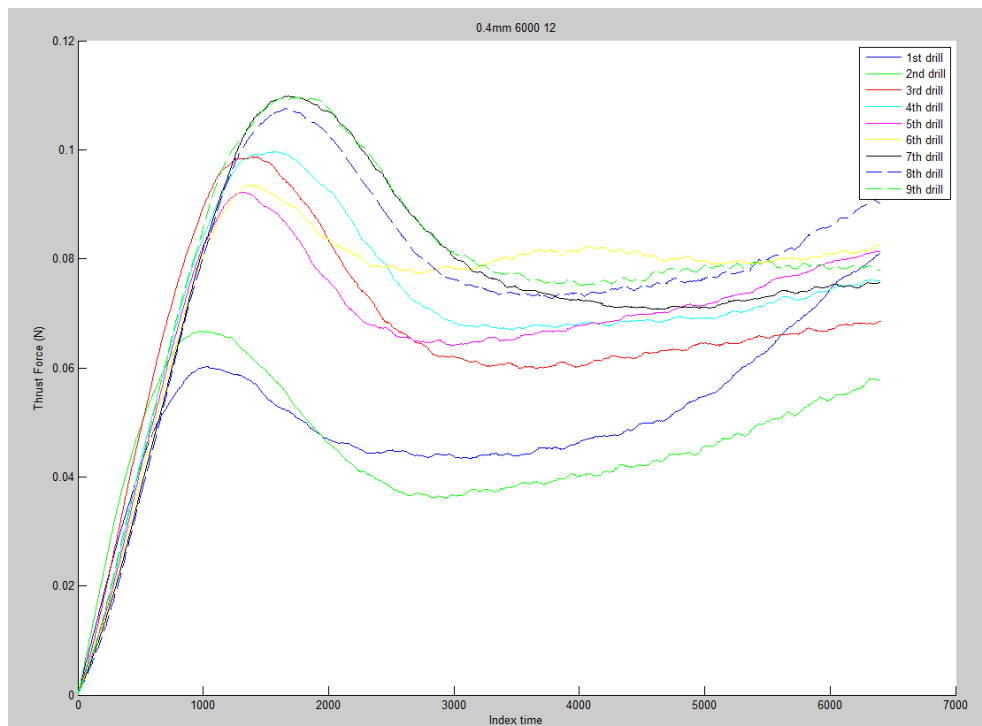


Figure 6-7: Thrust Force of all 1st pecking with Φ 0.4mm tool on Al work-piece

Experimental and theoretical of micro-drilling manufacturing

Figure 6-7 shows the thrust forces of the 1st pecking actions of all total 9 drilling processes. In this test the thrust force was recorded at 12mm/min feed rate, 6000 rpm and by 0.4mm drilling tool.

After 9 drilling processes, the data of 1st pecking actions were corrected by applying moving average with 1000 points and resulted in Figure 6-7, in which the maximum thrust force increases with the number of the drilling processes.

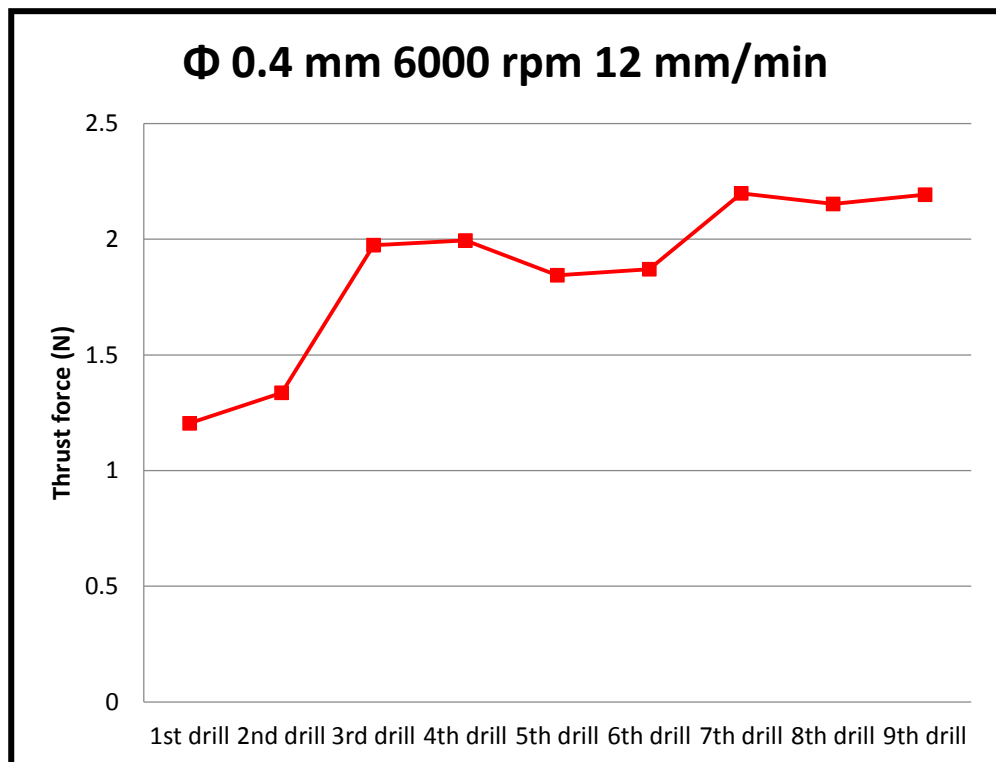


Figure 6-8: Variation of maximum thrust force over 9 drilling processes on Al work-piece with drilling parameters: Φ 0.4mm drilling tool, 6000 rpm, 12mm/min feed rate.

Figure 6-8 shows the Variation of maximum thrust force over 9 drilling processes on Al work-piece with the selected parameters. It can be seen that the thrust force gradually increases with the number of drilling process but not at significant amount. This is most likely due to the damage in cutting edge over repeated use although the damage is not enough to cause total failure.

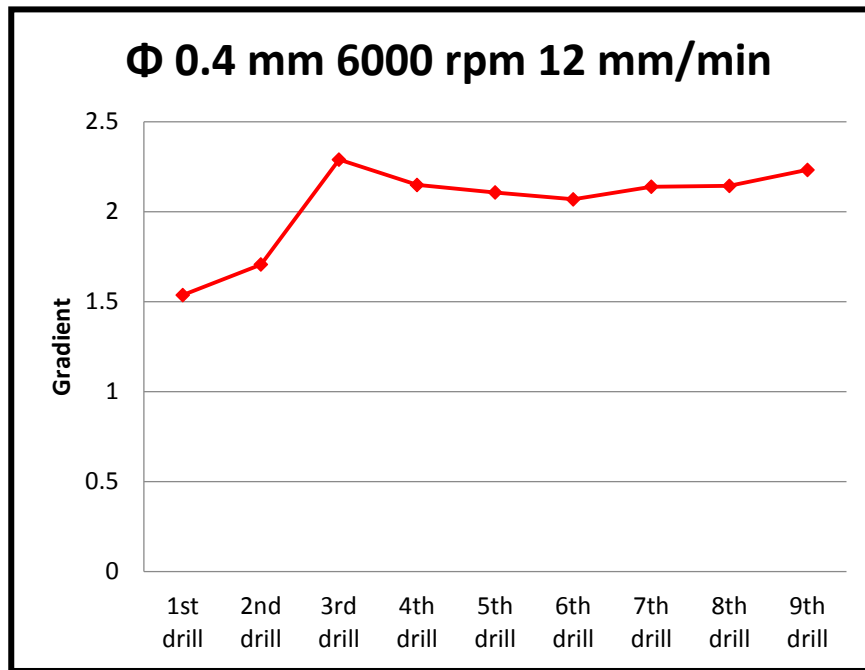


Figure 6-9: Variation of maximum force gradient over 9 drilling processes on Al work-piece with drilling parameters: Φ 0.4mm drilling tool, 6000 rpm, 12 mm/min feed rate.

Figure 6-9 shows the variation of maximum force gradient over 9 drilling processes on Al work-piece with the selected parameters. Unlike the previous case the first 3 drilling processes show significant gradient increase but level off from the 4th drilling process. The most probable explanation is that the cutting edge of tool was gradually worn and resulted in stable force gradient value.

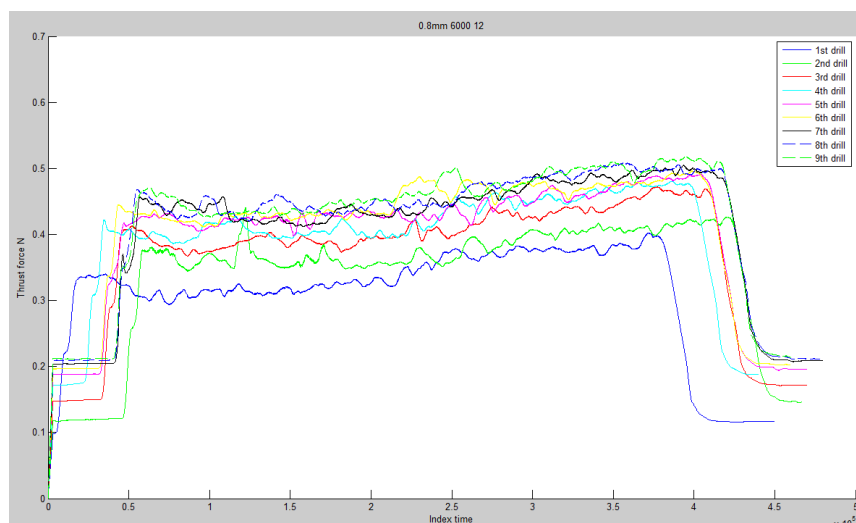


Figure 6-10: Variation of thrust force over 9 drilling processes on Al work-piece with drilling parameters: Φ 0.8mm drilling tool, 6000 rpm, 12 mm/min feed rate

Experimental and theoretical of micro-drilling manufacturing

Figure 6-10 shows Variation of thrust force over 9 drilling processes on Al work-piece with the selected parameters. Unlike the case with 0.2mm and 0.4mm drilling tool, the drilling process by 0.6mm, 0.8mm and 1.0mm did not involve pecking action. Due to the absence of pecking action a different correction involving moving average of 3000 points had to be used for the 0.8 mm drilling process.

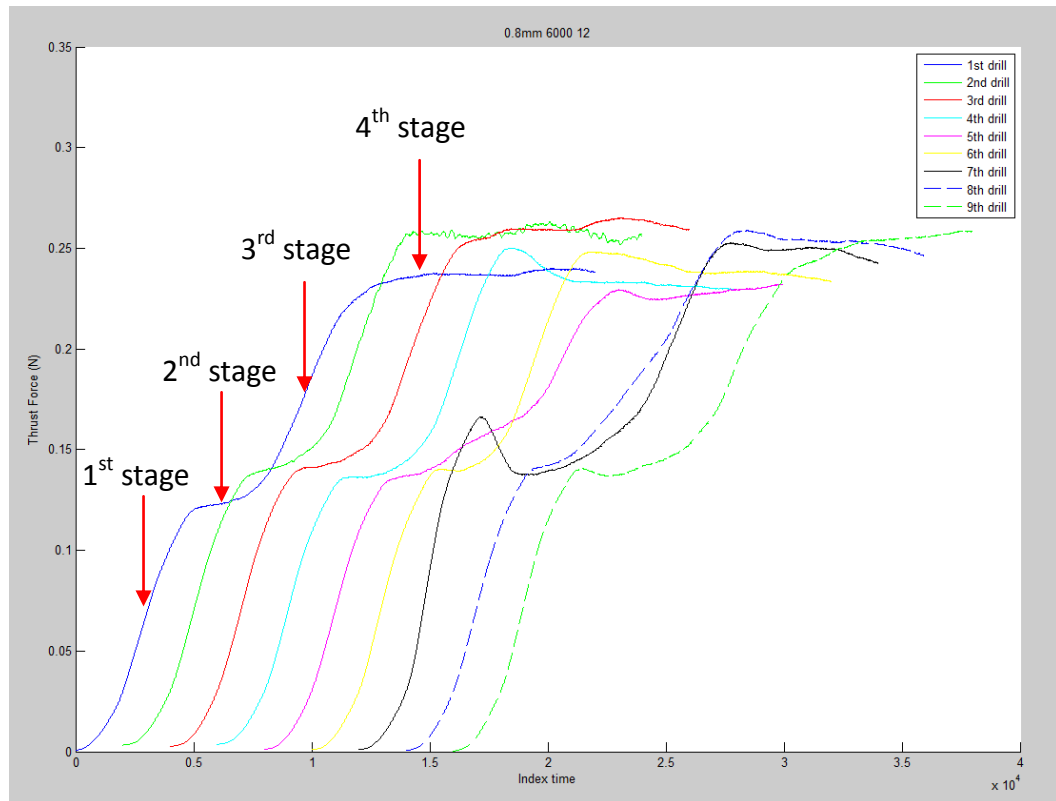


Figure 6-11: Section between index time 0 and 100000, extracted from Figure 5.10

It can be seen the thrust force in Figure 6-11 increases rapidly at the beginning of drilling process. This particular section, between index time 0 and 100000, was used for subsequent analysis and the extraction can be seen as Figure 6-11.

A clear four stage variation in thrust force matches the description in Chapter 5 that represents the four stages at the beginning of drilling process. The thrust force was then converted into force gradient, as Figure 6-12 shows.

Experimental and theoretical of micro-drilling manufacturing

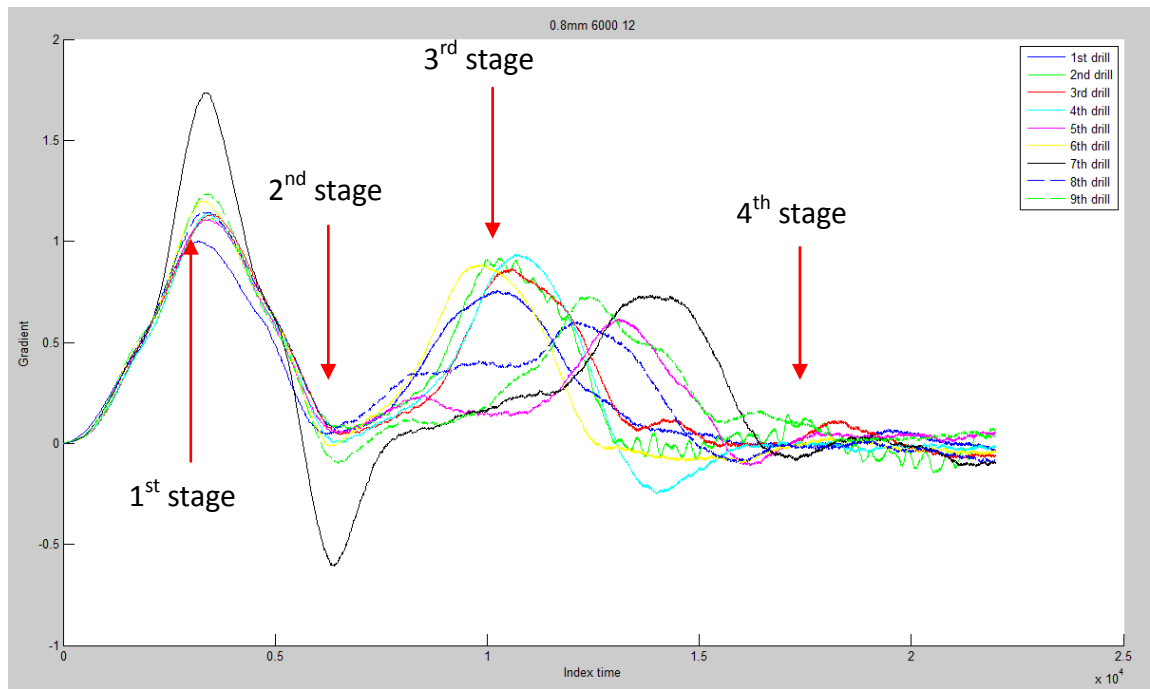


Figure 6-12: Variation of force gradient over 9 drilling processes on Al work-piece with drilling parameters: Φ 0.8mm drilling tool, 6000 rpm, 12 mm/min feed rate

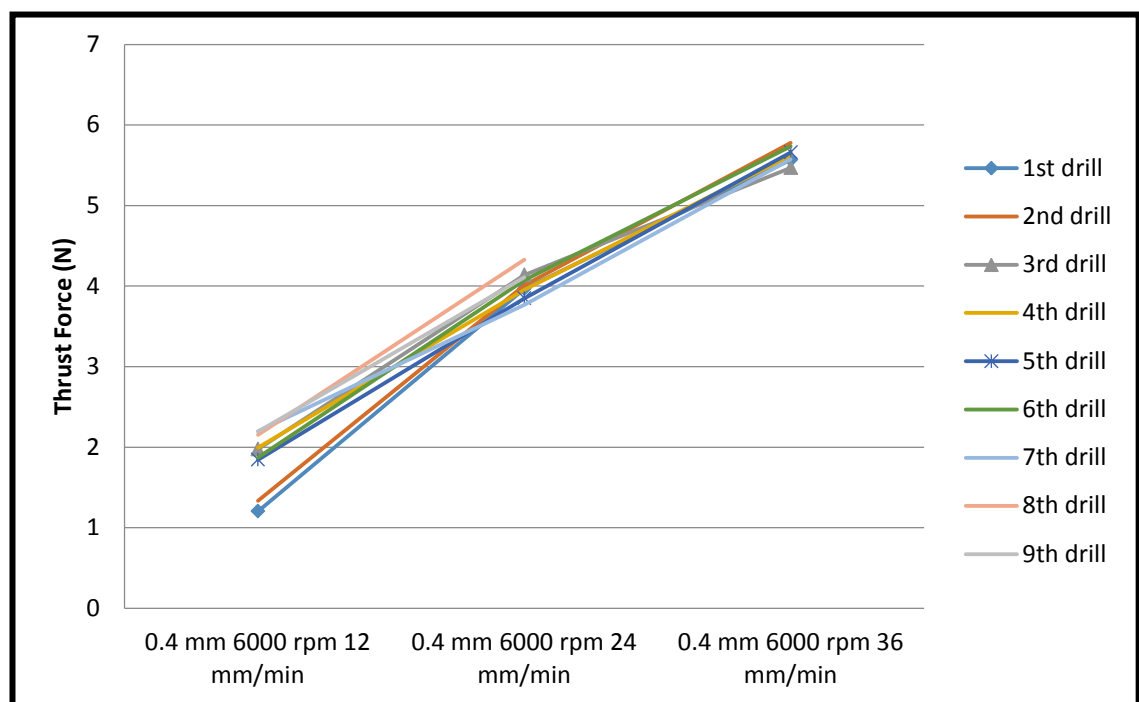


Figure 6-13: Influence of feed rates on thrust force over 9 drilling processes on Al work-piece with drilling parameters: Φ 0.4mm drilling tool, 6000 rpm

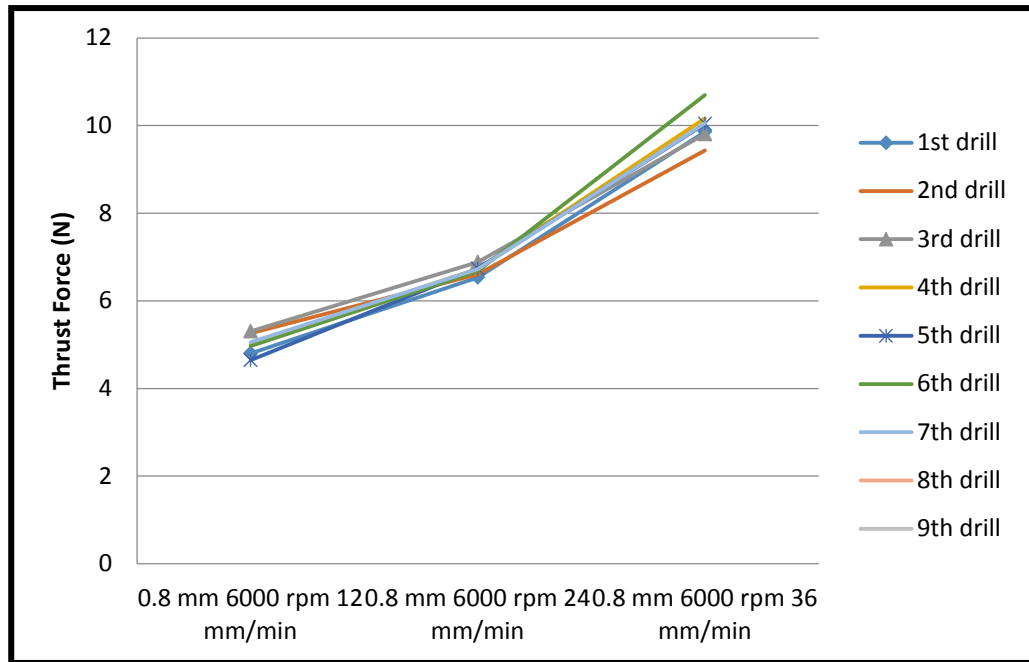


Figure 6-14: Influence of feed rates on thrust force over 9 drilling processes on Al work-piece with drilling parameters: 0.8mm drilling tool, 6000 rpm

Figure 6-13 and 6-14 show the influence of feed rates on thrust force over 9 drilling processes on Al work-piece with drilling selected parameters. Clearly thrust force is proportional to feed rate and the influence is not only significant to 0.8mm drilling tool but also to all other tools used in this research.

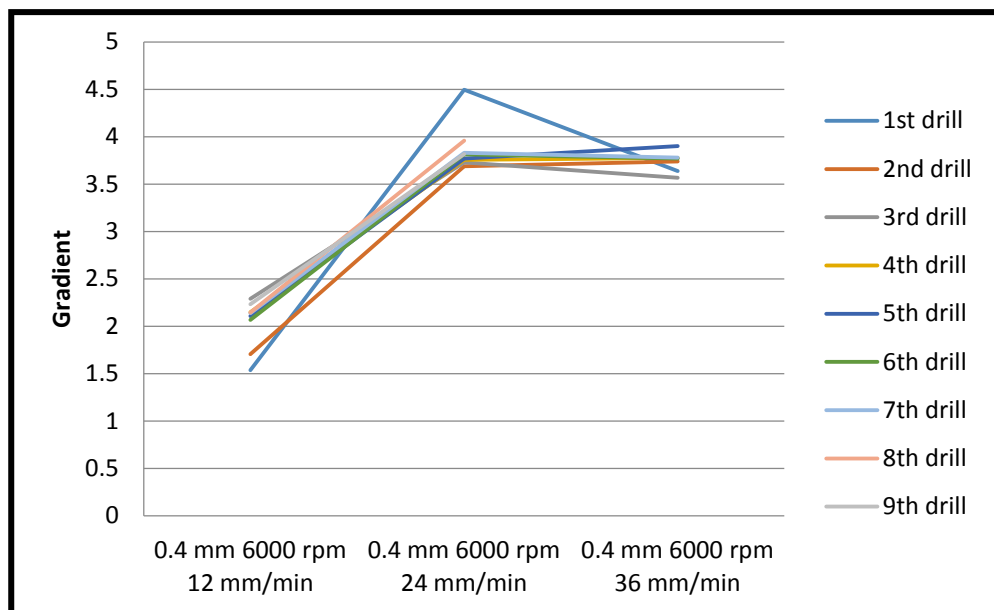


Figure 6-15: Influence of feed rates on force gradient over 9 drilling processes on Al work-piece with drilling parameters: Φ 0.4mm drilling tool, 6000 rpm

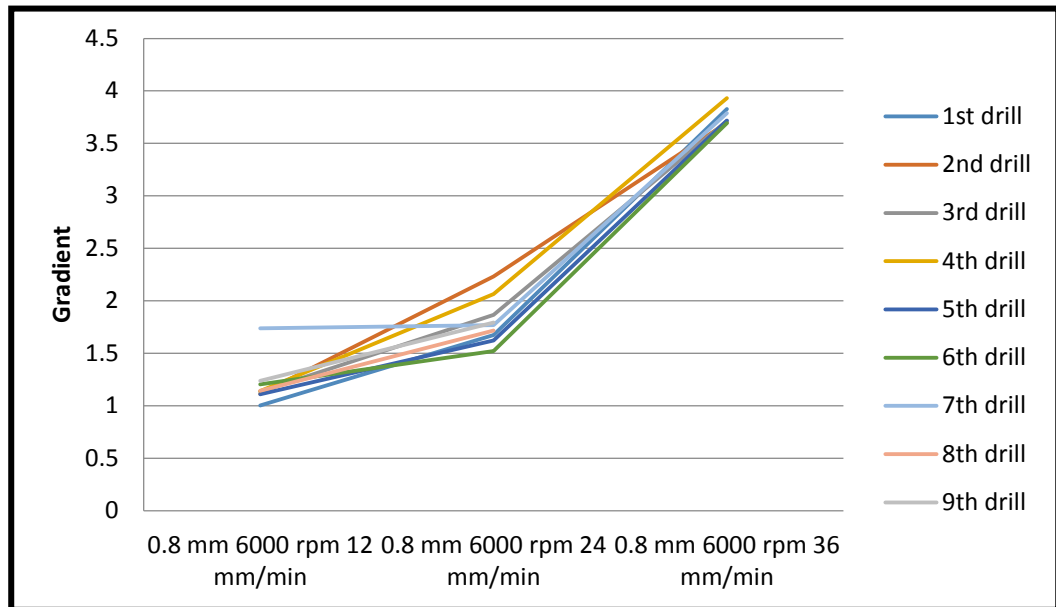


Figure 6-16: Influence of feed rates on force gradient over 9 drilling processes on Al work-piece with drilling parameters: Φ 0.8mm drilling tool, 6000 rpm

Figure 6-15 and 6-16 show the influence of feed rates on thrust force over 9 drilling processes on Al work-piece with drilling selected parameters. Feed rate variations influence force gradient in the way that is very similar to the case of thrust force, which points at the significant effect of feed rate.

However, in the cases of 0.2mm and 0.4mm drill tools there was no significant maximum force gradient difference between 24mm/min and 36mm/min feed rate. This suggests for both feed rates the increases in thrust force during the first and second stage of drilling process are very similar.

Figure 6-17, 6-18 and 6-19 show the influence of drilling tool size on thrust force over 9 drilling processes on Al work-piece with drilling selected parameters. It is apparent in all figures that thrust force increases proportionally to drilling tool size.

Although the repeated use of drilling tool does affect thrust force, its influence was found to be insignificant comparing to the effects caused by tool dimension and feed rate. This trend can be seen in all figures that thrust force has a clear dependency on drilling tool size although less apparent with the case of 0.2mm.

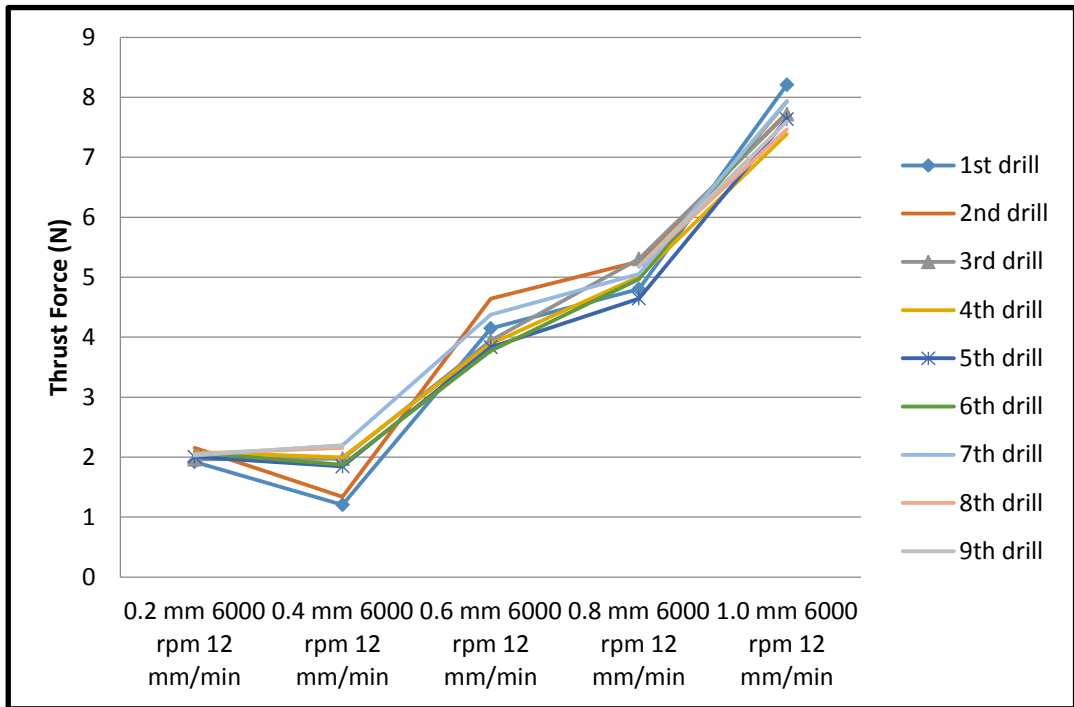


Figure 6-17: Influence of drilling tool size on thrust force over 9 drilling processes on Al work-piece with drilling parameters: 6000 rpm, 12/min feed rate

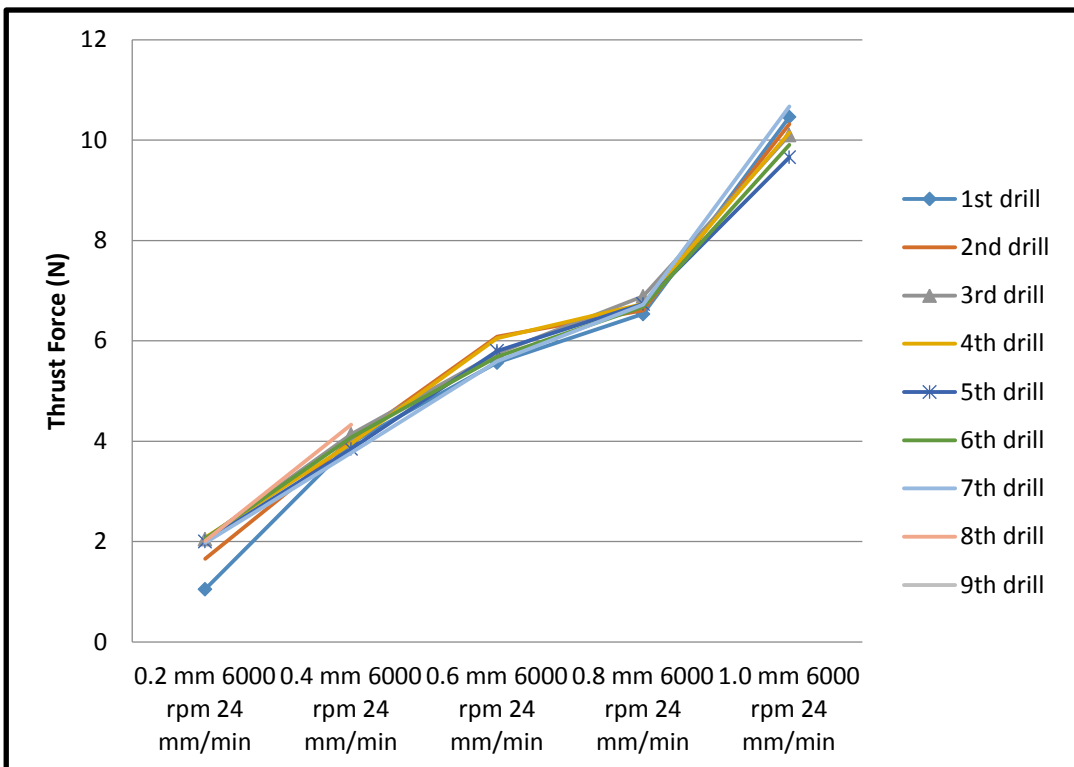


Figure 6-18: Influence of drilling tool size on thrust force over 9 drilling processes on Al work-piece with drilling parameters: 6000 rpm, 24/min feed rate

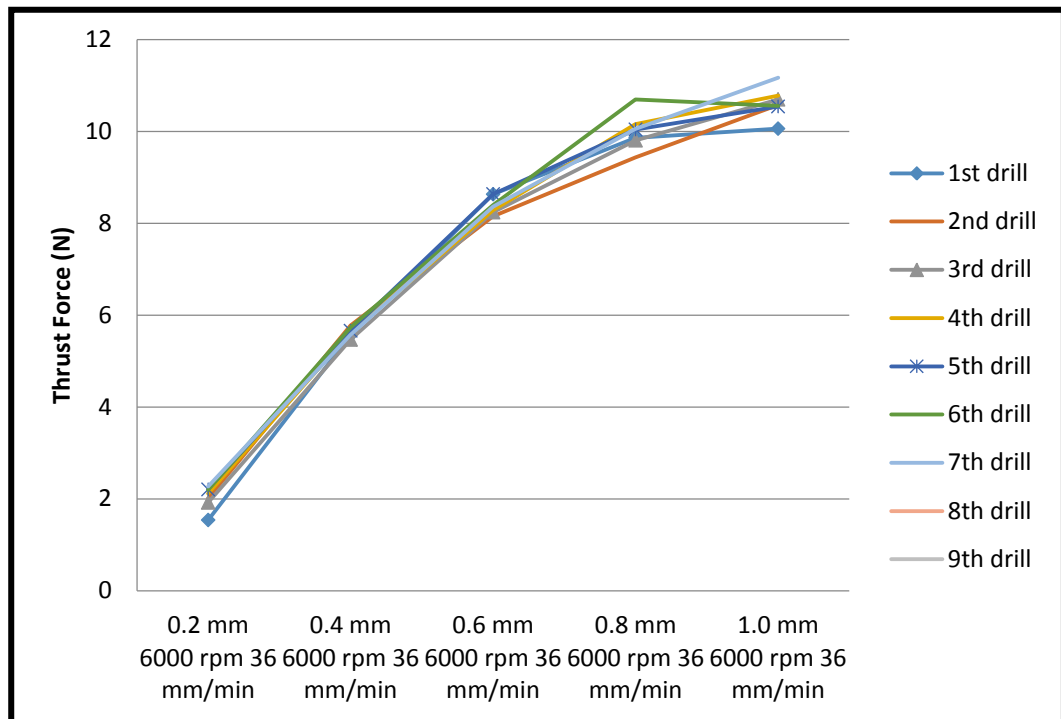


Figure 6-19: Influence of drilling tool size on thrust force over 9 drilling processes on Al work-piece with drilling parameters: 6000 rpm, 36/min feed rate

6.2.2 Al/Cu metal alloys

As shown in Figure 6-20, 3 repetitions were carried out for the drilling processes with 9000 rpm and 12000 rpm and 9 repetitions were done with the 6000 rpm drilling process. All data were recorded at a sampling rate of 51200 Hz with a 20x correction in order to obtain the true value. All the drilling data analyzed was corrected by the moving average of 6000 points in order to reduce the noise level and analyzed by MATLAB R2014a so the maximum thrust force and force gradient can be obtained.

Figure 6-20 shows the effect of spindle speed on thrust force during the drilling process with Al/Cu metal alloys work-piece. Figure 6-20 shows the thrust force increases with the spindle rotation speed, which means higher rotation speed results in the increase of thrust force. Another point can be noticed is that thrust force also increases with the repeating drilling processes.

The blue line in Figure 6-20 is a good example for this trend, which shows a 3-fold increase in the thrust force of 9th drilling process comparing to the much lower value

Experimental and theoretical of micro-drilling manufacturing

with the 1st drilling process. This is a clear difference found between the aluminum test and Al/Cu metal alloys test.

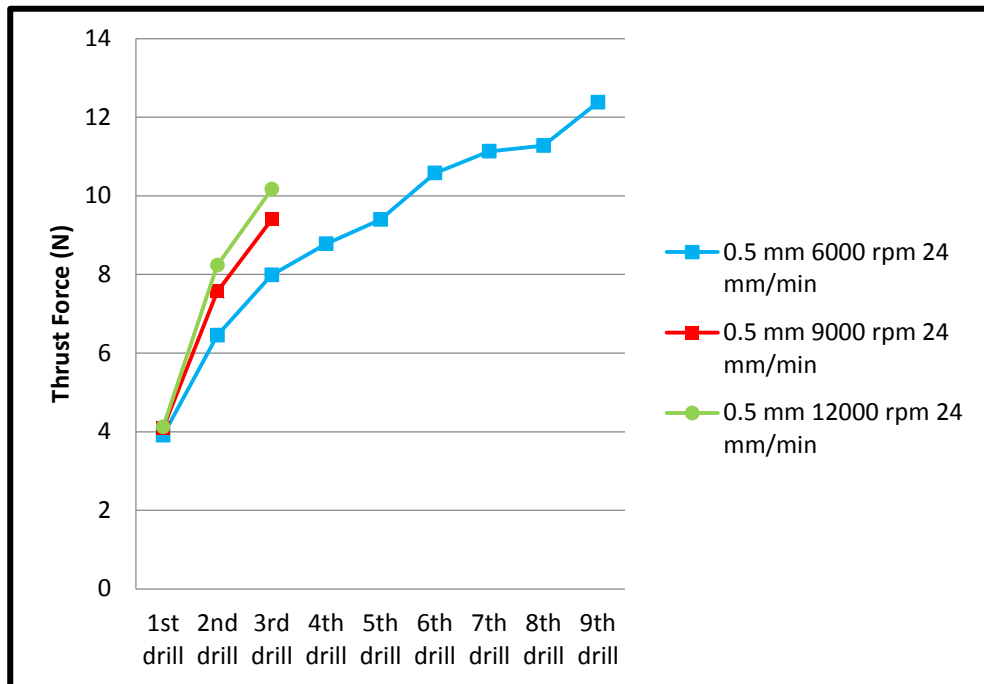


Figure 6-20: Influence of rotation speed on thrust force on Al/Cu metal alloys work-piece with drilling parameters: Φ 0.5mm drilling tool, 24/mm feed rate

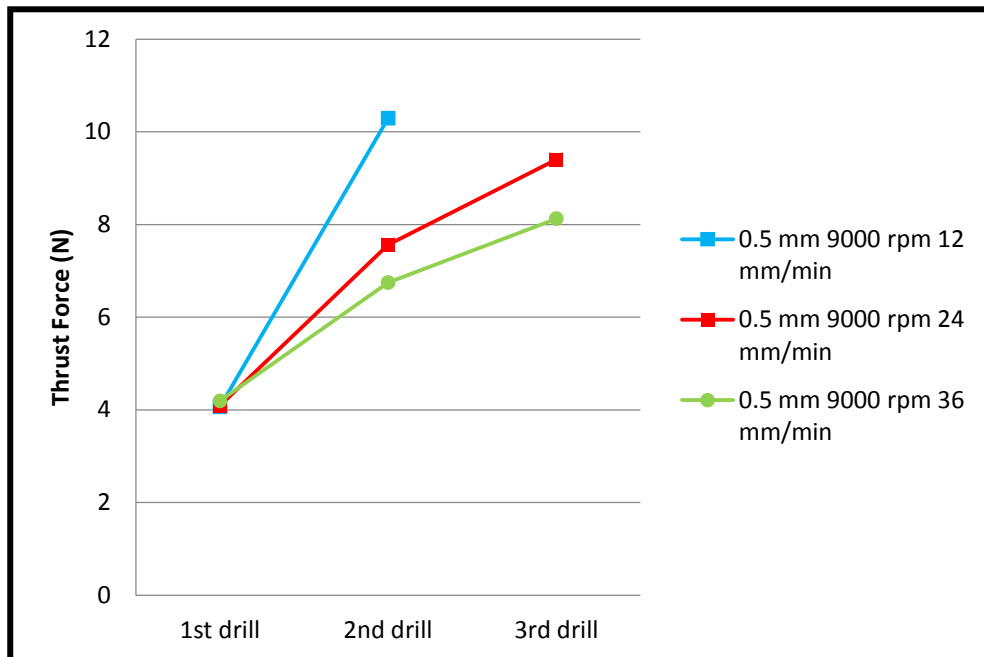


Figure 6-21: Influence of feed rate on thrust force on Al/Cu metal alloys work-piece with drilling parameters: 0.5mm drilling tool, 9000 rpm

Experimental and theoretical of micro-drilling manufacturing

It is worth mentioning that in Figure 6-21 the drilling process with lower feed rate resulted in higher thrust force readings, and higher feed rate ended up with less thrust forces. One of the possible reasons is that this was most likely to be caused by the related temperature differences. This is due to the absence of liquid coolant for Al/Cu metal alloy drilling processes, and naturally more friction resulted in higher temperature.

Similarly, this phenomenon can be found in Figure 6-21, in which the lower drilling feed rate led to longer drilling process and increased temperature. As the drilling process was repeated this heating effect became even more significant for the setup with lower feed rate. It was this high temperature that caused the chips to attach to the cutting edge and resulted in the increase of thrust force.

Figure 6-22 shows the maximum force gradient keeps growing with the repetition of drilling process. As the gradient describes the frictional force, it was found with a brand new drill tool the first drill gives much lower gradient than the subsequent drills. This difference is further compounded by increasing drilling rate as the higher the rate gets the higher frictional force gradient becomes.

In the meantime it was also noticed the duration of drilling time influences chip attachment significantly. With chips attached to the drill tool it is thought to have a further compounding effect on the increase of frictional force gradient.

The combined effect of brand new drill tool and drilling time duration suggests the quality/finishing of drill tool itself caused all the difference, most likely due to the wear/damage takes place during the first drilling process. Such wear or damage resulted in potentially rougher surface as well as slight difference in tool geometry; both have known significant connection to the outcome of drilling process.

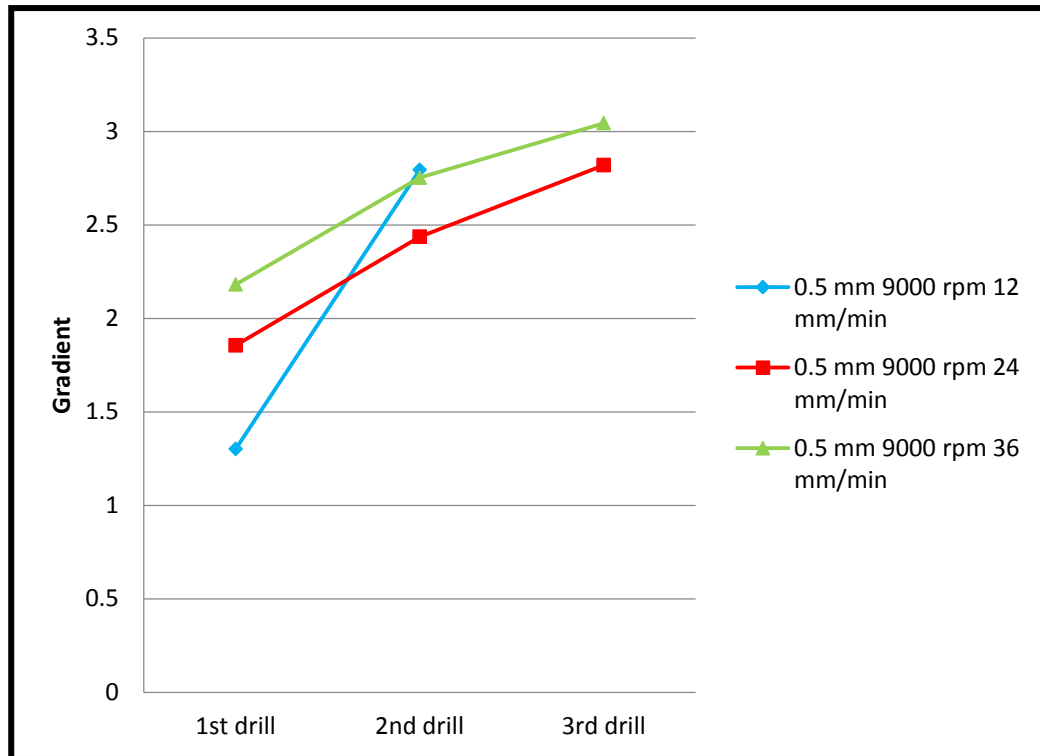


Figure 6-22: Influence of feed rate on gradient on Al/Cu metal matrix work-piece with drilling parameters: Φ 0.5mm drilling tool, 9,000 rpm

6.2.3 Carbon fibre reinforced composites

The drilling process on Carbon Fibre reinforced composites was conducted on ultra-high speed air bearing spindle, the cutting parameters can be found in Table 4-3. The force signal reading was recorded for the total 10 drilling processes at the sampling rate of 51,200 Hz.

All recorded data was corrected by the moving average of 6,000 points to reduce the noise level and analyzed in MATLAB R2014a in order to obtain the maximum thrust force.

Figures 6-23 and 6-24 show the effect of the feed rate and the spindle speed on the average thrust force. A clear trend can be found in Figure 6-23 showing the averaged thrust force increases with the feed rate at the set constant spindle speed of 20k rpm.

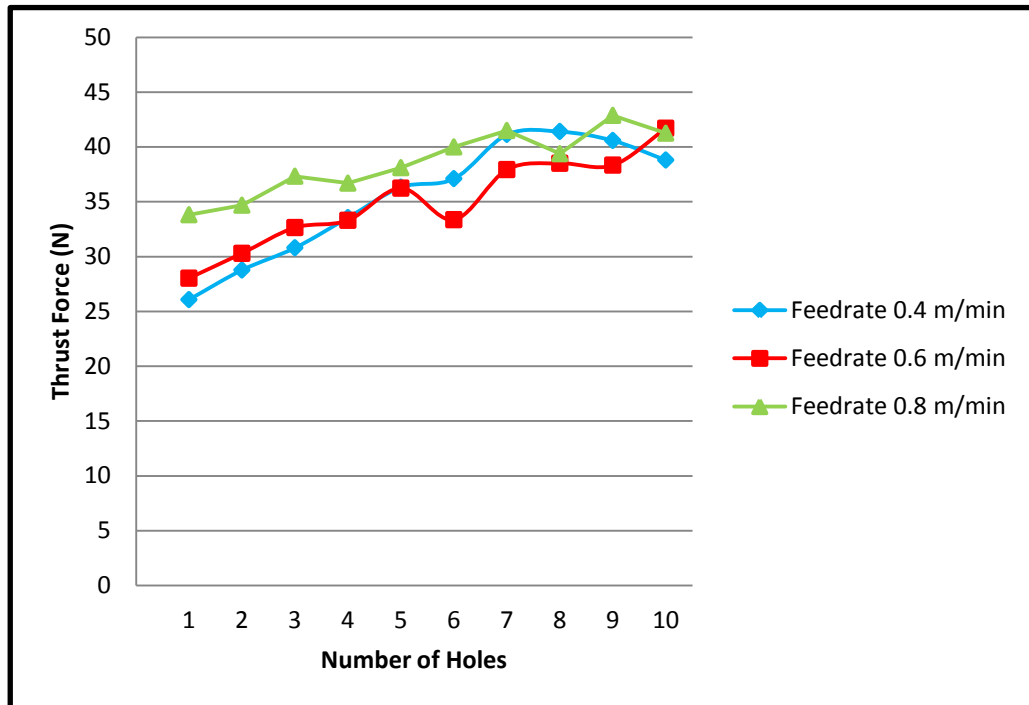


Figure 6-23: Comparison on the averaged thrust force with three levels of feed rate (0.4, 0.6 and 0.8 m/min) at a constant spindle speed of 20k rpm

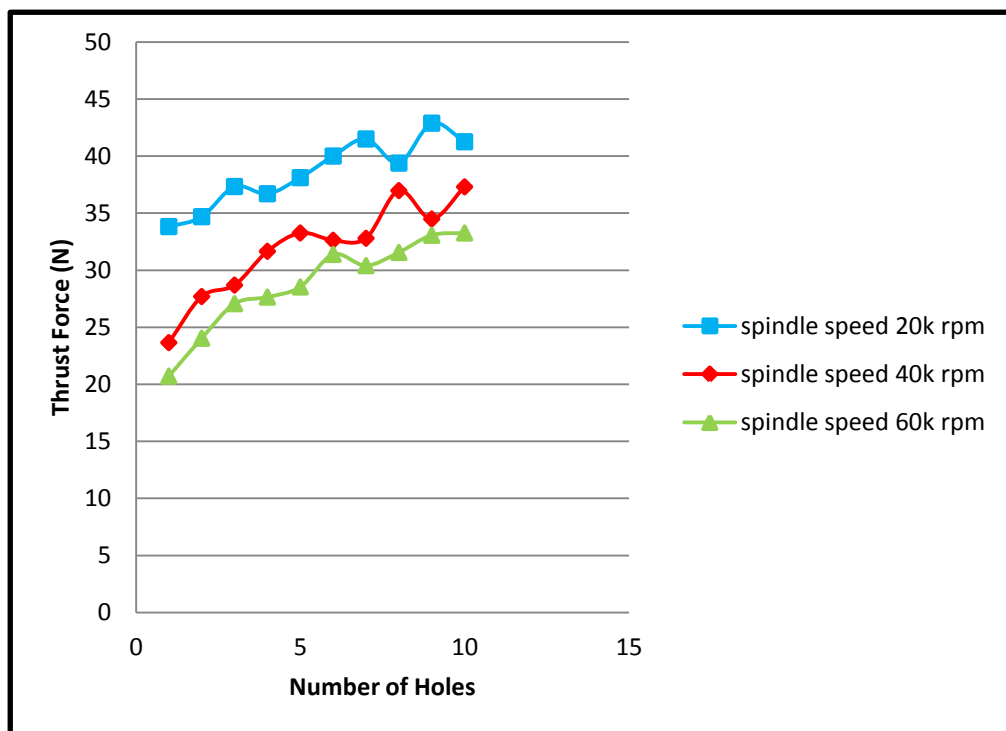


Figure 6-24: Comparison on the averaged thrust force with three levels of spindle speed (20k, 40k and 60k rpm) at a constant feed rate of 0.8 m/min.

Experimental and theoretical of micro-drilling manufacturing

This is primarily due to the fact that both the spindle speed and the feed rate chosen are relatively high compared the ones used in the low speed drilling, which leads the cutting process to be more dominant rather than mechanical push down force, whereas the latter is primarily responsible to the delamination.

To oppose the effect of the feed rate, the averaged thrust forces noticeably decrease with the spindle speed at a constant feed rate of 0.8 m/min as shown in Figure 6-24 due to the reduction of chip load. Thus, adopting the air bearing spindle to advance the spindle speed, a higher feed rate can be achieved without increasing the averaged thrust force during drilling.

6.3 Hole quality and tool wear

Significant tool wear could occur during the drilling process regardless the numbers of drilling or parameter settings; however, such wear can be observed by SEM imaging. This section will use the SEM images to compare the true circle and finished products so the quality of drilling process can be established.

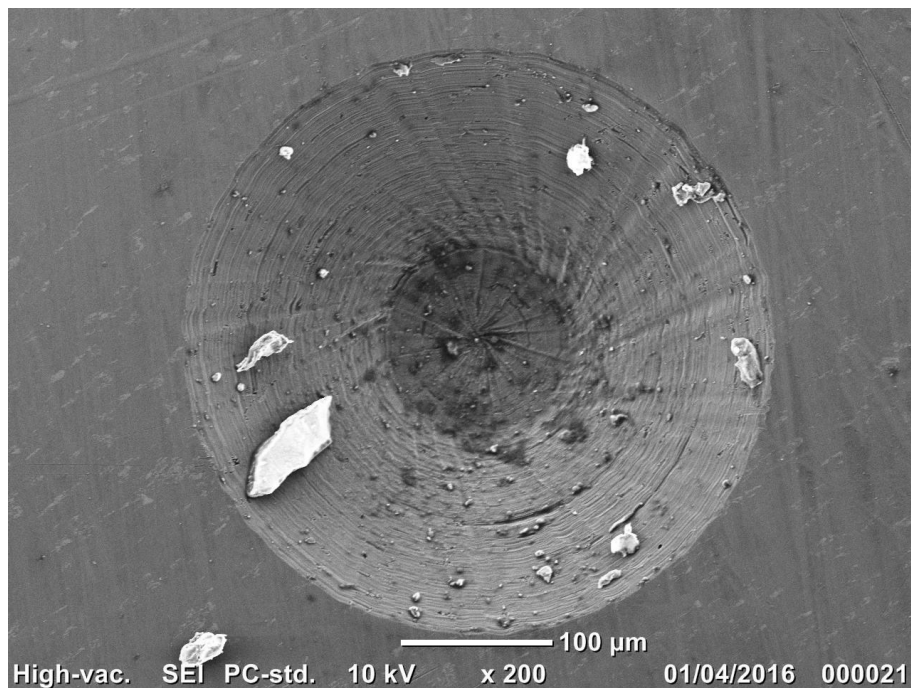


Figure 6-25: Countersink in Al work-piece

Experimental and theoretical of micro-drilling manufacturing

Figure 6-25 shows the countersink by spot drill on the aluminium work-piece. Two circular areas of the countersink can be seen clearly in Figure 6-25. The inner circular area was made by web of drilling tool and outer one was formed by the cutting lip.

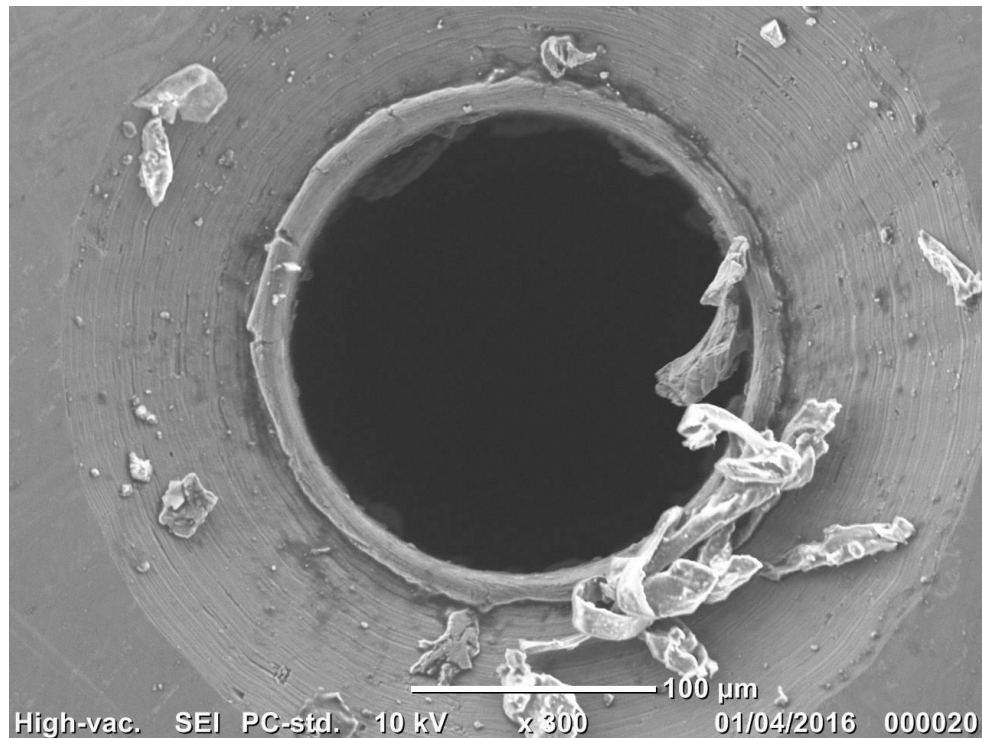
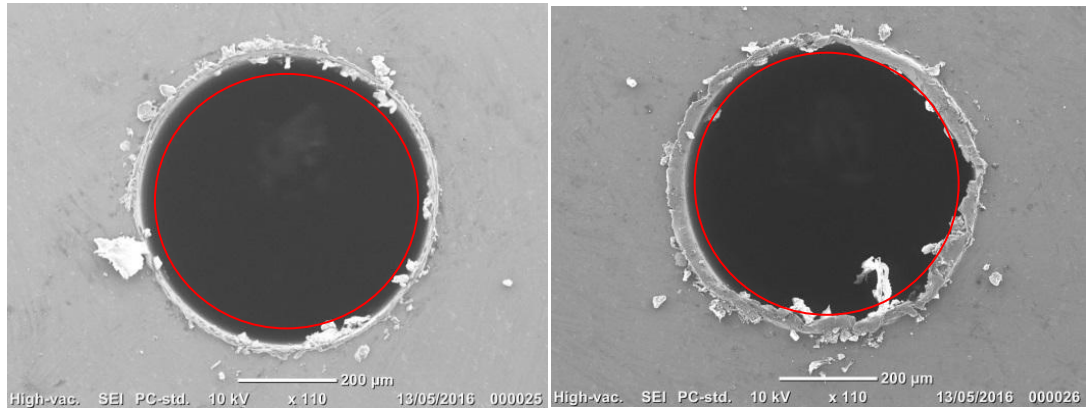


Figure 6-26: Φ 0.2mm drilled in Al work-piece entry side

Figure 6-26 shows the entry side of drilling product done by the 0.2mm tool on the aluminium work-piece. Due to the drilling tool diameter is smaller than the countersink diameter, it resulted in residual traces of countersink around of 0.2mm drilling. Furthermore, at the end of drilling, there is a build-up of chips around the cutting lips but with fewer chips attached to the edge of the hole.

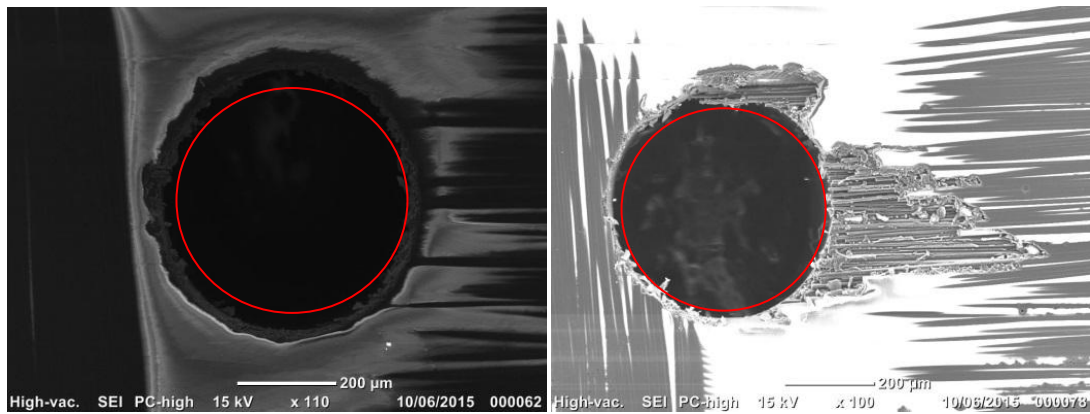
Figure 6-27 shows the entry and exit side of 0.6mm drilling process on the aluminium work-piece and the red circle marks the true circle of the drill tool. By comparing the images it was found although the entry hole in Figure 6-27(a) shows a good match, a slight shift to the right can be seen in the exit hole in Figure 6-27(b). Furthermore, it was also found generally speaking the build-up of chips is more significant on the exit side than the entry side.



(a)

(b)

Figure 6-27: Φ 0.6mm drilled in Al work-piece entry and exit side



(a)

(b)

Figure 6-28: Φ 0.5mm drilled in Carbon fibre reinforced composite entry and exit side

Figure 6.28 shows the entry and exit side of 0.5mm drilling process on the Carbon Fibre reinforced plastic and the red circle marks the true circle of the drill tool. No clear difference was found between entry and exit holes although some build-up of chips can be seen in Figure 6.28(a).

As to the exit hole in Figure 6.28(b), clear build-up of chips can be seen but also with significant damages to the fibres at the surfaces next to the hole.

Experimental and theoretical of micro-drilling manufacturing

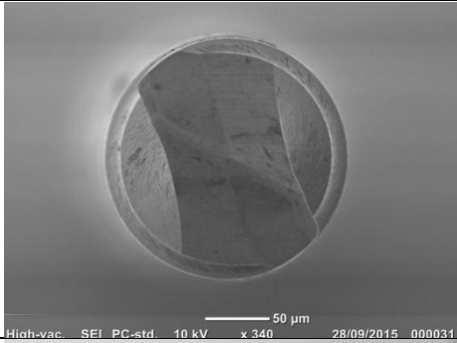
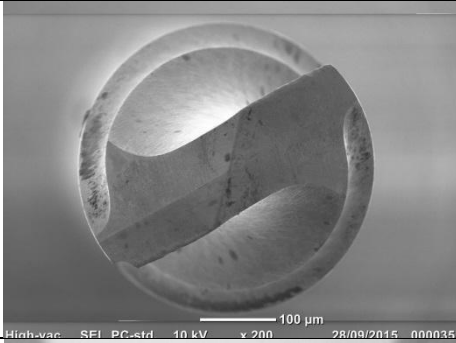
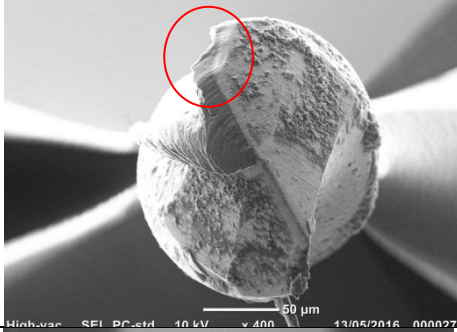
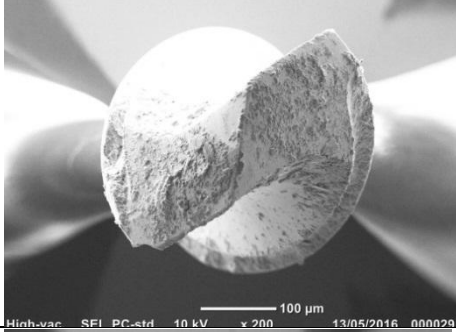
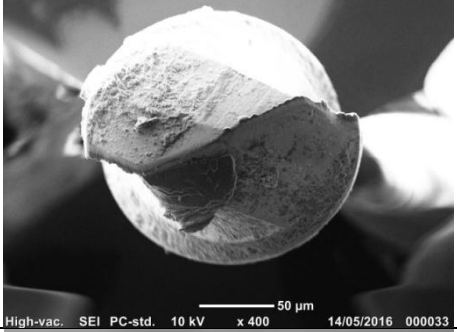
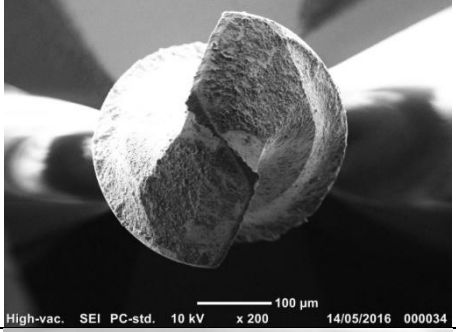
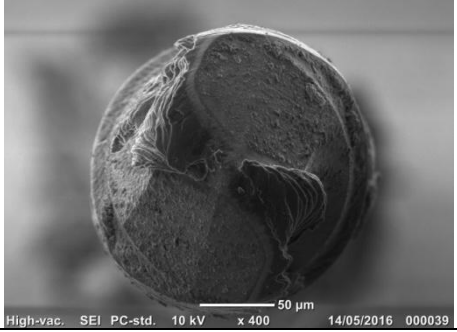
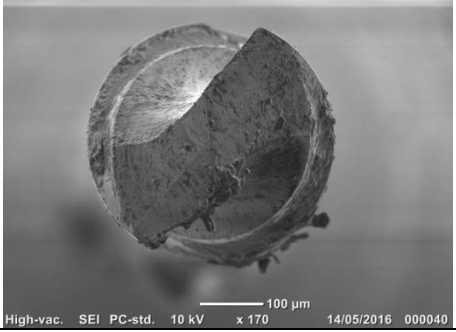
Size	Φ 0.2 mm	Φ 0.4 mm
new		
Feed rate: 12 mm/min		
Feed rate: 24 mm/min		
Feed rate: 36 mm/min		

Table 6-1: SEM photo of Φ 0.2 and Φ 0.4mm new drilling tool and drilled 9 times after with 12, 24 and 36 mm/min feed rate in aluminium work-piece

Experimental and theoretical of micro-drilling manufacturing

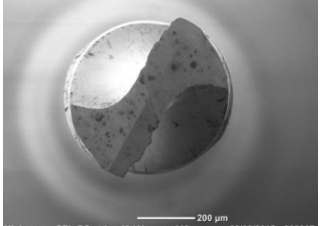
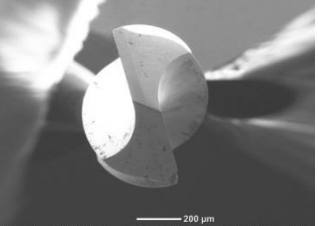
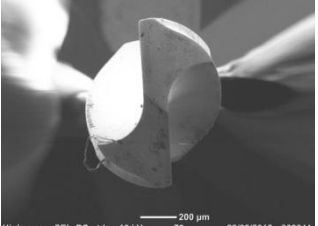
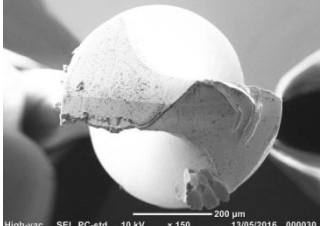
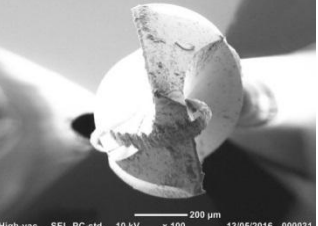
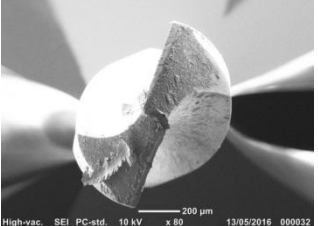
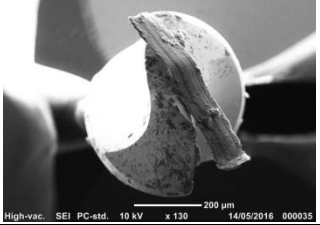
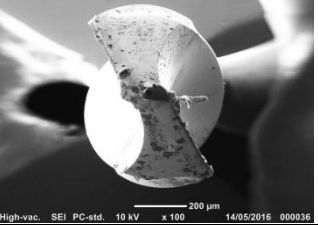
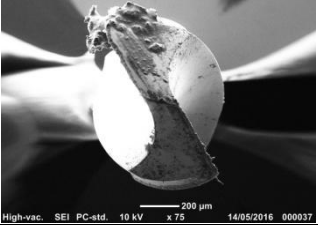
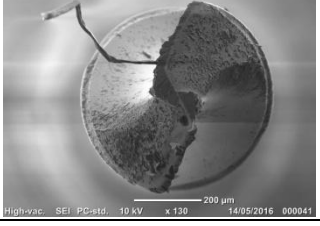
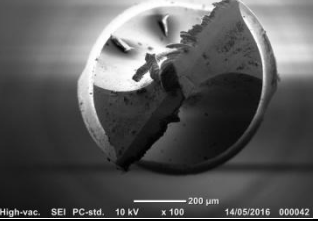
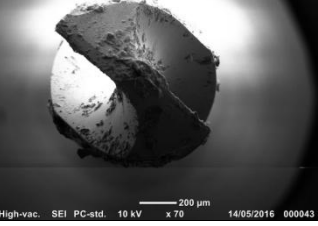
	Φ 0.6 mm	Φ 0.8 mm	Φ 1.0 mm
new			
Feed rate: 12 mm/min			
Feed rate: 24 mm/min			
Feed rate: 36 mm/min			

Table 6-2: SEM photo of Φ 0.6, 0.8 and 1.0mm new drilling tool and drilled 9 times after with 12, 24 and 36 mm/min feed rate in aluminium work-piece

Table 6-1 and 6-2 shows the SEM images of the drilling tool used in this research, before and after the total 9 drilling processes with respective feed rates.

The most significant wear was found on the 0.2mm drilling tool at 12mm/min feed rate, as marked in Table 6-1. No significant wear or damage was found with all other drilling tools although some build-up of chip can be seen around the web and cutting edge.

6.4 Discussion between the numerical calculation with the drilling model and force gradient

Comparison was carried out based on the results seen in Figure 6-5 and the drilling model presented in Figure 6-29. It can be found for 0.2mm drilling tool the web width on spot drill, or $r_0 = 0.0315\text{mm}$, and Web width on 0.2mm diameter twist drill, $R_0 = 0.0483\text{mm}$. Combine the above with the Countersunk hole depth ($x_1 = 0.1\text{mm}$) obtained through experiments results in:

$$a_0 = -\tan(130^\circ/2) = -2.1445 \quad (6-1)$$

This can be viewed with equation (5-1) and (5-2) and results in:

$$x_0 = x_1 - \frac{(r_0 - R_0)}{a_0} \quad (6-2)$$

$$x_0 = 0.0922 \quad (6-3)$$

To find the corresponding y , when $x_p = x_1$, we use (5-4) with the answer

$$y_s = (a_1 r_0) - (a_0 R_0) \quad (6-4)$$

$$y_s = 0.0610 \quad (6-5)$$

The drill diameter, being 0.2 mm (actual measured value is 0.189mm), is smaller than the rim diameter of the countersunk hole of 0.4 mm. Since the drill will begin to cut and continue to its full diameter, reaching x_2 and x_3 , the determination of x_3 can be done by using (5-4) again but this time let $x_p = x_3$ and $y_s = R_1$. Thus,

$$R_1 = \frac{0.189}{2} \quad (6-6)$$

$$x_3 = \left(\frac{a_1 - a_0}{a_0 a_1} \right) \times (R_1 - a_1 r_0 + a_0 R_0) + x_1 \quad (6-7)$$

$$x_3 = 0.1092 \quad (6-8)$$

Experimental and theoretical of micro-drilling manufacturing

Where the Feed rate = 12mm/min and recording sample frequency is 25600 Hz.

$x_0 \rightarrow x_1$ need 0.039 second, $x_1 \rightarrow x_3$ need 0.046 second

So if x_0 is the starting point then x_1 is located at index time 998.4 and x_3 is located at index time 2176.

By referencing Figure 6-5 it can be found that the highest point of gradient is at approximately 998.4 and the turning point indicating the levelling off is at 2176, as seen in Figure 6-29.

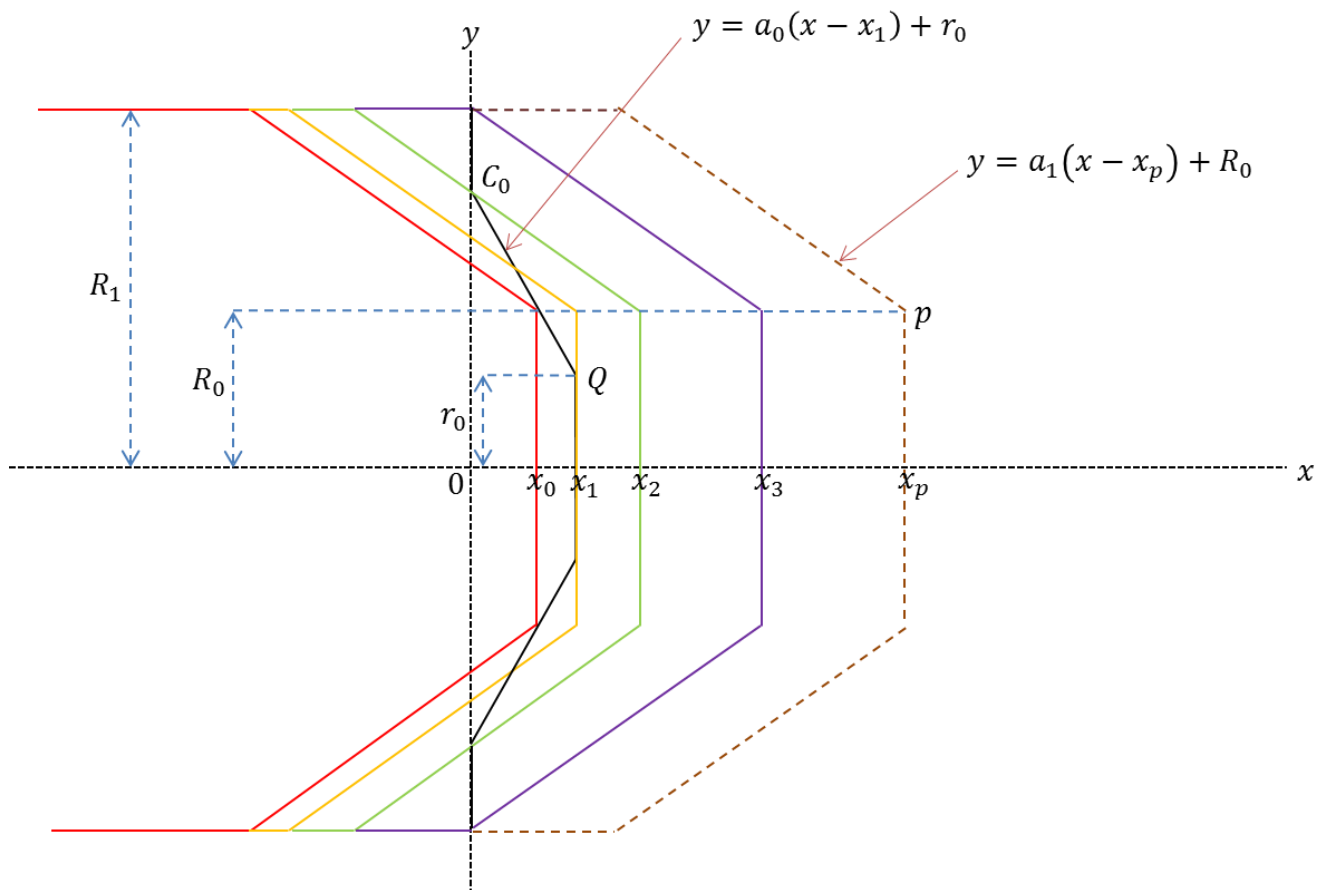


Figure 6-29: Twist drill tip model moves into a work-piece

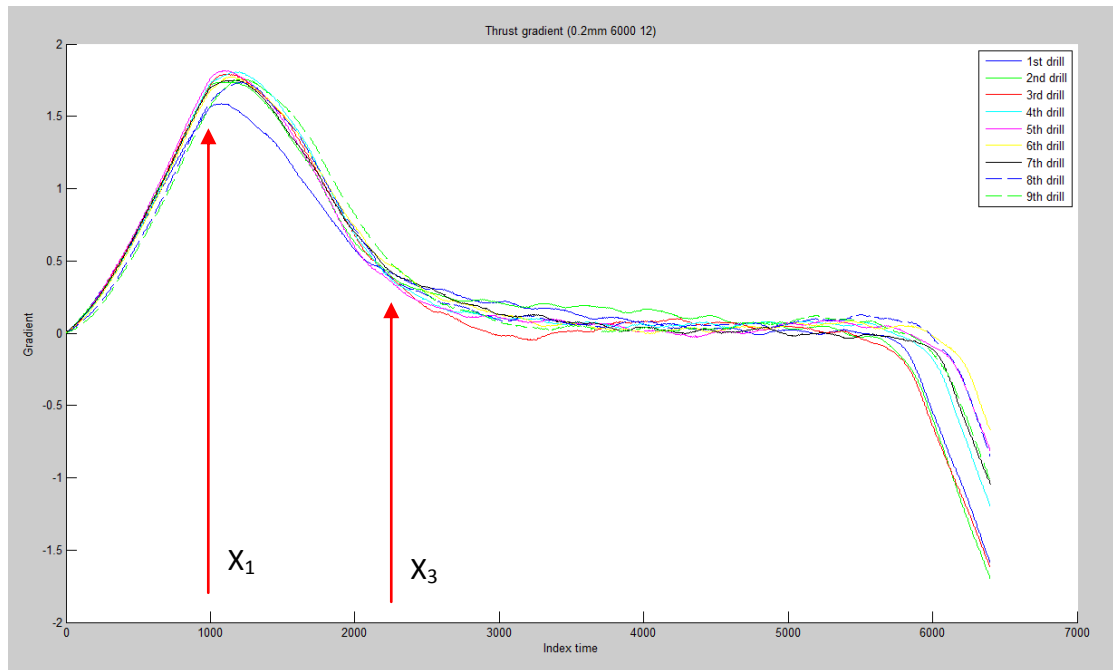


Figure 6-30: Drilling tool location after numerical calculation

6.5 Conclusion

Three work piece materials were selected in this research: Al 6061T, Al/Cu metal matrix alloy panel and Carbon fibre reinforced plastic. Various spindle rotation speed and feed rate were also investigated in order to establish their connection to thrust force. Moreover, in the case of Al 6061T work piece, five drill tool sizes (Φ 0.2, 0.4, 0.6, 0.8 and 1.0) were used for further understanding in thrust force variation.

SEM observation was carried out on both drill tool surface as well as the work piece to identify wear on the drill tool and the mechanics of composite delamination.

It was found both thrust force and drill tool wear are not only limited to the influence of feed rate and size. Further effects caused by countersink spot drill, step-wise operation and application of coolant were identified. From this viewpoint the direct contribution of spindle rotation speed turns to be relatively less significant than expected. Additional numerical calculation was also carried out and successfully demonstrated the application of drilling model described in previous chapter 5.

Chapter 7:

Conclusions and recommendations for future work

7.1 Conclusions

This chapter presents the summary of the main conclusions from micro-drilling process analysis based on research and investigation shown in earlier chapters. By combining actual measurements on micro-drilling and mathematical model this research hopefully would improve the understanding towards micro-drilling process. The main conclusions are presented as follows:

1. A four-stage thrust force variation was identified during the drilling process (Figure 6-11). This is most likely caused by the formation of countersink on the work-piece at the beginning. Such variation leads to the calculation of force gradient of each stage and through the mathematical model the approximate location corresponds to the gradient peak was then identified (Figure 6-30).
2. Pecking action was found to be important to Al work-piece, especially when the drilling tool is smaller than 0.4mm despite the 12mm/min feed rate. Such pecking action was found to reduce the occurrence of drilling tool failure, although it also resulted in a much more time-consuming drilling process. It was also found after applying the pecking action the four-stage increase of thrust force due to countersink formation became less significant (Figure 6-7 and 6-12).
3. Based on the experimental result in chapter 6, the work-piece material of Aluminium and Carbon Fibre reinforced composites has a characteristic of the thrust force that is proportional to feed rate, also this influence is applicable in any size of drilling tool. (Figure 6-13, 6-14 and 6-23)
4. Regarding Aluminium work-pieces, at the same rotation speed, the thrust force is proportional to tool dimensions. This influence is applicable to 12mm/min,

Conclusions and recommendation for future work

24mm/min and 36mm/min feed rates. (Figure 6-17, 6.18. and 6-19)

5. In the case of Al/Cu metal alloys, the thrust force was found to be proportional to the contact speed of spindle. High rotational speed and related friction resulted in higher temperature, and caused the chips to accumulate and attach to the cutting edge. It also leads to the increase in thrust force. (Figure 6-20)
6. During the drilling process, the thrust force gradually increases with the repetition of drilling process due to chip accumulation. This phenomenon is especially significant in the case of Al/Cu metal alloys. (Figure 6-21)
7. It was found in the cases of Al and Al/Cu work-piece thrust forces increase with the increasing feed rate. This is thought to be caused by the build-up of chips during the drilling process. However, in the case of carbon fibre reinforced plastic, instead of an increase, a decrease was observed and is most likely due to the fragmented chips that do not attach to surfaces easily. (Figure 6-23)
8. No significant wear or damage was found with most drilling tools after 9 holes were drilled; only some build-up of chips can be seen around the web and cutting edge. But significant tool wear was found in the case of 0.2mm tool on Al work-piece when 12mm/min feed rate was applied. It resulted in higher maximum thrust force value at the beginning of drilling process. (Figure 6-4)

7.2 Contribution to knowledge

From the research development above, the contribution to knowledge can be summarized as follows:

1. Modelled mathematically the metal removal rate of the drilling operation for the four stages of tool/work-piece engagement.
2. Used the moving average method to significantly reduce the signal-to-noise ratio of the thrust force signals.

Conclusions and recommendation for future work

3. Thrust force and force gradient were affected by feed rate, spindle speed, drill diameter, number of holes drilled and work-piece material; the force gradient was also affected by the shape of the pre-drilled countersunk hole. This could be the basis of a tool wear monitoring scheme.
4. Modelled by simulation of the thrust force in a micro-drilling operation.

7.3 Recommendations for future work

While this research has investigated some characteristics of micro-drilling, it still has lot of points that need to be improved and discussed; these recommendations and suggestions for future work should be indicated, including:

1. To use other material as the drilling work-piece. From this research, it was found characteristics vary between metal, metal matrix and carbon fibre reinforced plastic. More comprehensive investigation is needed involving other materials such as Copper, Nickel, metal composite or other metal matrix.
2. Other high-precision machining equipment such as air spindle drilling machine should be investigated in order to test the 0.1mm drilling tool since drilling tool smaller than 0.1 mm is not included in this research. This is also the main reason drilling tool smaller than 0.1mm was not included since signal recording would become much less effective as well as less accurate due to the limitation of KERN HSPC milling machine.
3. The measurement of skidding (X, Y-axis) in drilling process by displacement sensor and confirm the quality of drilling by SEM images. Also using a temperature sensing device to confirm the temperature variation at the tip of drilling tool.
4. At this moment, ANSYS simulation software cannot match the drilling parameter needs of this research exactly. It would be complementary to use the other

Conclusions and recommendation for future work

computer simulation methods and compare the result differences between simulation and actual measurement.

5. Further optimization for the drilling process model in the chapter 5. So far, the drilling process model does not consider the material characteristics and chips accumulation. Both could greatly affect the trend of thrust force during the process.

References

Amstead, B. H. (1987) 'Manufacturing Processes'. 8th. ed. New York, Wiley.

Anil, J. (2012) 'Analysis of Tool Wear Rate in Drilling Operation using Scanning Electron Microscope (SEM)'. *Journal of Minerals & Materials Characterization & Engineering*, Vol. 11, No.1, 43-54.

Armarego, E. (1988) 'A generic mechanics of cutting approach to predictive technological performance modelling of the wide spectrum of machining operations', *Machining Science and Technology*, 2, 191-211.

Astakhov, V. P. (2014) 'Drills: Science and Technology of Advanced Operations'. 4-8, 68-73, 85-99.

ASME (2008) 'Acceptance Test and Reverification Test for Coordinate Measuring Machines (CMMs)'. USA: ASME International. Vol. B89.4.10360, 2-2008.

Azlan, A.R., Azuddin, M., and Abdullah W. (2009) 'Effect of Machining Parameters on Hole Quality of Micro Drilling for Brass'. *The research is financed by University of Malaya Research University (RU) Grant No. FR072/2007A.*

Bailey, J.A. (1975) 'Friction in metal machining - mechanical aspects'. *Wear*, Vol. 31, 243-275.

Bateman, R. (2014) 'Manufacturing Paradigms, lecture notes distributed in the topic MN5502 Manufacturing Systems Design and Economics'. Ph.D. thesis, Brunel University, Lecture Centre on January.

Binayak, B., Young-Sun, H., Hae-Sung, Y., Jong-Seol, M., Minh-Quan, P., Gyu-Bong, L., Yu-chu, H., Barbara, S. Linkec., D.A. Dornfeldc, Sung-Hoon, A. (2013) 'Development of a micro-drilling burr-control chart for PCB drilling'. School of Mechanical & Aerospace Engineering, Seoul National University, Seoul 151-742, Republic of Korea.

Reference

Bishop, R.H. (2006) 'LabVIEW 7 Express'. Prentice Hall: Perason.

Bitter, R. (2006) 'LabVIEW: Advanced Proqraming Techniques'. 2nd edn. Taylor & Francis: CRC Press.

Bogdan, M. (2012) 'Cutting Force Modelling for Drilling of Fiber-Reinforced Composites'. Ph.D. thesis, FEDERAL POLYTECHNIC OF LAUSANNE.

Brodtt, M. and Lakes, R.S. (1996) 'Viscoelastic behaviour in indium alloys: InSn, InBi, InCd and InSnCd'. *JOURNAL OF MATERIALS SCIENCE*, Vol. 31, 6577-6581.

Cheng, K. (2008) 'Machining Dynamics: Fundamental, Applications and Practices', 33-37, 43-47.

Cheng, K. and Huo, D. (2013) 'Micro-Cutting Fundamental and Applications', 21-23, 30-31.

Cheong, M.S., Cho, D.W. and Ehmann, K.F. (1999) 'Identification and control for micro-drilling productivity enhancement'. *International Journal of Machine Tools and Manufacture*, Vol. 39 (10), 1539-1561.

David. R. (2001) 'Stress-Strain Curves, Massachusetts Institute of Technology'. Department of Materials Science and Engineering, Cambridge, MA 02139.

David, A.S. and John, S.A. (2006) 'Metal cutting theory and practice second edition' Library of Congress Cataloging – in – Publication Data.

Davim J.P., Reis P. (2003) 'Study of delamination in drilling carbon fiber reinforced plastics (CFRP) using design experiments', *J Compos Struct* 2003;59:481–7.

Ding, H., Chen, S.J. and Cheng, K. (2010) 'Two-dimensional vibration-assisted micro end milling: cutting force modelling and machining process dynamics'. *Proc. IMechE*,

Reference

Vol.224 Part B: J. Engineering Manufacturing, 1775-1783.

Ding, H., Ibrahim, R., Chen, S.J. and Cheng, K. (2010) 'Experimental study on machinability improvement of hardened tool steel using two dimensional vibration-assisted micro-end-milling'. *International Journal of Machine Tools & Manufacture*, Vol. 50, 1115-1118.

Dolinsek, S., Kopac, J. (2006) 'Mechanism and types of tool wear; particularities in advanced cutting materials'. *Journal of Achievements in Materials and Manufacturing Engineering*, Vol. 19.

Durao, L., Tavares, J., de Albuquerque, V., Marques, J. and Andrade, O. (2014) 'Drilling Damage in Composite Material', *Materials*, Vol. 7(5), 3802–3819.

Dwivedi, V.K. (2009) 'Heat and Mass Transfer'. 3. ed. Delhi: Umesh Publications.

Edwards, L.K., Lakes, R.S. and Nixon, W.A. (2000) 'Viscoelastic behaviour of 80In15Pb5Ag and 50Sn50Pb alloys: Experiment and Modelling'. *Journal OF Applied Physic*, Vol. 87(3), 1135-1140.

Ema, S., Fujji, H. and Marui, E. (1998) 'Whirling Vibration in Drilling. Part 3: Vibration Analysis in Drilling Workpiece with a Pilot Hole'. *Journal of Manufacturing Science and Engineering*, Vol. 110(4), 315-321.

Fang, N., Pai, P.S. and Edwards, N. (2010) 'Prediction of built –up edge formation in machining with round edge and sharp tools using aneural network approach'. *International Journal of Computer Integrated Manufacturing*, Vol. 23, 1002-1014.

Gao, C.H., Cheng, K. and Kirkwood, D. (2000) 'The investigation on the machining process of BTA deep hole drilling'. *Journal of Materials Processing Technology*, Vol. 107, 222-227.

Gao, W., Li, Z. and Sammes, N. (2011) 'An Introduction to Electronic Materials for

Reference

Engineers'. 2nd. ed. Singapore: World Scientific Publishing Co. Pte. Ltd.

Goel, B.K. and Goel, P.K. (2009) 'Machine Drawing'. 1st. ed. New Delhi: S.K. Kataria and sons.

Groover, M.P. (2010) 'Fundamentals of modern manufacturing : materials, processes, and systems Manufacturing Processes'. Hoboken, NJ. ed. New York, J. Wiley.

Han, D.C., Park, S.S., Kim, W.J. and Kim, J.W. (1994) 'A study on the characteristics of externally pressurized air bearings'. Department of Mechanical Design and Production Engineering, Seoul National University, Seoul, Korea, Vol. 16 (3), 164-173.

Hejun, D. and Yan, L. (2012) 'Investigation of head-disk interface and unloading process in HDD with an efficient scheme'. *International Journal of Modern Physics: Conference Series*, Vol. 19(1), 311-319.

Ho-cheng, H., and Dharan, C.K.H. (1990) 'Delamination during Drilling of Composite Laminates'. *Journal of Engineering for Industry*, Transactions of ASME, Vol.112, 236-239.

Ho-cheng, H., Chao, Y.C. and Puw, H.Y. (1995) 'A General Model for Thrust force-induced Delamination in Drilling of Composite Laminates'. *Machining of Advanced Material*, Vol.208, 29-39.

Huang, W.Z., Ding, Z., Wang, C.C., Yei, J., Zhao, Y. and Purnawali, H. (2010) 'Shape memory materials'. *Materials Today*, Vol. 13 (7-8), 54-61.

Hughes, J.P. (2012) 'Analysis of a Toggle Mechanism: Sensitivity to Link Sizes and Compliance Material'. M.Sc. thesis, Rensselaer Polytechnic Institute Hartford, Connecticut.

Huo, D. and Cheng, K. (2009) 'Experimental investigation on micromilling of oxygen-free, high-conductivity copper using tungsten carbide, chemistry vapour

Reference

deposition, and single-crystal diamond micro tools'. *Proc. IMechE*, Vol.224 Part B: J. Engineering Manufacturing, 995-1003.

Ibrahim, N.T. (1992) 'Identification of the prefigure phase in micro drilling operations using multiple sensors'. *Int. J. Mach. Tools Manufact.* Vol. 34, No. 3, 351-364.

Islam, S. and Suzanne, B. (2010) 'Effect of laminate configuration and feed rate on cutting performance when drilling holes in carbon fibre reinforced plastic composites'. *Journal of materials processing technology*. Volume 210, 1023-1034.

Jani, J.M., Leary, M., Subic, A. and Gibson, M.A. (2013) 'A review of shape memory alloy research, applications and opportunities'. *Material and Design*, Vol. 56 (1), 1078-1113.

Jay, P. P. (2003). 'Design, assembly, and testing of an ultra-high-speed micro-milling spindle'. PhD Thesis, University of Florida. University of Florida, USA.

Jun, M.B., Liu, X., Devor, R.E. and Kapoor, S.G. (2006) 'Investigation of the Dynamics of Micro end Milling'. *Journal of Manufacturing Science and Engineering*, Vol. 128 (4), 893-900.

Kauffman, G.B. and Mayo, I. (1997) 'The Story of Nitinol: The Serendipitous Discovery of the Memory Metal and Its Applications'. *The Chemical Educator*, Vol.2 (2), 1-21.

Kim, J.S., Jim, J.H., Kang, M.C. and Seo. Y.W. (2007) 'A mechanistic model of cutting force in the micro and milling process'. *Journal of Material Processing Technology*, 187, 250-255.

Konig, W. (1990). 'Fertigungsverfahren - Drehen, Bohren, Frasen'. Vol. 1, 3rd ed., VDI-publishing, ISBN 3-18-400180-X, 11.

Laroux, G. (1992) 'Countersinking Handbook'. Industrial Press Inc. 989 Avenue of the Americas New York, NY 10018.

Reference

Le Dref, J., Eyma, F., Dessein, G., Denaud, L.E. and Landon, Y. (2013) 'Comparative study of tool in drilling composites T700-M21 and T800-M21'. *Advanced Materials Research*, ISSN 1662-8985, Vol. 698, 59-68.

Liu, X.W., Cheng, K., Webb, D. and Luo, X.C. (2002) 'Improved Dynamic Cutting Force Model in Peripheral Milling. Part I: Theoretical Model and Simulation'. *The International Journal of Advanced Manufacturing Technology*, Vol. 20, 9, 631-638.

Liu, X.W., Cheng, K., Webb, D., Longstaff, A.P. and Widiyanto, M.H. (2004) 'Improved Dynamic Cutting Force Model in Peripheral Milling. Part II: experimental verification and prediction'. *The International Journal of Advanced Manufacturing Technology*, Vol. 24, 794-805.

Liu, X.W., Cheng, K., Webb, D. and Luo, X.C. (2002) 'Prediction of cutting force distribution and its influence on dimensional accuracy in peripheral milling'. *International Journal of Machine Tools & Manufacture*, Vol. 42, 791-800.

Luís Miguel, P., Durão 1, João Manuel R.S. Tavares 2, Victor Hugo C. de Albuquerque 3, Jorge Filipe, S. Marques 1 and Oscar, N.G.A. (2014) 'Drilling Damage in Composite Material'. ISEP/CIDEM – Instituto Superior de Engenharia do Porto, Instituto Politécnico do Porto R. Dr. António Bernardino de Almeida, 431 – 4200-072 Porto, Portugal.

Luo, X., Cheng, K., Ward, R. and Holt, R. (2003) 'Modelling and simulation of the tool wear in nanometric cutting'. *Wear*, Vol. 255, 1427-1432.

Luo, X., Cheng, K., Webb, D. and Wardle, F. (2005) 'Design of ultraprecision machine tools with applications to manufacturing of miniature and micro components'. *Journal of Materials Processing Technology*, Vol. 167, 515-528.

Machinery's Handbook (2000). 'Mechanical Engineering', Vol. 122, no. 9, 866-872.

Reference

Marinov, V. (2008) 'Drilling and Reaming'. Dubuque, USA: Kendall Hunt Publishing Company.

Meyers, M.A. and Chawla, K.K. (2009) 'Mechanical Behaviour of Materials'. 2nd. ed. Cambridge: Cambridge University Press.

Miller, S.F., Wang, H., Li, R. and Shih, A.J. (2006) 'Experimental and numerical analysis of the friction drilling process'. *Journal of Manufacturing Science and Engineering*, Vol. 128 (3), 802-810.

Mondelin, A., Furet, B. and Rech, J. (2010) 'Characterisation of friction properties between a laminated carbon fibres reinforced polymer and monocrystalline diamond under dry or lubricated conditions'. *Tribology International*, Vol. 43, No. 1665.

Natebi, A., Mauvoisin, G. and Vaghepour, H. (2008) 'Modelling of twist drills wear by a temperature-dependent friction law'. *Journal of Materials Processing Technology*, Vol. 207, 98-106.

Niu, Z.C and Cheng, K. (2015) ' Multiscale Multiphysics-Based Modelling and Analysis on the Tool Wear in Micro Drilling'. *Journal of Mutiscale Modeling*, Vol.7, No.1, 164002, 1-22.

Palanikumar, K. and Muiaraj, A. (2014) 'Experimental investigation and analysis of thrust force in drilling cast hybrid metal matrix (Al-15% SiC-4% graphite) composite'. *Measurement*, Vol.53, 240-250.

Pathak, J.P. (2003) 'Design, Assembly, and Testing Of an Ultra-High-Speed Micro Milling Spindle', University Of Florida.

Popov, K. (2014) 'Introduction to Ansys', lecture notes distributed in the topic MN5561 Computer Aided Engineering 2. Brunel University, TA312, Tower-A on January.

Reference

PSG College of Engineering (2011) 'Design Data'. 2nd. ed. Coimbatore, India: M/s Kalaikathir Achchagam.

Qin, Y., Brockett, A., Ma, Y., Razali, A., Zhao, J., Harrison, C., Pan, W., Dai, X. and Loziak D. (2009) 'Micro-manufacturing: research, technology outcomes and development issues'. *Int J Adv Manuf Technol* Vol. 47, 821–837.

Rajput, R.K. (2006) 'Strength of Materials'. 4th. ed. New Delhi: S Chand Publication.

Rajput, R. K. (2007) 'A Textbook of Manufacturing Technology: Manufacturing Processes'. Laxmi Publications (P) LTD 113, Golden House, Daryaganj, New Delhi-110002.

Ross, P.J. (1996) 'Taguchi Techniques for Quality Engineering', second Edition. McGrawHill, New York.

Saiful Anwar Bin Che Ghani (2013) 'Design and analysis of the internally cooled smart cutting tools with the applications to adaptive machining'. PhD Thesis, Brunel University, UK.

Shyha, I.S., Aspinwall, D.K., Soo, S.L. and Bradley, S. (2009) 'Drill geometry and operating effects when cutting small diameter holes in CFRP'. *International Journal of Machine Tools & Manufacture*, Vol. 49, 1008-1014.

Shyha, I., Soo, S.L., Aspinwall, D. and Bradley, S. (2010) 'Effect of laminate configuration and feed rate on cutting performance when drilling holes in carbon fibre reinforced plastic composites'. *Journal of Materials Processing Technology*, Vol. 210(8), 1023–1034.

Sreekumar, M., Nagarajan, T. and Singaperumal, M. (2009) 'Application of trained NiTi SMA actuators in a spatial compliant mechanism: Experimental investigations'. *Web of Knowledge Scopus*, Vol. 30, 320-3029.

Reference

Stolarski, T.A., Nakasone, Y., and Yoshimoto, S. (2006) 'Engineering Analysis with Ansys software'. ANSYS Inc: Elsevier.

Su, J.C., Huang, C.K. and Tarn, Y.S. (2006) 'An automated flank wear measurement of microdrills using machine vision'. *Journal of Materials Processing Technology*, Vol.180, 328–335.

Taskesen, A. and Kutuke, K. (2015) 'Non-contact measurement and multi-objective analysis of drilling temperature when drilling B4C reinforced aluminum composite'. *Trans. Nonferrous Met. Soc. China*, Vol. 25, 271-283.

Thomas, C., Katsuhiko, M., Toshiyuki, O., and Yasuo, Y. (2000) 'Metal Machining Theory and Applications'. LONDON First published in Great Britain in 2000 by Arnold, a member of the Hodder Headline Group.

Tian, Y., Shirinzadeh, B., Zhang, D. and Zhong, Y. (2010) 'Three flexure hinges for compliant mechanism designs based on dimensionless graph analysis'. *Precision Engineering*, Vol. 34, 92-100.

Tlusty, J. and MacNeil, P. (1975) 'Dynamics of cutting force in end milling'. *Annals of the CIRP*, 24, 21-25.

Todd, R.H., Allen, D.K. and Alting, L. (1994). 'Manufacturing Processes Reference Guide'. 1st. ed. New York: Industrial Press Inc.

United States Cutting tool Institute (1989) 'Metal Cutting Tool Handbook' Industrial Press Inc. 200 Madison, New York, New York, 10016-4078.

Victor, P.A. (2014) 'Manufacturing design and technology drills science and technology of advanced operations', *Wiley*, New York.

Vijayakumar, P. (2002) 'Finite element simulation of 3D drilling in unidirectional crop composite'. Bachelor of Engineering, University of Madras, India.

Reference

Westwind Air Bearings Ltd. (2002) 'High speed drill holders'. U.S. Pat. - US 6,443,462 B2.

Winston, C. (1941) 'Basic Definitions and Cutting Tool Geometry, Single Point Cutting Tools'. Winston Churchill's message to President Roosevelt.

Worapong, S. (2014) 'An Investigation on Micro Cutting Mechanics: Modelling, Simulations and Experimental Case Studies'. PhD Thesis, Brunel University, UK.

Xie, T. (2010) 'Tunable polymer multi-shape memory effect'. *Nature*. Vol. 464 (1), 267-270.

Zettl, B., Szyszkowsk, W. and Zhang, W.J. (2005) 'Accurate low DOF modelling of a planar compliant mechanism with flexure hinges: the equivalent beam methodology'. *Precision Engineering*. Vol. 29, 237-245.

Zheng, L.J., Wang, C.Y. and Fub, L.Y. (2012) 'Wear mechanisms of micro-drills during dry high speed drilling of PCB'. *Journal of Materials Processing Technology*, Vol.212, 1989-1997.

Zong, W.J., Li, D., Cheng, K., Sun, T. and Liang, Y.C. (2006) 'Finite element optimization of diamond tool geometry and cutting-process parameters based on surface residual stresses'. *Int J Adv Manuf Technol (2007)*. 32: 666-674

Alan, M. (2014) 'Printed Circuit Board'. [online]. Available from:
<<http://www.madehow.com/Volume-2/Printed-Circuit-Board.html>>.
[Accessed 28 December 2015].

American Machinist (2010) 'Cutting Tool Applications, Chapter 8: Drills and drilling operations'. [online]. Available from:
<<http://americanmachinist.com/machining-cutting/cutting-tool-applications-chapter-8-drills-and-drilling-operations>>. [Accessed 13 Jan 2016]

Reference

Ansys (2010) 'Introduction to Contact'. [online]. Available from:

<http://inside.mines.edu/~apetrell/ENME442/Labs/1301_ENME442_lab6_lecture.pdf>. [Accessed 20 Jan 2016].

Ansys (2010) 'Rate Independent Plasticity'. [online]. Available from:

<http://inside.mines.edu/~apetrell/ENME442/Labs/1301_ENME442_lab7.pdf>. [Accessed 7 April 2016].

ArcelorMittal (2014) 'Steels for hot stamping'. [online]. Available from:

<http://automotive.arcelormittal.com/saturnus/sheets/catalogue.pl?id_sheet=E>. [Accessed 21 March 2015].

Bam Lab (2013) 'Introduction to Viscoelasticity'. [online]. Available from:

<<https://www.youtube.com/watch?v=5ZIH9pidAdc>>. [Accessed 18 February 2016].

British Standards Institution (2010) 'BS ISO 8573-1:2010 Compressed air British Standards Online'. [online]. Available through: Brunel University Library website

<<https://bsol-bsigroup-com.v-ezproxy.brunel.ac.uk>> [Accessed 18 February 2016].

CircuitPeople (2014) 'Introduction to Gerber Files'. [online]. Available from:

<<http://circuitpeople.com/Blog/WhatIsAGerberFile.aspx>>. [Accessed 19 December 2015].

Cobon Engineering (2013) 'Mechanical Engineering'. [online]. Available from:

<<http://cobanengineering.com/mechanicalengineering/MechanicalEngineering.asp>>. [Accessed 17 January 2016].

Dan B. (2005) 'Tangent Modulus' [online]. Available from:

<<http://www.xansys.org/forum/viewtopic.php?p=87964>>. [Accessed 10 January 2016].

Dyneema® (2013) 'Understanding Creep'. [online]. Available from:

Reference

<<https://www.youtube.com/watch?v=opPWceW-YKc>>. [Accessed 21 March 2016].

eBay (2014) 'How to Choose the Right Drill Bit Material'. [online]. Available from: <<http://www.ebay.co.uk/gds/How-to-Choose-the-Right-Drill-Bit-Material-/10000000177630330/g.html>>. [Accessed 28 December 2015].

Engscope (2014) 'PCB Basics'. [online]. Available from: <<http://www.engscope.com/pcb-fab-tutorial/02-pcb-basics/>>. [Accessed 28 December 2015].

Grablab, Y. (2012) 'OpenHand Model T (Flexure Base) Performance (Autonomous Grasping)'. [online]. Available from: <<http://www.youtube.com/watch?v=2k8kBe9S3BY>>. [Accessed 19 January 2016].

Higgins, J. (2012) 'Obtaining and Optimizing Structural Analysis Convergence'. [online]. Available from: <<http://www.ansys.com/staticassets/ANSYS/Conference/Confidence/Boston/Downloads/obtaining-and-optimizing-convergence.pdf>>. [Accessed 15 March 2016].

Lakes, R. (2015) 'Viscoelasticity Notes'. [online]. Available from: <<http://silver.neep.wisc.edu/~lakes/VEnotes.html>>. [Accessed 21 December 2015].

LOADPOINT BEARINGS (2012) 'How Air Bearings work'. [online]. Available from: <<http://www.loadpoint-bearings.co.uk/about/how-air-bearings-work/>>. [Accessed 12 January 2016].

Marcel T. (2012) 'UROP Flexure Animation'. [online]. Available from: <<http://www.youtube.com/watch?v=P0moT7nPkG8>>. [Accessed 22 January 2016].

Marinov, V. (2015) 'DRILLING AND REAMING'. Dubuque, USA: Kendall Hunt Publishing Company. Available from: <http://me.emu.edu.tr/me364/ME364_machining_drilling.pdf>. [Accessed 3 January 2016].

Reference

National Physical Laboratory (2007) 'Manual for the Calculation of Elastic -Plastic Materials Models Parameters'. [online]. Available from:

<<http://www.npl.co.uk/upload/pdf/elastic-plastic-materials-manual.pdf>>.

[3 January 2016].

Ntlworld (2015) 'Drilling History'. [online]. Available from:

<http://homepage.ntlworld.com/leslie.foster/drilling_history.htm>.

[Accessed 3 December 2015].

NUMEN MACHINERY CO., LTD. (2011) 'Micro hole drilling'. [online]. Available from:

<<http://www.youtube.com/watch?v=GNMXxbqzi-Y>>. [5 January 2016].

PADT, Inc. (2012) 'User defined results'. [online]. Available from:

<<http://www.padtinc.com/blog/wp-content/uploads/oldblog/pic4.png>>. [Accessed

22 March 2016].

Pennsylvania State University (2014) 'Stress-Strain Diagrams'. [online]. Available from:<http://www.esm.psu.edu/courses/emch213d/tutorials/animations/stress_strain.php>.

[15 January 2016].

Prabha, M. (2011) 'Piezo Element and Arduino'. [online]. Available from:

<<https://www.youtube.com/watch?v=wMI4QRsCyEo>>. [Accessed 20 December

2015].

Ramirez, A. (2011) 'Material Marvels with Ainissa Ramirez - Shape Memory Alloys'.

[online]. Available from: <<http://www.youtube.com/watch?v=WREwKx0qF7o>>.

[Accessed 20 January 2016].

Roylane, D. (2001) 'Stress-Strain Curves, Massachusetts Institute of Technology'.

[online]. Available from:

<<http://ocw.mit.edu/courses/materials-science-and-engineering/3-11-mechanics-of-materials-fall-1999/modules/ss.pdf>>.

[Accessed 10 December 2015].

Reference

Sankararaj, S. (2013) 'Introduction of Unconventional Manufacturing Process'. [online]. Available from: <<http://www.newagepublishers.com/samplechapter/001566.pdf>>. [Accessed 19 December 2015].

SpecSearch® (2014) 'Stainless Steel AISI Type 440B'. [online]. Available from: <http://www.efunda.com/materials/alloys/stainless_steels/show_stainless.cfm?ID=AISI_Type_440B>. [Accessed 7 January 2016].

Tooling University (2014) 'CNC Training'. [online]. Available from: <<http://www.toolingu.com/class-300310-canned-cycles-310.html>>. [Accessed 3 January 2016].

Westwind, Inc. (2012) 'Air Bearing Technology'. [online]. Available from: <http://www.westwind-airbearings.com/pdfs/Air_Bearing_Technology.pdf>. [Accessed 5 December 2015].

Wolfram Demonstrations Project (2014) 'Square-Hole Drill in Three Dimensions'. [online]. Available from: <<http://demonstrations.wolfram.com/SquareHoleDrillInThreeDimensions/>>. [Accessed 8 Decemberber 2015].

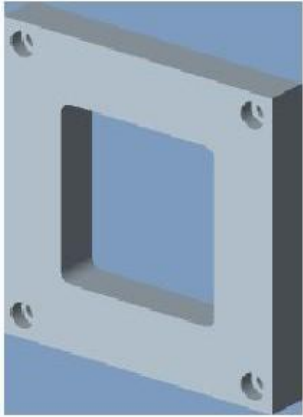
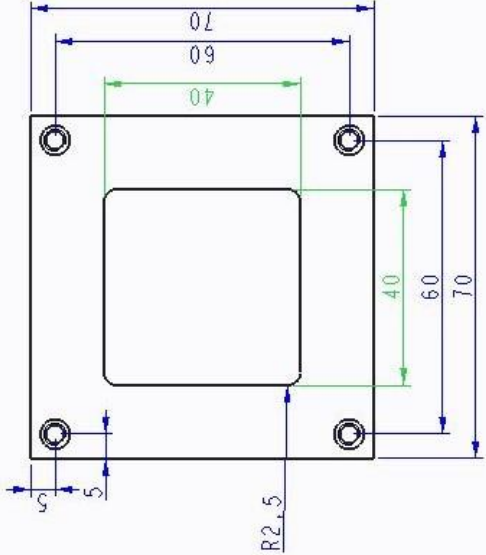
Zheng, Z. (2011) 'Sinco Machining'. [online]. Available from: <<http://www.sincomachine.com/sincomachine/Product.aspx?id=43>>. [Accessed 15 December 2015].

**Appendix A:
Engineering drawings for fixture
design**

Appendix A

Smaller work-piece fixture square cover

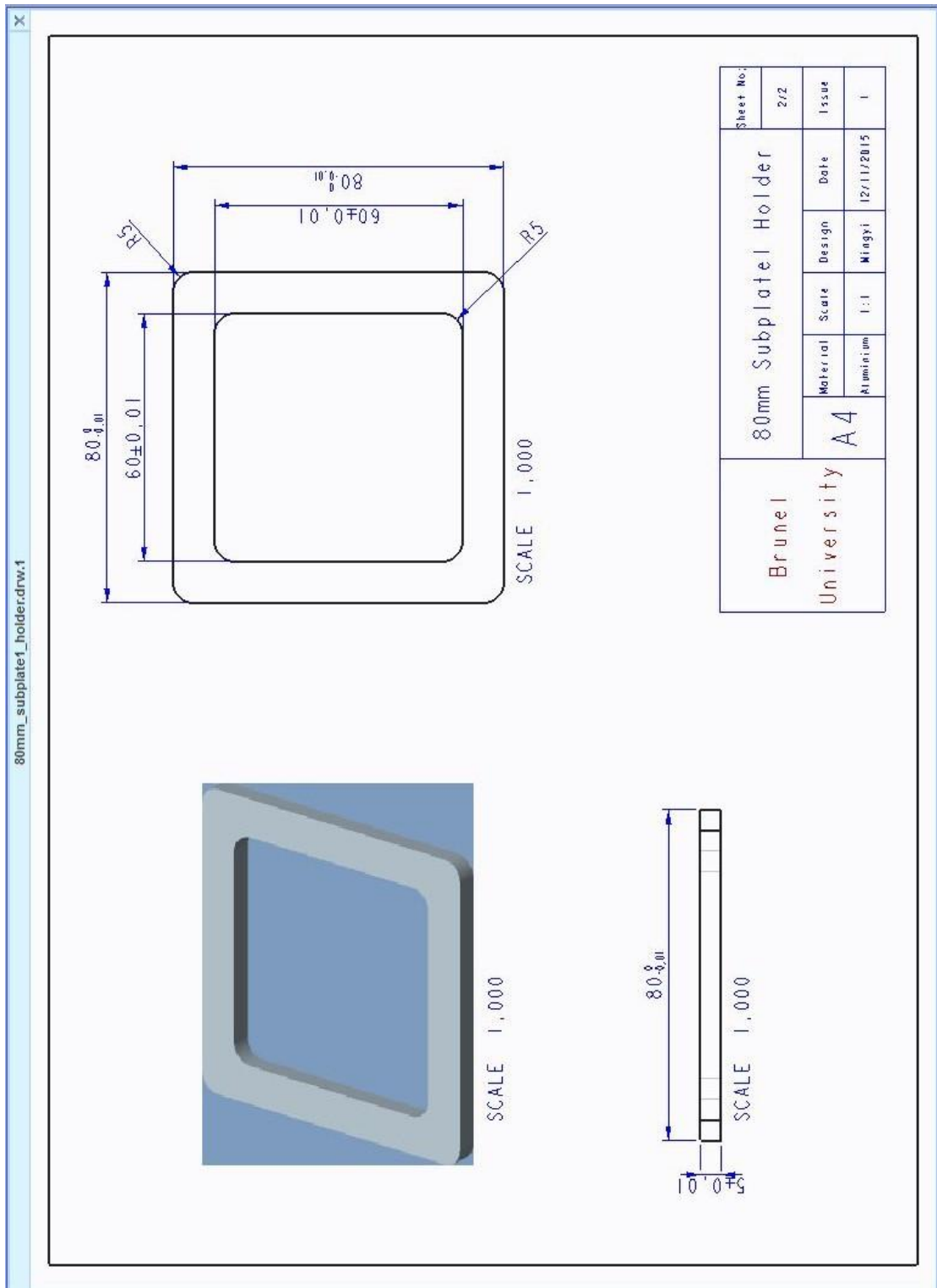
70mmsquarecover.drw.2


Brunel University	A4	Material Aluminium	Scale 1:1	Design Miegyi	Date 09/05/2014	Sheet No.
						Issue
						1/2
						1

Appendix A

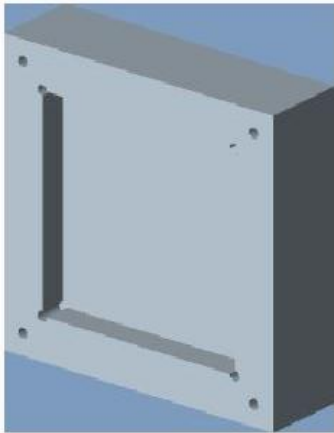
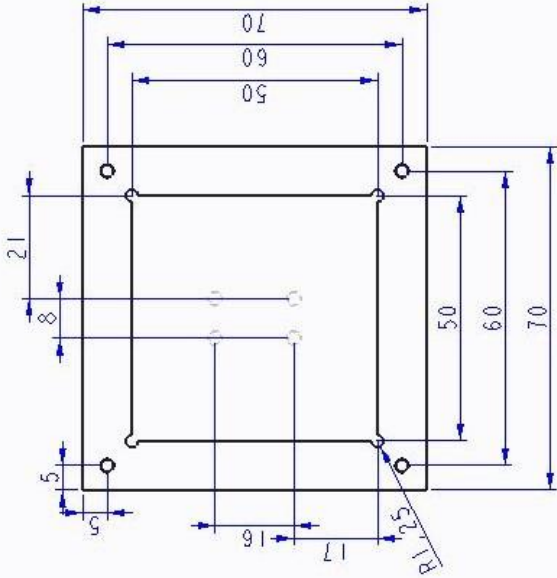
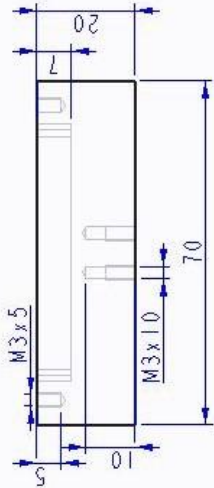
Sub-plate holder



Appendix A

Smaller work-piece fixture square plate

70mmsquareplate.drw.1

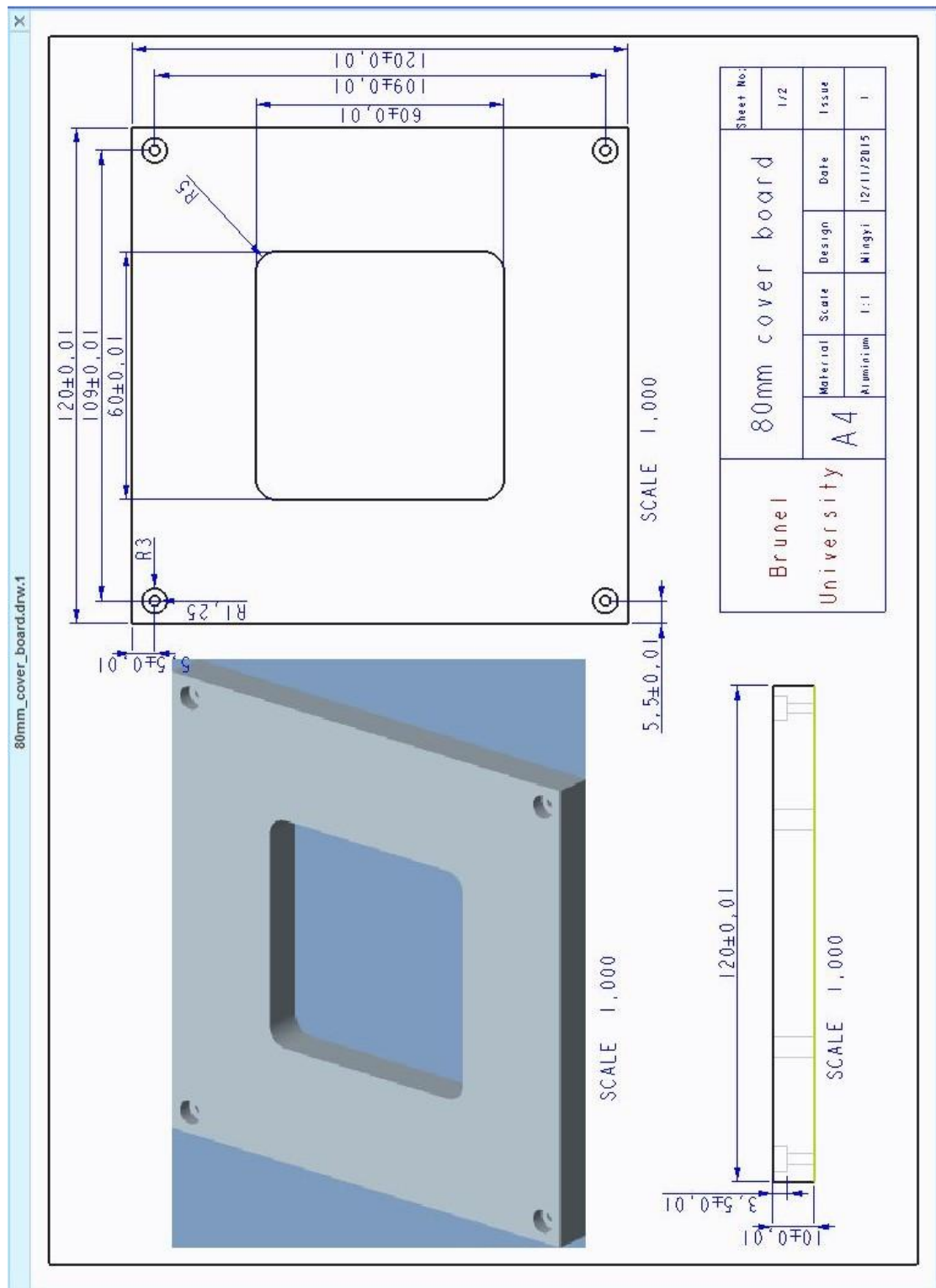




Brunel University	A4	Material Aluminium	Scale 1:1	Design Mingyi	Date 09/08/2014	Issue	Sheet No:
						1	2/2

70mm square plate

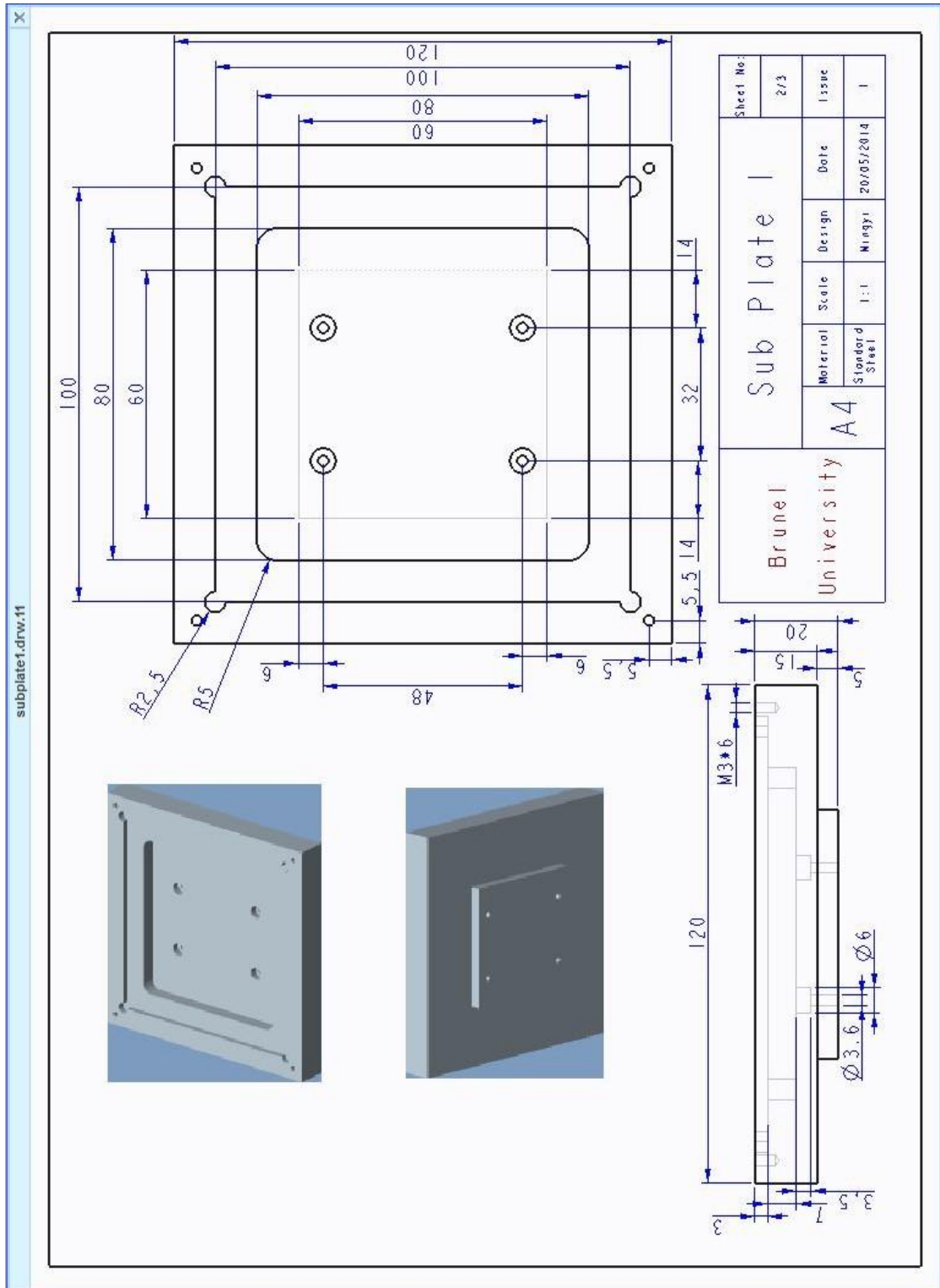
Appendix A

Lager work-piece fixture square cover



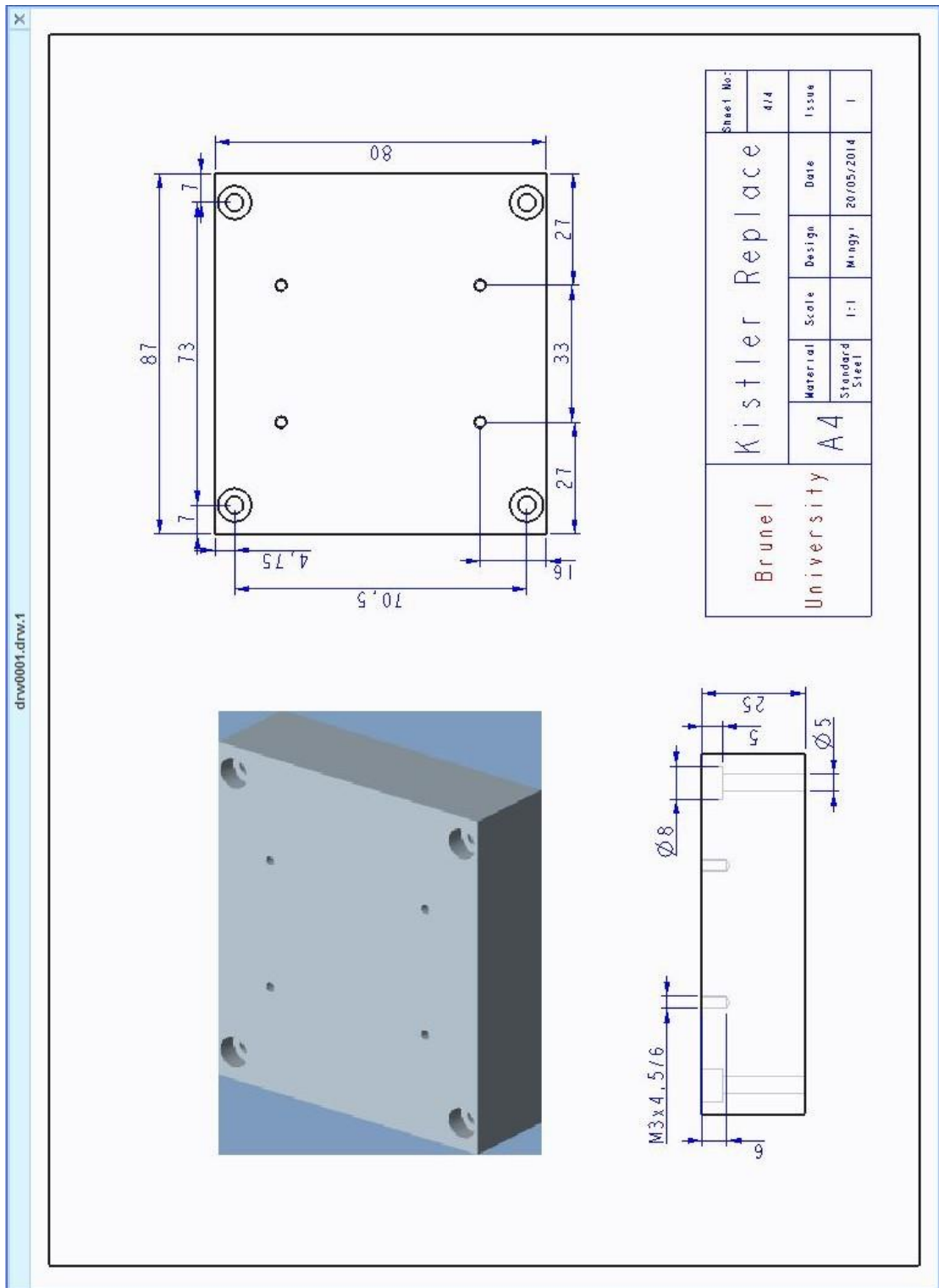
Appendix A

Lager work-piece fixture square plate



Appendix A

Kistler replace



Appendix B
MATLAB programming for
experimental data analysis

Appendix B

B-1 Data signal loading

```
function filtThrust = loadsignal(fname, N)
    % Load file into the force variable
    load(fname)
    % extract the time and thrust values
    thrust = [force(:,3)];
    filtThrust = movavg(thrust, N);
    clf;
    figure(1);
    plot(filtThrust)
```

B-2 Data move average

```
function y=movavg(x,n)
    % function y=movavg(x,n)
    % x = signal matrix to be filtered using the moving average method; a two
    %     column matrix: first column is time and second column is thrust
    % n = number of data points to be averaged over
    % y = the filter signal matrix: first column holds the filtered values
    %     whilst the second column holds the time values
    %
    % set the coefficient a and b for the filter
    a=1;
    b=ones(1,n). *1/n;
    % call the filter function
    y=filter(b,a,x);
```

B-3 Data elements remove

```
function J=removeElements(I, indices)
    % J=removeElements(I, indices)
    % Remove elements in array I at the index position contained in vector indices
```

Appendix B

```
for i=1:length(indices)
l(indices(i))=0;
J = l(l>0);
end
```

B-4 Signal separate

```
function hole = separateSig(sig, l, span)

for i = 1:length(l)
    hole(:,i)=sig(l(i):l(i)+span);
end
```

B-5 Drilling separate

```
function Dhole = slope(hole, gtitle)

[m, n] = size(hole);
for i=1:n
    Dhole(:,i)=movavg(diff(hole(:,i)),1000).*25600;
end
```

B-6 Start point

```
function out=startInd(sig, thres)
% out=startInd(sig, thres)
% find the start indices of the positive slopes
% at which the signal sig crosses the threshold thres
% create a logical array logicalSig in which each element
% whose value is greater than thres is set to unity, elements
% below thres is set to zero
logicalSig = (sig>thres);

% find the indices of elements corresponding to the point at which
```

Appendix B

```
% the signal sig cross the threshold thres; 1 is added to restore
% the correct index value caused by the diff function
out = find(diff(logicalSig)==1)+1;
```

B-7 restore drilling signal

```
function [startrecord] = startpoint(name)

%UNTITLED4 Summary of this function goes here
% Detailed explanation goes here
j=1;
n = length(name);
startrecord = zeros(n,1);
for i = 1:n
if name(i) > 0.02;
startrecord(j) = name(i);
j=j+1;
end
plot (startrecord(j), j-1000);
end
```

B-9 0.5mm drilling tool signal on Al/Cu

```
% Step 1
% Procedure for analysing gradients of thrust-time signals
% Run filtThrust = loadsignal(fname, N);
% fname is filename of force file (a six-column matrix, fifth column containing the thrust force
% fifth column containing the thrust force which is extracted and filtered using moving average of N
points
% N = 3000. Outputs: filtered thrust signal for all holes drilled
% filtThrust and a graph depicting the thrust against array index.
filtThrust = loadsignal('slot_6000 12.mat', 3000);

% plot thrust-time graph
clf;
```

Appendix B

```
figure(1);
plot(filtThrust);

% Run out = startInd(sig, thres)
% by visual inspection of graph in step 1
% set a threshold for the rising edges of the signal to cross
I = startInd(filtThrust,0.018);

% these crossing points indicating the thrust when the rotating drill makes contact with the specimen
% inspect the values returned in 'out' and visually check to ensure their correctness.
I =

    974257
    2113298
    3255083
    4386710
    5504208
    6621619
    7752190
    8893595

% Step 2
% Run hole = separateSig(sig, J, span) - sig is filtThrust from Step 1,
% span is the index range wide enough to cover the signal length of interest,
hole = separateSig(filtThrust,I,100000);

% plot startInd graph
figure(2);
plot(hole);
hold on;
warning off;
title('Thrust(N) vs index')
hleg1=legend('hole 1', 'hole 2', 'hole 3', 'hole 4', 'hole 5', 'hole 6', 'hole 7', 'hole 8', 'hole 9');
```

Appendix B

```
set(hleg1,'Location','NorthEast');
warning on;
hold off;

% J = out - backjump where out is obtained from Step 2 and backjump the left shift required to reveal
the zero
% thrust level before drill makes contact with specimen,
% typically from drill first contact to full diameter drilling;
hole = separateSig(filtThrust,I-6000,100000);

% plot startInd graph
figure(3);
plot(hole);
hold on;
warning off;
title('Thrust(N) vs index')
hleg1=legend('hole 1', 'hole 2', 'hole 3', 'hole 4', 'hole 5', 'hole 6', 'hole 7', 'hole 8', 'hole 9');
set(hleg1,'Location','NorthEast');
warning on;
hold off;

% Step 4
% Run Dhole = slope(hole, gradient-title)
% to obtain the gradients of signals in hole from Step 3 and plot graphs
% thrust-time gradient vs index position
% The argument gtitle is a string variable denoting the graph title.
Dhole=slope(hole,'Thrust gradient (6000 12)');

% plot slop graph
figure(4);
plot(Dhole);
hold on;
warning off;
```

Appendix B

```
title('Thrust gradient (6000 12)')
xlabel('thrust time gradient')

hleg1=legend('hole 1', 'hole 2', 'hole 3', 'hole 4', 'hole 5', 'hole 6', 'hole 7', 'hole 8', 'hole 9');
set(hleg1,'Location','NorthEast');

warning on;
hold off;

% Step 5
% Run slopemax=maxSlope(Dhole, lowerIndex, upperIndex, gtitle)
% returns a vector slopemax containing the maximum gradient values of hole signals in the range
lowerIndex to upperIndex
% plots a graph of these values against hole numbers.
slopemax1=maxSlope(Dhole,1, 30000, 'First gradient');
slopemax2=maxSlope(Dhole,30000, 90000, 'Second gradient');
```

B-10 0.2mm drilling tool signal on AI (pecking action)

```
%% Step 1
% Procedure for analysing gradients of thrust-time signals

load('0.2mm_6000_12_1st.mat');
hole1 = B;

load('0.2mm_6000_12_2nd.mat');
hole2 = B;

load('0.2mm_6000_12_3rd.mat');
hole3 = B;

load('0.2mm_6000_12_4th.mat');
hole4 = B;

load('0.2mm_6000_12_5th.mat');
hole5 = B;

load('0.2mm_6000_12_6th.mat');
hole6 = B;

load('0.2mm_6000_12_7th.mat');
hole7 = B;
```

Appendix B

```
load('0.2mm_6000_12_8th.mat');
hole8 = B;
load('0.2mm_6000_12_9th.mat');
hole9 = B;

%% Step 2
% fifth column containing the thrust force which is extracted and filtered using moving average of N
points
% N = 100. Outputs: filtered thrust signal for all holes drilled
% filtThrust and a graph depicting the thrust against array index.

filtH1=movavg(hole1,100);
filtH2=movavg(hole2,100);
filtH3=movavg(hole3,100);
filtH4=movavg(hole4,100);
filtH5=movavg(hole5,100);
filtH6=movavg(hole6,100);
filtH7=movavg(hole7,100);
filtH8=movavg(hole8,100);
filtH9=movavg(hole9,100);

%% Step 3
%% Run out = startInd(sig, thres)
% by visual inspection of graph in step 1
% set a threshold for the rising edges of the signal to cross
% J = out - backjump where out is obtained from Step 2 and backjump the left shift required to reveal
the zero
% thrust level before drill makes contact with specimen,
% typically from drill first contact to full diameter drilling;

I = startInd(filtH1,0.16);
J = I(1)
hole1plough1 = hole1(J-1000: J+6400);
```

Appendix B

```
I = startInd(filtH2,0.16);
J = I(1)
hole2plough1 = hole2(J-1000: J+6400);
I = startInd(filtH3,0.16);
J = I(1)
hole3plough1 = hole3(J-1000: J+6400);
I = startInd(filtH4,0.16);
J = I(1)
hole4plough1 = hole4(J-1000: J+6400);
I = startInd(filtH5,0.16);
J = I(1)
hole5plough1 = hole5(J-1000: J+6400);
I = startInd(filtH6,0.16);
J = I(1)
hole6plough1 = hole6(J-1000: J+6400);
I = startInd(filtH7,0.16);
J = I(1)
hole7plough1 = hole7(J-1000: J+6400);
I = startInd(filtH8,0.16);
J = I(1)
hole8plough1 = hole8(J-1000: J+6400);
I = startInd(filtH9,0.16);
J = I(1)
hole9plough1 = hole9(J-1000: J+6400);

%% Step 4
% fifth column containing the thrust force which is extracted and filtered using moving average of N
% points
% N = 1000. Outputs: filtered thrust signal for all holes drilled
% filtThrust and a graph depicting the thrust against array index.
filtH1plough1=movavg(hole1plough1,1000);
filtH2plough1=movavg(hole2plough1,1000);
filtH3plough1=movavg(hole3plough1,1000);
```

Appendix B

```
filtH4plough1=movavg(hole4plough1,1000);
filtH5plough1=movavg(hole5plough1,1000);
filtH6plough1=movavg(hole6plough1,1000);
filtH7plough1=movavg(hole7plough1,1000);
filtH8plough1=movavg(hole8plough1,1000);
filtH9plough1=movavg(hole9plough1,1000);

% plot filter graph
figure(1);
hold on;
plot(filtH1plough1,'b')
plot(filtH2plough1,'g')
plot(filtH3plough1,'r')
plot(filtH4plough1,'c')
plot(filtH5plough1,'m')
plot(filtH6plough1,'y')
plot(filtH7plough1,'k')
plot(filtH8plough1,'--b')
plot(filtH9plough1,'--g')
title('Thrust(N) vs index')
hold off

%% Step 5
% run filter signal backjump from the same start level to reveal the zero
% thrust level before drill makes contact with speciment,
% typically from drill first contact to full diameter drilling;
    filtH1plough1 = filtH1plough1 - filtH1plough1(1000);
    filtH2plough1 = filtH2plough1 - filtH2plough1(1000);
    filtH3plough1 = filtH3plough1 - filtH3plough1(1000);
    filtH4plough1 = filtH4plough1 - filtH4plough1(1000);
    filtH5plough1 = filtH5plough1 - filtH5plough1(1000);
    filtH6plough1 = filtH6plough1 - filtH6plough1(1000);
    filtH7plough1 = filtH7plough1 - filtH7plough1(1000);
```

Appendix B

```
filtH8plough1 = filtH8plough1 - filtH8plough1(1000);
```

```
filtH9plough1 = filtH9plough1 - filtH9plough1(1000);
```

```
%% plot filter graph
```

```
figure(2);
```

```
hold on;
```

```
plot(filtH1plough1,'b')
```

```
plot(filtH2plough1,'g')
```

```
plot(filtH3plough1,'r')
```

```
plot(filtH4plough1,'c')
```

```
plot(filtH5plough1,'m')
```

```
plot(filtH6plough1,'y')
```

```
plot(filtH7plough1,'k')
```

```
plot(filtH8plough1,'--b')
```

```
plot(filtH9plough1,'--g')
```

```
title('Thrust(N) vs index')
```

```
hold off
```

```
%% Step 6
```

```
%% run removeElements to pick the first pecking signal
```

```
filtH1plough1 = removeElements(filtH1plough1, [1:1000]);
```

```
filtH2plough1 = removeElements(filtH2plough1, [1:1000]);
```

```
filtH3plough1 = removeElements(filtH3plough1, [1:1000]);
```

```
filtH4plough1 = removeElements(filtH4plough1, [1:1000]);
```

```
filtH5plough1 = removeElements(filtH5plough1, [1:1000]);
```

```
filtH6plough1 = removeElements(filtH6plough1, [1:1000]);
```

```
filtH7plough1 = removeElements(filtH7plough1, [1:1000]);
```

```
filtH8plough1 = removeElements(filtH8plough1, [1:1000]);
```

```
filtH9plough1 = removeElements(filtH9plough1, [1:1000]);
```

```
%%plot the pecking signal
```

```
figure(3);
```

```
hold on;
```

Appendix B

```
plot(filtH1plough1,'b')
plot(filtH2plough1,'g')
plot(filtH3plough1,'r')
plot(filtH4plough1,'c')
plot(filtH5plough1,'m')
plot(filtH6plough1,'y')
plot(filtH7plough1,'k')
plot(filtH8plough1,'--b')
plot(filtH9plough1,'--g')
title('0.2mm 6000 12')
xlabel('Index time')
ylabel('Thrust Force (N)')
hleg1=legend('1st drill', '2nd drill', '3rd drill', '4th drill', '5th drill', '6th drill', '7th drill', '8th drill', '9th
drill');
set(hleg1,'Location','NorthEast');hold off

% Step 7
% Run Dhole = slope(hole, gradient-title)
% to obtain the gradients of signals in hole from Step 3 and plot graphs
% thrust-time gradient vs index position
% The argument gtitle is a string variable denoting the graph title.
Dhole1=slope(filtH1plough1,'Thrust gradient (12000 12)');
Dhole2=slope(filtH2plough1,'Thrust gradient (12000 12)');
Dhole3=slope(filtH3plough1,'Thrust gradient (12000 12)');
Dhole4=slope(filtH4plough1,'Thrust gradient (12000 12)');
Dhole5=slope(filtH5plough1,'Thrust gradient (12000 12)');
Dhole6=slope(filtH6plough1,'Thrust gradient (12000 12)');
Dhole7=slope(filtH7plough1,'Thrust gradient (12000 12)');
Dhole8=slope(filtH8plough1,'Thrust gradient (12000 12)');
Dhole9=slope(filtH9plough1,'Thrust gradient (12000 12)');

%%plot gradient graph
figure(4);
```

Appendix B

```
hold on;
plot(Dhole1,'b')
plot(Dhole2,'g')
plot(Dhole3,'r')
plot(Dhole4,'c')
plot(Dhole5,'m')
plot(Dhole6,'y')
plot(Dhole7,'k')
plot(Dhole8,'--b')
plot(Dhole9,'--g')
title('Thrust gradient (0.2mm 6000 12)')
xlabel('Index time')
ylabel('Gradient')
hleg1=legend('1st drill', '2nd drill', '3rd drill', '4th drill', '5th drill', '6th drill', '7th drill', '8th drill', '9th
drill');
set(hleg1,'Location','NorthEast');
hold off
```

B-11 0.6mm drilling tool signal on Al (non-pecking action)

```
%% Step 1
%% separate thrust signal for individual holes
load('0.6mm_6000_12_1st.mat');
hole1 = B;
load('0.6mm_6000_12_2nd.mat');
hole2 = B;
load('0.6mm_6000_12_3rd.mat');
hole3 = B;
load('0.6mm_6000_12_4th.mat');
hole4 = B;
load('0.6mm_6000_12_5th.mat');
hole5 = B;
load('0.6mm_6000_12_6th.mat');
hole6 = B;
```

Appendix B

```
load('0.6mm_6000_12_7th.mat');
hole7 = B;

load('0.6mm_6000_12_8th.mat');
hole8 = B;

load('0.6mm_6000_12_9th.mat');
hole9 = B;

%% Step 2
%% apply moving average to smooth the signals
% number of average points used: 3000
filtH1=movavg(hole1,3000);
filtH2=movavg(hole2,3000);
filtH3=movavg(hole3,3000);
filtH4=movavg(hole4,3000);
filtH5=movavg(hole5,3000);
filtH6=movavg(hole6,3000);
filtH7=movavg(hole7,3000);
filtH8=movavg(hole8,3000);
filtH9=movavg(hole9,3000);

%% plot the smoothed thrust-time graphs
% one for each hole drilled
figure(1);
hold on;
plot(filtH1,'b')
plot(filtH2,'g')
plot(filtH3,'r')
plot(filtH4,'c')
plot(filtH5,'m')
plot(filtH6,'y')
plot(filtH7,'k')
plot(filtH8,'--b')
plot(filtH9,'--g')
```

Appendix B

```
title('0.8mm 6000 12')
xlabel('Index time')
ylabel('Thrust force N')
hleg1=legend('1st drill', '2nd drill', '3rd drill', '4th drill', '5th drill', '6th drill', '7th drill', '8th drill', '9th
drill');
set(hleg1,'Location','NorthEast');
hold off

%% Step 3
%% restore each hole start from 0
restoreH1=filtH1-filtH1(4000);
restoreH2=filtH2-filtH2(10000);
restoreH3=filtH3-filtH3(10000);
restoreH4=filtH4-filtH4(10000);
restoreH5=filtH5-filtH5(10000);
restoreH6=filtH6-filtH6(10000);
restoreH7=filtH7-filtH7(10000);
restoreH8=filtH8-filtH8(10000);
restoreH9=filtH9-filtH9(10000);

%% plot the restore thrust-time graphs
% one for each hole drilled
figure(2);
hold on;
plot(restoreH1,'b')
plot(restoreH2,'g')
plot(restoreH3,'r')
plot(restoreH4,'c')
plot(restoreH5,'m')
plot(restoreH6,'y')
plot(restoreH7,'k')
plot(restoreH8,'--b')
plot(restoreH9,'--g')
```

Appendix B

```
title('Thrust(N) vs index')
hold off

%% Step 4
%% set a value to be the zero point.
%% go back 2000 points to be the start point
k = find(restoreH1>0.03, 1);
restartpointH1 = removeElements(restoreH1, [1: k-2000, k+20000: 450000]);
k = find(restoreH2>0.03, 1);
restartpointH2 = removeElements(restoreH2, [1: k-2000, k+20000: 467001]);
k = find(restoreH3>0.03, 1);
restartpointH3 = removeElements(restoreH3, [1: k-2000, k+20000: 470001]);
k = find(restoreH4>0.03, 1);
restartpointH4 = removeElements(restoreH4, [1: k-2000, k+20000: 440001]);
k = find(restoreH5>0.03, 1);
restartpointH5 = removeElements(restoreH5, [1: k-2000, k+20000: 470001]);
k = find(restoreH6>0.03, 1);
restartpointH6 = removeElements(restoreH6, [1: k-2000, k+20000: 460001]);
k = find(restoreH7>0.03, 1);
restartpointH7 = removeElements(restoreH7, [1: k-2000, k+20000: 480001]);
k = find(restoreH8>0.03, 1);
restartpointH8 = removeElements(restoreH8, [1: k-2000, k+20000: 480001]);
k = find(restoreH9>0.03, 1);
restartpointH9 = removeElements(restoreH9, [1: k-2000, k+20000: 460001]);

%% plot the restartpoint thrust-time graphs
%% one for each hole drilled
figure(3);
hold on;
plot(restartpointH1,'b')
plot(restartpointH2,'g')
plot(restartpointH3,'r')
plot(restartpointH4,'c')
```

Appendix B

```
plot(restartpointH5,'m')
plot(restartpointH6,'y')
plot(restartpointH7,'k')
plot(restartpointH8,'--b')
plot(restartpointH9,'--g')
title('0.8mm 6000 12')
xlabel('Index time')
ylabel('Thrust Force (N)')
hleg1=legend('1st drill', '2nd drill', '3rd drill', '4th drill', '5th drill', '6th drill', '7th drill', '8th drill', '9th
drill');
set(hleg1,'Location','NorthEast')
hold off

%% Step 5
%% each drilled has a 2000 points gap
% one for each hole drilled

figure(4);
hold on;
n = length(restartpointH1)
x = [1:1:n]
plot(x, restartpointH1,'b')
n = length(restartpointH2)
x = [1:1:n]
plot(x+2000, restartpointH2,'g')
n = length(restartpointH3)
x = [1:1:n]
plot(x+4000, restartpointH3,'r')
n = length(restartpointH4)
x = [1:1:n]
plot(x+6000, restartpointH4,'c')
n = length(restartpointH5)
x = [1:1:n]
plot(x+8000, restartpointH5,'m')
```

Appendix B

```
n = length(restartpointH6)
x = [1:1:n]
plot(x+10000, restartpointH6, 'y')
n = length(restartpointH7)
x = [1:1:n]
plot(x+12000, restartpointH7, 'k')
n = length(restartpointH8)
x = [1:1:n]
plot(x+14000, restartpointH8, '--b')
n = length(restartpointH9)
x = [1:1:n]
plot(x+16000, restartpointH9, '--g')
title('0.8mm 6000 12')
xlabel('Index time')
ylabel('Thrust Force (N)')
hleg1=legend('1st drill', '2nd drill', '3rd drill', '4th drill', '5th drill', '6th drill', '7th drill', '8th drill', '9th
drill');
set(hleg1, 'Location', 'NorthEast')
hold off

%% Step 6
% Run Dhole = slope(hole, gradient-title)
% to obtain the gradients of signals in hole from Step 3 and plot graphs
% thrust-time gradient vs index position
% The argument gtitle is a string variable denoting the graph title.

Dhole1=slope(restartpointH1, 'Thrust gradient (20000 12)');
Dhole2=slope(restartpointH2, 'Thrust gradient (20000 12)');
Dhole3=slope(restartpointH3, 'Thrust gradient (20000 12)');
Dhole4=slope(restartpointH4, 'Thrust gradient (20000 12)');
Dhole5=slope(restartpointH5, 'Thrust gradient (20000 12)');
Dhole6=slope(restartpointH6, 'Thrust gradient (20000 12)');
Dhole7=slope(restartpointH7, 'Thrust gradient (20000 12)');
```

Appendix B

```
Dhole8=slope(restartpointH8,'Thrust gradient (20000 12)');
Dhole9=slope(restartpointH9,'Thrust gradient (20000 12)');

%%plot gradient graph
figure(5);
hold on;
plot(Dhole1,'b')
plot(Dhole2,'g')
plot(Dhole3,'r')
plot(Dhole4,'c')
plot(Dhole5,'m')
plot(Dhole6,'y')
plot(Dhole7,'k')
plot(Dhole8,'--b')
plot(Dhole9,'--g')
title('0.8mm 6000 12')
xlabel('Index time')
ylabel('Gradient')
hleg1=legend('1st drill', '2nd drill', '3rd drill', '4th drill', '5th drill', '6th drill', '7th drill', '8th drill', '9th
drill');
set(hleg1,'Location','NorthEast');
hold off
```